

1 Comparison of a Semi-Implicit and a Fully-Implicit Time Integration Method for a  
2 Highly Degenerate Diffusion-Reaction Equation Coupled with an Ordinary  
3 Differential Equation

4 by

5 Eric M. Jalbert

6 A Thesis  
7 presented to  
8 The University of Guelph

9 In partial fulfilment of requirements  
10 for the degree of  
11 Master of Science  
12 in  
13 Applied Mathematics

14 Guelph, Ontario, Canada

15 © E.M. Jalbert, January, 2015

## ABSTRACT

17    **Comparison of a Semi-Implicit and a Fully-Implicit Time Integration Method  
18    for a Highly Degenerate Diffusion-Reaction Equation Coupled with and  
19    Ordinary Differential Equation**

20    Eric M. Jalbert  
University of Guelph, 2015

Adviser  
Professor Hermann J. Eberl

21    A certain class of highly degenerate diffusion equations arises when modelling biofilm growth and  
22    propagations. We focus on the cellulolytic *Clostridium thermocellum*, because of its potential in  
23    the field of energy biotechnology. From this system a spatially implicit model was proposed in the  
24    literature before. Here we study a spatially explicit model. In contrast to other biofilm systems, a  
25    special feature of this system is that the growth promoting nutrient is not diffusive but bound in the  
26    substratum on which the biofilm grows. As a consequence one obtains a highly degenerate diffusion-  
27    reaction equation for the bacteria that is coupled to an ordinary differential equation for nutrients.  
28    The degeneracy of the biomass equation introduces gradient blow-up at the interface which makes  
29    numerical treatment difficult. For this, a fully-implicit time integration method is formulated so that  
30    it generalises a previously used semi-implicit method to solve the problem with increased accuracy.  
31    The fully-implicit method uses, at each time-step, a fixed-point iteration to solve the arising nonlinear  
32    algebraic equation and can be controlled by the required tolerance for convergence.

33    This method is validated and tested to investigate numerous issues that arise with numerical com-  
34    putations: mass conservations, preservation of symmetries in the initial data, and convergence with  
35    respect to grid refinement. Furthermore, a difference is quantified between the fully-implicit and the  
36    simpler semi-implicit methods which it generalises. The trade-off between improved accuracy and  
37    increased computational effort is found to be optimal for tolerances that force a single extra iteration  
38    of the fully-implicit method.

39    The numerical method is then used to simulate *C.thermocellum* biofilm formation on cellulose sheets  
40    with the main objectives of (i) understanding patterns of biofilm formation and (ii) understanding how  
41    including the spatial diffusion terms in the biomass affect the results of the simulations at a reactor-  
42    scale. Our simulation results strongly suggest the formation of travelling wave solutions that describe  
43    how the biofilm moves across the substratum. To test the effect of the spatial effects on overall  
44    biofilm performance, two extremes of initial biomass distributions were simulated. A quantitative  
45    difference between the behaviour in both cases is found, but not a qualitative one. This suggests  
46    that in applications where spatial heterogeneity is important then a two dimensional spatially explicit  
47    model that includes the spatial diffusion must be used instead of the earlier, simple spatially implicit  
48    reactor-scale ordinary differential equation model that consolidated the spatial effects with a carrying  
49    capacity on the growth term.

# 50 **Contents**

51	<b>Abstract</b> . . . . .	ii
52	<b>1 Introductions</b>	1
53	1.1 Introduction . . . . .	1
54	1.2 Objectives . . . . .	7
55	1.3 Thesis Outline . . . . .	8
56	<b>2 Model Definition</b>	9
57	2.1 Model Description . . . . .	9
58	2.2 Nondimensionalization . . . . .	13
59	<b>3 Numerical Methods</b>	16
60	3.1 Discretization . . . . .	16
61	3.2 Solution Technique . . . . .	19
62	3.3 Computational Setup . . . . .	25
63	3.4 Method Validation . . . . .	26
64	3.5 Comparison of Semi-implicit and Fully-implicit Method . . . . .	32
65	<b>4 Simulation Results</b>	36
66	4.1 Typical Simulation . . . . .	36
67	4.2 Travelling Wave Analysis . . . . .	42
68	4.3 Spatial Effects . . . . .	52
69	<b>5 Conclusions</b>	58
70	5.1 Lessons Learned . . . . .	58
71	5.2 Future Work . . . . .	59
72	<b>Bibliography</b>	60
73	<b>A Default Parameter Values</b>	63
74	<b>B Source Code</b>	64

75 **Chapter 1**

76 **Introductions**

77 **1.1 Introduction**

78 Bacterial biofilms are microscopic depositions of organisms that attach themselves on immersed sur-  
79 faces whenever environmental conditions can sustain microbial growth. These bacteria, when sessile,  
80 surround themselves in a self-produced viscous layer of extracellular polymeric substances. As a  
81 result of this, the cells are extraordinarily resistant to mechanical washout or antibiotic attacks. Most  
82 bacterial populations live in communities within the extracellular polymeric substances. They can be  
83 found in many different aspects of life in both positive ways (wastewater treatments, soil remediation,  
84 and groundwater protection) and negative ways (bacterial infections, dental plaque, biocorrosion of  
85 facilities and water pipes).

86 The first biofilm models, like that in Rittmann and McCarty (1980), assumed that biofilms developed  
87 as a flat layer and were posed as ordinary differential equations or one-dimensional partial differential  
88 equations. This simplified the calculation for the speed of propagation but was limited in non-spatially  
89 heterogenous biofilm morphologies. To this end, many models for spatially heterogenous biofilms  
90 were proposed. These included stochastic individual based models (Kreft et al., 2001), cellular au-  
91 tomata models (Picioreanu et al., 1998), and deterministic continuum models (Eberl et al., 2001). The  
92 added complexity helped in modelling more of the multi-dimensional aspects of biofilms, namely the

93 intrinsic structures that most biofilms grew. These models considered the changes the biofilms made  
 94 at the meso-scale instead of the reactor-scale which simpler models tended to do.

95 The recent field of energy biotechnology has led to researching biofilms as a potential means of  
 96 using plant biomass to generate sustainable fuels. These fuels, such as ethanol, are generated through  
 97 conversion of terrestrial or aquatic biomass (Lynd, 2008). The main benefits for using these fuel  
 98 sources is that they produce much less greenhouse gases as seen in Figure 1.1. Using cellulolytic  
 99 biofilms (cellulose degrading biofilms) to produce biofuels means that only non-edible cellulose is  
 100 utilized instead of edible plants like corn. *Clostridium thermocellum* is a possible choice for achieving  
 101 large scale biomass conversion. Because of this there has been a surge of studies based around  
 102 its behaviours and characteristics. An interesting feature of *C.thermocellum* is that it grows as a  
 103 thin cellulolytic monolayer and does not produce any extracellular polymeric matrix (Dumitrache  
 104 et al., 2013a). This is a stark contrast to typical biofilms which are notorious for forming complex  
 105 mushroom or pillar shaped morphologies.

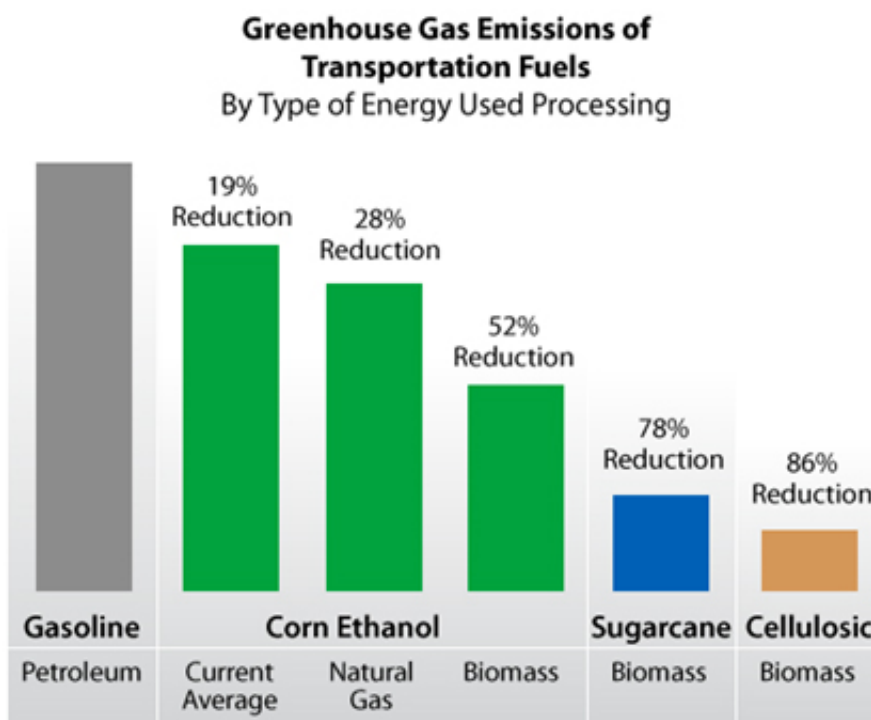


**Figure 1.1:** A comparison graph of greenhouse gas emissions for transportation fuels produced based on different fuel types. Each are related to the decreased emissions when compared to Petroleum. Graph indicating high greenhouse gas emissions for gasoline, then reductions with corn ethanol and further reductions with sugarcane biomass (78% reduction) and cellulosic biomass (86% reduction). Figure originally from Alternative Fuel Data Center (2014).

106 Dumitrache et al. (2015) have made a number of *in situ* and *in vitro* observations for *C.thermocellum*.  
107 Here they linked the cellulose consumption rate of the bacteria to the rate of  $CO_2$  produced. The  
108 experiments ran in a continuous-flow reactor that used Whatman cellulose paper sheets inoculated  
109 with *C.thermocellum* strains. The bacteria consumed the fibers of the cellulose sheets as they grew. By  
110 tracking only the  $CO_2$  production, they were only focused on the activity of the bacteria at a reactor-  
111 scale. The smaller spatial movements of the bacteria were ignored for simplicity of the experiment.

112 A simple mathematical model for cellulolytic biofilm activity and growth on model cellulosic sub-  
113 strate was proposed in Dumitrache et al. (2015). Here the production of carbon dioxide was used as  
114 an indicator of culture metabolism. Because of this indicator, they focused on overall biofilm per-  
115 formance rather than on detailed biofilm structure. This led to a reactor-scale model that attributed  
116 the spatial effects into logistic-like growth and carrying capacities to limit the bacteria activity in the  
117 models. The model was based on a number of observations on the metabolic activity gathered by  
118 online carbon dioxide measurements. For this model, attention was also put on high-resolution imag-  
119 ing of different stages of biofilm development (Dumitrache et al., 2013a) and to the physiological  
120 behaviour of substrate modification (Dumitrache et al., 2013b).

121 The conceptual model of cellulolytic biofilm growth that was followed for their model is shown in  
122 Figure 1.2. This model is based on the relation between *C.thermocellum* growth and cellulose sheet  
123 consumption. The relation is, when *C.thermocellum* grows there exist cellulose sheet consumption,  
124 limiting the area of substratum available for bacteria attachment. Here they express the growth of  
125 the biomass in terms of an *ideal* and an *actual* carrying capacity. The ideal carrying capacity,  $M_\infty$ ,  
126 refers to the maximum amount of biomass that can be supported when the only limitations are from  
127 a deficiency of local space. This value depends on the properties of the substratum and is assumed to  
128 be constant since it is independent of the substrate concentration. The actual carrying capacity,  $M_\alpha$ ,  
129 references the amount of biomass that can be supported when the local concentration of substrate  
130 mass is limited. This value is not constant since it is a function of the current substrate concentration.  
131 In essence, Dumitrache et al. (2015) use the carrying capacity as a means to account for the limitations  
132 due to spatial effects.

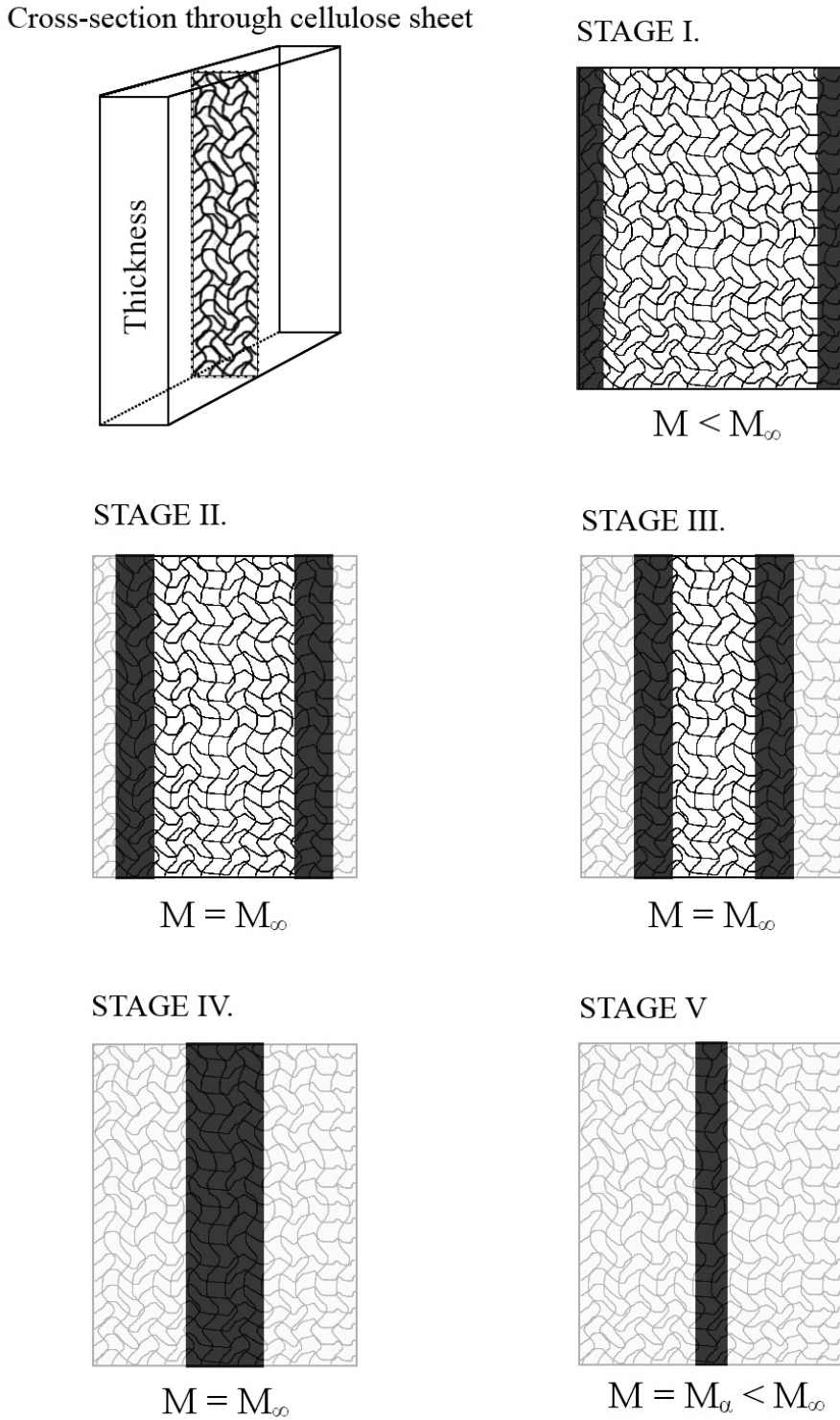


**Figure 1.2:** Conceptual model of cellulolytic biofilm growth and consumption of cellulose sheets. Attachment and growth occurs on both sides of the sheet, individual monolayers form on each fiber and result in a band of active biofilm (i.e., the effective sessile biomass)  $M$  (dark band). The ideal carrying capacity,  $M_{\infty}$ , and the actual carrying capacity,  $M_{\alpha}$ , are explained in Dumitrache et al. (2015). Consumed substrate is represented by the light gray areas. Figure originally from Dumitrache et al. (2015).

133 The model developed by Dumitrache et al. (2015) followed the five different conceptual growth stages  
134 of *C.thermocellum*. These stages were:

- 135 • Stage I: Independent colonies of cells grow on the matrix of fibers in the substrate. This occurs  
136 initially for all the isolated regions of the biofilm.
- 137 • Stage II: The biofilm grows inwards. The superficial fibres are consumed and newly unsup-  
138 ported biofilms are released from the cellulose sheet into the aqueous stream.
- 139 • Stage III: The active biofilm band stabilizes somewhere around the point where superficial fiber  
140 deconstruction rate is the equivalent to the inwards penetration rate of the biofilm.
- 141 • Stage IV: The progression of the biofilm band continues until the remaining amount of usable  
142 substrate becomes limited.
- 143 • Stage V: The remaining cellulose gets consumed without new biofilm being produced. Instead  
144 a new generation of non-adherent cells is formed locally.

145 This formulated a system of ordinary differential equation because of the non-diffusivity of the sub-  
146 strate. These ordinary differential equations resembled traditional growth models in batch cultures  
147 more then the typically complex biofilm model seen in studies (Wanner et al., 2005).

148 The model developed in Wang et al. (2011) focused more on detailing the qualitative aspects of a  
149 single *C.thermocellum* colony in terms of spatio-temporal development. The reaction kinetics were  
150 ignored as they assumed that when bacteria occupied a new space all the substrate would be immedi-  
151 ately utilised. This was completed by use of a nine-neighbour square cellular automata on a  $30 \times 15$   
152 grid with a single grid cell as an inoculation point. The model results matched the experimental re-  
153 sults they gathered. This was the first model to consider the spatial development of *C.thermocellum* at  
154 a small scale. Using cellular automata with such a coarse grid gave them a discrete representation of  
155 the system they modelled. One purpose of this thesis is to extend this concept to a continuous model  
156 similar to Eberl et al. (2001) but instead using the assumptions and growth function that match the  
157 behaviour of *C.thermocellum*.

158 There are problems with trying to extend *C.thermocellum* to a spatially considerate continuum model.  
159 Because the substratum used for attachment is consumed with biofilm growth and the stationary  
160 nature of the cellulose sheets, this problem becomes significantly different from other biofilm models  
161 which are based on the aqueous, free-floating environment where biofilms typically develop. At  
162 the meso-scale, our *C.thermocellum* system must model the development of the biofilm along the  
163 non-diffusing individual fibers of the cellulose sheet structure. Thus, these two categories of biofilm  
164 models differ mainly in their consideration of substrate diffusion, with *C.thermocellum* there is none.

165 Our problem originates from the ordinary differential equation model from Dumitache et al. (2015).  
166 Here we include the double-degenerate parabolic model of biofilm formation from Eberl et al. (2001)  
167 for the spatial consideration. This type of model arises when a volume filling problem has a finite  
168 speed of interface propagation (Khassehkhan et al., 2009). A density-dependent diffusion model with  
169 reaction terms that match with the behaviour of *C.thermocellum* is what is handled here. The spatial  
170 operator for biofilm spreading shows two non-standard diffusion effects:

- 171     • A power law degeneracy similar to the porous medium equation for local biomass at the inter-  
172         face of the biofilm (Gurtin, 1977).
- 173     • A singularity in the diffusion coefficient when the biofilm approaches maximum biomass den-  
174         sity.

175 Both of these effects together lead to the development of sharp and steep interfaces in the model  
176 solutions that mark the separation of the actual biofilm from its liquid environment. Such propagating  
177 interface problems in partial differential equations often are difficult to treat numerically.

178 The mathematical models which focus on the growth dynamics of biological films are usually systems  
179 of partial differential equations. These models are built on some of the significant features of biofilm  
180 growth observed throughout the practice, such as:

- 181     a) the presence of a sharp front of biomass at the solid to fluid transition region,

- 182 b) the existence of a threshold of biomass density,
- 183 c) the spreading of biomass is only notable when local densities approach the threshold of sustain-
- 184 ability,
- 185 d) the use of reaction kinetics mechanisms to model the production of biomass,
- 186 e) the compatibility of biomass spreading with nutrient transfer and consumption mechanism models.

187 There exists mathematical background for these systems of equations that prove existence and unique-

188 ness of positive and bounded solutions. However, the complexity of these nonlinear partial differential

189 equations have made providing analytical expressions of the solutions practically impossible, when

190 given biologically meaningful initial conditions.

191 This forces numerical computational approaches to be taken for simulating the growth of these micro-

192 bial colonies. Some techniques with the finite-difference method have been used for these problems.

193 This approach has been proposed in Eberl and Demaret (2007) for deterministic models.

194 In this thesis, the finite-difference method is treated as a semi-implicit numerical method similar to

195 Eberl and Demaret (2007). Here, the method is extended to use a fixed-point iteration to facilitate the

196 computations of the degeneracy from the biomass diffusion. This turns the semi-implicit method into

197 a fully-implicit method. The validity of this method is unknown and put under scrutiny by simulating

198 the *C.thermocellum* system during this thesis. This system has a partial differential equation for the

199 diffusion-reaction equation of biomass and an ordinary differential equation for the non-diffusing

200 substrate concentrations.

201 **1.2 Objectives**

202 There are three main objectives of this thesis:

- 203 1. Formulate and test a fully-implicit method for a highly degenerate, highly nonlinear coupled
- 204 PDE-ODE system modelling *C.thermocellum* biofilms.

- 205        2. Compare the fully-implicit method of Objective 1 with a previously introduced semi-implicit  
206        method, which it generalizes. This is done based on the trade-off between improved accuracy  
207        of the method and increased computational effort.
- 208        3. Use the numerical methods developed in Object 1 and 2 to simulate *C.thermocellum* biofilm for-  
209        mation on cellulose sheets, with the goal of understanding better the spatio-temporal dynamics  
210        of this system biofilms.

211 **1.3 Thesis Outline**

212 In Chapter 1 of the thesis, a brief background for the research project is provided. The objectives of  
213 the thesis and the outline of how each objective will be addressed is also presented here.

214 In Chapter 2, the underlying model of *C.thermocellum* biofilm growth on cellulose sheets is stated and  
215 transformed into a non-dimensional model. This model is a coupled system comprised of a highly-  
216 degenerate partial differential equations for bacterial biomass and a ordinary differential equation for  
217 the growth limiting substrate.

218 In Chapter 3, a fully-implicit time-integration scheme is introduced that generalizes an earlier semi-  
219 implicit method. The implementation of the method is discussed and validated by testing it against  
220 typical settings and running a grid convergence test. Finally a comparison between the fully-implicit  
221 method and the earlier semi-implicit method is conducted.

222 In Chapter 4, the fully-implicit method of Chapter 3 is used to simulate *C.thermocellum* biofilm  
223 formation on cellulose fibers. The numerical solution suggests that the model permits travelling wave  
224 solutions that describe the spatio-temporal breakdown of the cellulose fibers. The results of the two  
225 dimensional simulations are compared qualitatively against a conceptual model of fiber breakdown  
226 and against lumped experimental data from the literature.

227 In Chapter 5, concluding statements are made concerning the main objectives of the thesis, based on  
228 the results from chapter 3 and 4. Future extensions of the works done here are also discussed.

229 **Chapter 2**

230 **Model Definition**

231 **2.1 Model Description**

232 The model used for simulations is based on the deterministic biofilm model developed in Eberl et al.  
233 (2001), which was designed for modelling the development of spatially heterogenous biofilm struc-  
234 tures. Since *C.thermocellum* grows as a monolayered biofilm and consumes a solid carbon fibrous  
235 substrate, there are mechanical differences between the two systems. Our model is based on the  
236 following assumptions:

- 237 1. The growth of sessile biomass is limited locally by the availability of nutrients and by the  
238 availability of colonizable space.
- 239 2. The number of cells per unit area of substratum is limited to a finite value because *C.thermocellum*  
240 forms only a thin monolayer.
- 241 3. Biomass does not spread until its density approaches the physical limit. Near the physical limit  
242 it expands spatially into neighbouring regions. Because of this, the physical limit of biomass  
243 density is never attained.
- 244 4. The carbon fibrous substrate consumed as nutrition for biomass growth is the substratum to  
245 which the biofilm attaches. Carbon is bound in the fibers of the substratum and does not diffuse.

246 The propagation of biofilm is based on the lack of available substrate locally, not the physical  
 247 degradation of the substratum.

- 248 5. Cell death and cell loss into the aqueous environment is assumed to be proportional to cell  
 249 density.
- 250 6. Biomass growth is proportional to substrate consumption.

251 Assumption 1, 2, 3, 5, and 6 are similar to those made in Eberl et al. (2001). The main difference  
 252 here is 4; our substrate is sessile. With a sessile substrate, there is no diffusion for the substrate  
 253 concentration. Another difference is that *C. thermocellum* does not grow from the substratum into  
 254 the aqueous phase. Instead our biofilm grows across the substratum making this a two dimensional  
 255 setting.

256 The model is formulated in a spatial domain  $\Omega \subset \mathbb{R}^2$ . The independent variables  $t > 0$  denote  
 257 time and  $x \in \Omega$  denotes the location within the physical domain. The dependent variables are the  
 258 local fraction of the surface occupied by biomass  $M(t, x)$  and the substrate density  $C(t, x)$ . The net  
 259 growth rate of biomass is denoted by  $f(C)$  and the substrate consumption rate is denoted by  $g(C)$ ,  
 260 both are dependent upon available substrate. The diffusion coefficient that describes spatial expansion  
 261 of biomass is given by the function  $d(M)$ .

262 From the above assumptions, a PDE-ODE-coupled system that models *C. thermocellum* growth on  
 263 carbonous fibres can be formulated as,

$$M_t = \nabla_x (d(M) \nabla_x M) + f(C)M \quad (2.1)$$

$$C_t = -g(C)M \quad (2.2)$$

264 where

$$265 d(M) = d \frac{M^\alpha}{(1 - M)^\beta} \quad (2.3)$$

266

$$f(C) = u \frac{C}{k_C + C} - n \quad (2.4)$$

267

$$g(C) = y \frac{C}{k_C + C} \quad (2.5)$$

268

269 with all parameters non-negative. Here we have a pair of equations, (2.1) and (2.2), that represent  
 270 the biomass density and substrate concentration respectively. This is a model for spatially explicit  
 271 biomass growth. This agrees with assumption 3 since for  $0 < M \ll 1$  the spreading effect is negli-  
 272 gible but when  $0 \ll M \approx 1$  there is considerable spreading. This choice for a spatially considerate  
 273 model is based on the work done in Khassehkhan et al. (2009). By assumption 1, the only factors  
 274 affecting the biomass density is growth from nutrient conversion and diffusion from local spatially-  
 275 full colonized space. For equation (2.3), the density-dependent diffusion equation,  $d$  is the diffusion  
 276 coefficient which controls the magnitude of the diffusion and the parameters  $\alpha$  and  $\beta$  are selected to  
 277 control the strength of the diffusion. For equation (2.3) the diffusion term is shown to have the wanted  
 278 behaviour since it has a near-zero finite value until  $M \rightarrow 1$ , which leads to  $d(M) \rightarrow \infty$  as seen in  
 279 Figure 2.1. The production rate is the difference between simple Monod kinetic growth term, with  
 280 growth rate  $u$ , and a constant death rate term,  $n$ , to agree with assumption 1 and 5. Monod kinetic  
 281 growth was selected, with half-saturation carbon concentration  $k_C$ , since it matches the growth of  
 282 bacteria when limited by available nutrients.

283 Equation (2.2) describes the consumption of carbon substrate due to biomass growth. Parameter  $y$  is  
 284 the consumption rate, measured in mass carbon per unit time. Substrate consumption is proportional  
 285 to the local biomass density  $M$ . Parameter  $k_C$ , same as in the growth term for (2.1), is again the half-  
 286 saturation carbon concentration. Here assumption 4 and 6 are satisfied since there exists no diffusion  
 287 term for the substrate and its growth is a scalar multiple of the biomass growth rate.

288 There has been shown to exist a finite speed of interface propagation for the solutions of these kinds  
 289 of degenerate problems, where  $d(0) = 0$  and  $\alpha > 1$  from (2.3) (Jalbert and Eberl, 2014). These  
 290 problems have a blow up in the biomass gradient at the interface because of the degeneracy that exists  
 291 there. For this system, we have  $M < 1$  always since the diffusion when  $M \approx 1$  is great enough to  
 292 always ensure this (Jalbert and Eberl, 2014).

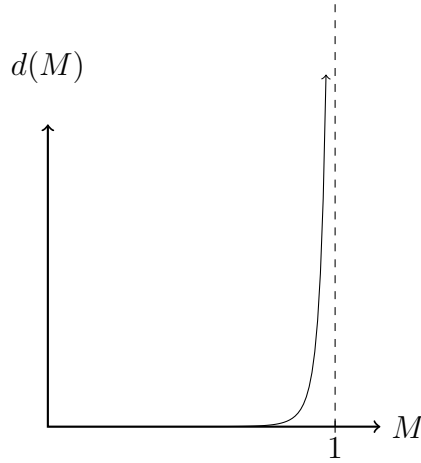


**Figure 2.1:** A graph of  $d(M) = d \frac{M^\alpha}{(1-M)^\beta}$  showing the way diffusion increases asymptotically as  $M \rightarrow 1$ .

293 The dimensions of the parameters and variables are in Table 2.1. Note that since we have a two  
 294 dimensional problem, due to the lack of complex biofilm structures from *C. thermocellum* growth,  
 295 the spatial considerations are all strictly for area and not volume, as is typically done for biofilm  
 modelling.

Description	Symbol	Dimensions
Spatial region	$\Omega$	$NA$
Time	$t$	[days]
Location in $\Omega$	$x = (x_1, x_2)$	[meters <sup>2</sup> ]
Biomass fraction	$M$	[—]
Substrate concentration	$C$	[grams / meters <sup>2</sup> ]
Diffusion coefficient	$d$	[meters <sup>2</sup> / days]
Density-dependent exponent	$\alpha$	[—]
Density-dependent exponent	$\beta$	[—]
Growth rate	$u$	[days <sup>-1</sup> ]
Half-saturation carbon concentration	$k_C$	[grams / meters <sup>2</sup> ]
Maximum consumption rate	$y$	[grams carbon / days]
Death constant	$n$	[days <sup>-1</sup> ]

**Table 2.1:** List of parameters and their dimensions

296  
 297 The model (2.1), (2.2) is completed by boundary conditions for the biomass density,  $M$ , and ini-  
 298 tial conditions for both  $M$  and substrate concentration  $C$ . For  $M$  we pose homogeneous Neumann  
 299 boundary conditions such that,

300 
$$\partial_n M = 0, \quad x \in \partial\Omega. \quad (2.6)$$

<sup>301</sup> The initial conditions for the biomass density is,

$$\text{302} \quad M(0, x) = M_0(x), \quad x \in \Omega, \quad (2.7)$$

<sup>303</sup> where  $0 \leq M_0(x) < 1$  and  $M_0(x)$  non-zero in specific pockets on the substratum. These are specified  
<sup>304</sup> below for each individual, simulation experiments. The initial conditions for the substrate concentra-  
<sup>305</sup> tion is,

$$\text{306} \quad C(0, x) = C_\infty, \quad x \in \Omega, \quad (2.8)$$

<sup>307</sup> where  $C_\infty$  describes the initial carbon density in the substratum.

## <sup>308</sup> 2.2 Nondimensionalization

<sup>309</sup> To help facilitate the analysis of this system, the full removal of all physical units is preferred and  
<sup>310</sup> so we nondimensionalize the parameters. From this point on, we assume that  $\Omega$  is a square two  
<sup>311</sup> dimensional region of length,  $L$ . Here the parameters used are: the biomass growth rate,  $u$ ; the length  
<sup>312</sup> of the region,  $L$ ; and the maximum density for biomass and substrate,  $M_\infty$  and  $C_\infty$ . The biomass  
<sup>313</sup> density fraction represents the current density of biomass divided by the maximum biomass density,  
<sup>314</sup>  $M_\infty$ . From using the following parameter changes, the system can be made unitless.

$$\chi = \frac{x}{L} \implies L\nabla_\chi = \nabla_x \quad (2.9)$$

$$\tau = ut \implies \frac{1}{u}d\tau = dt \quad (2.10)$$

$$\mathcal{C} = \frac{C}{C_\infty} \quad (2.11)$$

$$\delta = \frac{1}{uL^2}d \quad (2.12)$$

$$\kappa = \frac{k_C}{C_\infty} \quad (2.13)$$

$$\nu = \frac{n}{uC_\infty} \quad (2.14)$$

$$\gamma = \frac{M_\infty}{C_\infty}y \quad (2.15)$$

<sup>315</sup> Using these, (2.1) and (2.2) can be simplified and nondimensionalized into,

$$M_\tau = \nabla_\chi (D(M)\nabla_\chi M) + F(\mathcal{C})M \quad (2.16)$$

$$\mathcal{C}_\tau = -G(\mathcal{C})M, \quad (2.17)$$

<sup>316</sup> where,

$$\begin{aligned} D(M) &= \delta \frac{M^\alpha}{(1-M)^\beta} \\ F(\mathcal{C}) &= \frac{\mathcal{C}}{\kappa + \mathcal{C}} - \nu \\ G(\mathcal{C}) &= \gamma \frac{\mathcal{C}}{\kappa + \mathcal{C}}. \end{aligned} \quad (2.18)$$

<sup>317</sup> <sup>318</sup> with only  $\delta, \alpha, \beta, \kappa, \nu, \gamma$  as model parameters. For convenience, we henceforth use

$$C := \mathcal{C}, \quad x := \chi, \quad t := \tau. \quad (2.19)$$

<sup>319</sup> <sup>320</sup> Each of the dimensionless parameters in (2.18) have a biological representation based on the trans-

321 formations done. The parameter  $\delta$  is the dimensionless biomass motility coefficient. It affects the  
322 change in biomass from adjacent biomass sources, a greater  $\delta$  results in faster biofilm expansion.  
323 The parameter  $\kappa$  is the half-saturation point, it is exactly the value for which substrate concentration  
324 results in 0.5-optimum growth rate. Parameter  $\nu$  is the decay and loss rate for biomass. These can  
325 be from starvation in cases where substrates are depleted or from loss into the aqueous environment.  
326 Lastly,  $\gamma$  is the dimensionless maximum substrate consumption rate. It signifies the ratio of substrate  
327 consumed to biomass growth. Here, a larger  $\gamma$  value results in more substrate being consumed to  
328 produce the same amount of biomass.

329 With (2.16) being reduced to these parameters the numerical analysis become more simplified while  
330 still retaining the same significance in results. From this point on, since  $L$ , the length of the region,  
331 was used for nondimensionalization  $\Omega$  is now the unit square.

332 **Chapter 3**

333 **Numerical Methods**

334 **3.1 Discretization**

335 In order to approximate the solution for (2.16) spatial and temporal discretizations must be made.

336 First the equations are discretized in time,

$$\frac{M^{k+1} - M^k}{\Delta t} = \nabla_x(D(M^{k+1})\nabla_x M^{k+1}) + F(C^{k+1})M^{k+1}, \quad (3.1)$$

$$\frac{C^{k+1} - C^k}{\Delta t} = \frac{1}{2}(G(C^{k+1})M^{k+1} + G(C^k)M^k). \quad (3.2)$$

340 Here, (3.1) follows the ideas of the Backwards Euler Method; (3.2) follows Trapezoidal Rule (Burden  
341 and Faires, 2010). The index variable  $k$  has been introduced in (3.1) - (3.2) such that  $M^k(x) \approx$   
342  $M(t^k, x)$ , allowing an approximation at a certain time,  $t^k$ , to be used; this changes the spatial-temporal  
343 continuum model into a spatial continuum model with discrete temporal time steps.

344 Now, only (3.1) requires spatial considerations since the substrate does not diffuse across the region.  
345 The spatial discretization will be through the Finite Difference Method as described in Saad (2003).  
346 Here, a uniform  $n \times m$  grid is used to discretize  $\Omega$ . Since all the calculations will be done on the grid  
347 intersections the discretization will be grid-point based. This means that a  $n \times m$  grid implies there  
348 are  $(n - 1) \times (m - 1)$  grid boxes. The distance between grid points is the same in both  $x_1$  and  $x_2$

349 dimensions; we have  $\Delta x_1 = \Delta x_2 = \Delta x$ . Since we work on a nondimensionalized domain, and we  
 350 known the number of grid boxes in our region, we have that  $\Delta x = \frac{1}{n-1}$ . A five-point stencil is used  
 351 to approximate the solution of (3.1) at each grid point. This spatial discretization allows the use of  $i$   
 352 and  $j$  to index across the region such that  $x_{1_i} = i * \Delta x$  for  $i \in \{0, 1, \dots, n-1\}$  and  $x_{2_j} = j * \Delta x$  for  
 353  $j \in \{0, 1, \dots, m-1\}$ . To index the grid point,  $i$  and  $j$  are used such that  $M_{i,j}^k \approx M(t^k, x_{1_i}, x_{2_j})$ . To  
 354 account for the dependency on neighbouring grid points, we introduce  $\sigma$  as the index pair from the  
 355 set

$$356 \quad \mathcal{N}_{ij} = \{n_{ij}, e_{ij}, s_{ij}, w_{ij}\} \quad (3.3)$$

357 where,

$$358 \quad \begin{aligned} n_{ij} &= \begin{cases} (i, j+1) & \text{if } j < m \\ (i, j-1) & \text{if } j = m \end{cases} & e_{ij} &= \begin{cases} (i+1, j) & \text{if } i < n \\ (i-1, j) & \text{if } i = n \end{cases} \\ s_{ij} &= \begin{cases} (i, j-1) & \text{if } j > 0 \\ (i, j+1) & \text{if } j = 0 \end{cases} & w_{ij} &= \begin{cases} (i-1, j) & \text{if } i > 0 \\ (i+1, j) & \text{if } i = 0 \end{cases}. \end{aligned} \quad (3.4)$$

359 With  $\mathcal{N}_{ij}$  and  $\sigma$  we can account for the difference in boundary points and interior points. The different  
 360 branches of (3.4) are based on the second order discretisation of the Neumann boundary conditions.

361 The equation for (3.1), after following the spatial discretization for finite-difference method listed in  
 362 Saad (2003), is

$$363 \quad \frac{M_{i,j}^{k+1} - M_{i,j}^k}{\Delta t} = \frac{1}{\Delta x^2} \sum_{\sigma \in \mathcal{N}_{ij}} \left( \frac{D(M_{\sigma}^{k+1}) + D(M_{i,j}^{k+1})}{2} \right) \cdot (M_{\sigma}^{k+1} - M_{i,j}^{k+1}) + F(C_{i,j}^{k+1}) M_{i,j}^{k+1} \quad (3.5)$$

364 For completeness, we spatially discretize (3.2) as

$$365 \quad \frac{C_{i,j}^{k+1} - C_{i,j}^k}{\Delta t} = \frac{1}{2} (G(C_{i,j}^{k+1}) M_{i,j}^{k+1} + G(C_{i,j}^k) M_{i,j}^k). \quad (3.6)$$

366 Notice that for (3.5), the arithmetic mean of the diffusion function,  $D$ , is taken because of the steep  
 367 gradient at the interface. Since this discretization requires  $D(M)$  to be evaluated at points that lie

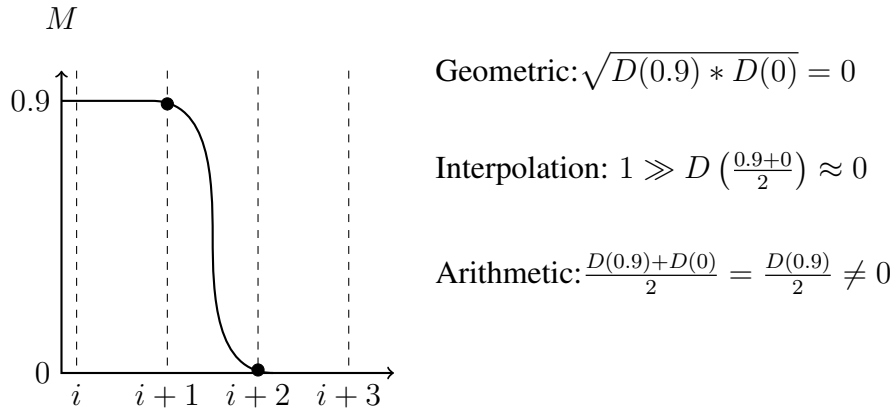


**Figure 3.1:** An illustration of the three methods for approximating the value of  $D(M)$  at ghost points located in between the existing grid points. The two black circles represent the two points in consideration for the calculations of geometric mean, interpolation of values, and arithmetic mean. The problem with Geometric mean is that  $D(0)$  evaluates to 0, resulting in no diffusion effects. With interpolation, the value of  $D(0.45)$  is near-zero because  $M \ll 1 \implies D(M) \approx 0$ . For the arithmetic mean, since  $D(0.9)$  is a larger value than the other methods some spatial diffusion actually work.

368 in between the existing grid points, which do not exist, an approximation is made. Between the  
 369 three common choices for approximating a point (arithmetic mean, geometric mean, and interpola-  
 370 tion) arithmetic mean is the best suited for this situation. This is illustrated in Figure 3.1, where the  
 371 geometric mean and interpolation approximation are shown to result in a zero diffusion term, thus  
 372 stopping the spreading of the biomass. Taking the arithmetic mean eliminates this result because the  
 373 average value of  $D$  would not be zero at the interface.

374 To simplify the spatial indexing, the grid functions are converted into vector functions by use of a  
 375 bijective mapping defined as:

$$\begin{aligned} \pi : \{1, \dots, n\} \times \{1, \dots, m\} &\rightarrow \{1, \dots, nm\} \\ 376 (i, j) &\mapsto \pi(i, j) \end{aligned} \tag{3.7}$$

377 Now, a single index can be used to iterate over the vector,  $l$ . Lexographical ordering is used here  
 378 resulting in a bijective function  $\pi(i, j) = j + (i - 1)m$ . This gives the system,

$$\frac{M_l^{k+1} - M_l^k}{\Delta t} = \frac{1}{\Delta x^2} \sum_{\sigma \in \mathcal{N}_{\pi^{-1}(l)}} \left( \left( \frac{D(M_{\pi(\sigma)}^{k+1}) + D(M_l^{k+1})}{2} \right) \cdot (M_{\pi(\sigma)}^{k+1} - M_l^{k+1}) \right) + F(C_l^{k+1}) M_l^{k+1} \tag{3.8}$$

$$\frac{C_l^{k+1} - C_l^k}{\Delta t} = \frac{1}{2} (G(C_l^{k+1}) M_l^{k+1} + G(C_l^k) M_l^k). \tag{3.9}$$

### 382 3.2 Solution Technique

383 Assuming the values for  $C$  and  $M$  at time level  $k$  are known, (3.8) and (3.9) are a coupled system  
 384 of  $2nm$  highly nonlinear equation for  $2nm$  unknown  $M_l^{k+1}, C_l^{k+1}$ . To solve this coupled system, we  
 385 define a fixed point iteration which we apply to (3.8) and (3.9). In a single time step, the solutions for  
 386  $M$  and  $C$  can be solved using the previous time step solution in the follow manner:

$$\frac{M_l^{(p+1)} - M_l^k}{\Delta t} = \frac{1}{\Delta x^2} \sum_{\sigma \in \mathcal{N}_{\pi^{-1}(l)}} \left( \frac{D(M_{\pi(\sigma)}^{(p)}) + D(M_l^{(p)})}{2} \right) \cdot (M_{\pi(\sigma)}^{(p+1)} - M_l^{(p+1)}) + F(C_l^{(p)}) M_l^{(p+1)} \quad (3.10)$$

$$\frac{C_l^{(p+1)} - C_l^k}{\Delta t} = \frac{1}{2} (G(C_l^{(p+1)}) M_l^{(p+1)} + G(C_l^k) M_l^k) \quad (3.11)$$

390 where  $(p) \in (0, 1, 2, \dots)$ ,  $(p+1)$  is the next iteration solution fo  $p$ , and  $k$  is the solution of the previous  
 391 timestep. An initial guess is made such that,

$$392 M_l^{(p)} := M_l^k, \quad C_l^{(p)} := C_l^k. \quad (3.12)$$

393 The fixed-point iteration is stopped when convergence is achieved. This is when the difference be-  
 394 tween consecutive iterations is below a selected tolerance, i.e.

$$395 \sum_{l=1}^{nm} \left( |M_l^{(p+1)} - M_l^{(p)}| + |C_l^{(p+1)} - C_l^{(p)}| \right) < tol. \quad (3.13)$$

396 At the end of the fixed-point iteration, the number of iterations is recorded as  $P$ , and we define,

$$397 M_l^{k+1} := M_l^{(P)}, \quad C_l^{k+1} := C_l^{(P)}. \quad (3.14)$$

398 In this fixed point format, given by (3.10) - (3.11), the equations can be rearranged and solved by  
 399 conventional methods.

400 In each iteration step, (3.10) is a simultaneous linear system for the  $nm$  unknown  $M_l^{(p+1)}$ . From this  
 401 a linear system of equations can be created following Saad (2003).

402 From (3.10), we get the matrix equation:

403

$$A^{(p)} M^{(p+1)} = \frac{1}{\Delta t} M^k. \quad (3.15)$$

404 Here,  $A^{(p)}$  is a five-diagonal  $nm \times nm$  matrix, defined as

405

$$A^{(p)} = \begin{bmatrix} a_{1,1} & a_{1,2} & & a_{1,m} & & \\ a_{2,1} & \ddots & \ddots & \ddots & \ddots & \\ a_{n,1} & \ddots & \ddots & \ddots & \ddots & \\ & \ddots & \ddots & \ddots & \ddots & \\ & & & a_{nm,nm-m} & a_{nm,nm-1} & a_{nm,nm} \\ & & & & a_{nm-n,nm} & a_{nm-1,nm} \end{bmatrix} \quad (3.16)$$

406 where each  $a_{i,j}$  is the coefficient for specific grid indices based on (3.10).

407 **Proposition 3.2.1.** If  $\Delta t < \left(F(C_l^{(p)})\right)^{-1}$  then the matrix  $A$  is positive definite and symmetric.

408 *Proof.* Matrix  $A$  is positive definite if all the eigenvalues are positive. Using the Gershgorin's Circle theorem described by Varga (2004), the eigenvalues can be shown to be positive. Gershgorin's Circle theorem tells us that each eigenvalue must be contained in the union of all Gershgorin's discs (Varga, 2004). There exist one disc for each row of  $A$ , with radius equal to the sum of the off-diagonals and center equal to the value of the main diagonal. By showing that, independently on all rows, the sum of the off-diagonals values is less than the diagonal value we have that all the Gershgorin's discs must be in the positive region when the main diagonal is positive. This can be shown by manipulating (3.10) for just the main diagonal element,

416

$$\sum_{\sigma \in \mathcal{N}_{\pi^{-1}(l)}} \left( \left( \frac{D(M_{\pi(\sigma)}^{(p)}) + D(M_l^{(p)})}{2\Delta x^2} \right) - F(C_l^{(p)}) + \frac{1}{\Delta t} \right) M_l^{(p+1)} \quad (3.17)$$

<sup>417</sup> and for just the off-diagonal elements,

$$\sum_{\sigma \in \mathcal{N}_{\pi^{-1}(l)}} \left( \left( \frac{D(M_{\pi(\sigma)}^{(p)}) + D(M_l^{(p)})}{2\Delta x^2} \right) M_{\pi(\sigma)}^{(p+1)} \right). \quad (3.18)$$

<sup>419</sup> Comparing the coefficients to the vector elements in (3.17) - (3.18) results in the inequality necessary  
<sup>420</sup> for Gershgorin's Circle theorem.

$$\left| \sum_{\sigma \in \mathcal{N}_{\pi^{-1}(l)}} \frac{D(M_{\pi(\sigma)}^{(p)}) + D(M_l^{(p)})}{2\Delta x^2} \right| < \left| \sum_{\sigma \in \mathcal{N}_{\pi^{-1}(l)}} \left( \frac{D(M_{\pi(\sigma)}^{(p)}) + D(M_l^{(p)})}{2\Delta x^2} \right) - F(C_l^{(p)}) + \frac{1}{\Delta t} \right| \quad (3.19)$$

<sup>422</sup> This simplifies to,

$$\Delta t < \left( F(C_l^{(p)}) \right)^{-1} \quad (3.20)$$

<sup>424</sup> When this inequality is true, we have that the off-diagonals are smaller than the main diagonal and  
<sup>425</sup> the main diagonal values are positive thus Gershgorin's Circle theorem says that the eigenvalues are  
<sup>426</sup> all positive. Therefore we have positive definite when (3.20) is true.

<sup>427</sup> The symmetry of  $A$  can be trivially shown if one considers the formation of the diagonals. On a  
<sup>428</sup> single row, each element corresponds to the adjacent grid points of grid  $l$ . As the grid ordering counts  
<sup>429</sup> along, the elements that are equi-distance from the diagonal actually reference the same grid point.  
<sup>430</sup> Therefore we have symmetry.  $\square$

<sup>431</sup> It is important to remark that the time-step constraint in Proposition 3.2.1 is not a severe constraint,  
<sup>432</sup> practically. The condition,  $\frac{1}{F(C)} < \Delta t$ , relates the growth of the biomass to the size of time step  
<sup>433</sup> selected. In order to resolve any biomass growth,  $\Delta t$  must obviously be chosen smaller than the  
<sup>434</sup> characteristic time scale of growth,  $\frac{1}{F(C)}$ .

<sup>435</sup> Given that  $A$  is positive definite and symmetric, the conjugate gradient method can be used to compute  
<sup>436</sup> the solution.

<sup>437</sup> **Proposition 3.2.2.** *The matrix  $A$  is diagonally dominant when  $\Delta t < \left( F(C_l^{(p)}) \right)^{-1}$ .*

438 *Proof.* This is trivially shown to be true when one considers (3.19). It was shown that this simplifies  
439 to

$$\Delta t < \left( F(C_l^{(p)}) \right)^{-1} \quad (3.21)$$

441 This means that when the above is true the diagonal elements of  $A$  will be strictly larger than the sum  
442 of off-diagonals. Therefore we have diagonal dominance.  $\square$

443 Since we have  $A$  positive definite, symmetric, and diagonally dominant we know that  $A$  is an M-  
444 matrix. This is important because this ensures that if  $M^k$  is non-negative we have that  $M^{(p)}$  is also  
445 non-negative.

446 For solving (3.11), the equation can be rearranged into a quadratic form, substituting in  $G(C)$  from  
447 (2.18)

$$(C^{(p+1)})^2 + \left( \kappa - C^k + \frac{\Delta t}{2} \gamma M^{(p+1)} + \frac{\Delta t}{2} \frac{\gamma C^k M^k}{\kappa + C^k} \right) C^{(p+1)} + \left( -\kappa C^k + \frac{\Delta t}{2} \frac{\gamma \kappa C^k M^k}{\kappa + C^k} \right) = 0. \quad (3.22)$$

449 Using the quadratic equation results in,

$$C^{(p+1)} = \frac{-b \pm \sqrt{b^2 - 4c}}{2} \quad (3.23)$$

451 for which,

$$\begin{aligned} b &= \kappa - C^k + \frac{\Delta t}{2} \gamma M^{(p+1)} + \frac{\Delta t}{2} \frac{\gamma C^k M^k}{\kappa + C^k} \\ c &= -\kappa C^k + \frac{\Delta t}{2} \frac{\gamma \kappa C^k M^k}{\kappa + C^k} \end{aligned} \quad (3.24)$$

453 Unless  $b^2 - 4c = 0$ , we have two different solutions to  $C^{(p+1)}$ . The problem with that is that if both  
454 solutions are positive we have two valid values to be used. Here, we can show that there will always  
455 be only one positive solution.

456 **Proposition 3.2.3.** *The quadratic equation defined as (3.22) will always have one positive solution  
457 and one negative solution for non-zero parameter choices.*

458 *Proof.* For the duration of this proof, we let  $C := C^{(p+1)}$  to make equations easier to read. Rearrang-  
 459 ing (3.22) so that all the  $\Delta t$  terms are on the right-hand-side, we get

460 
$$(C)^2 + (\kappa - C^k) C - \kappa C^k = \left( \frac{\gamma C^k M^k}{2(\kappa + C^k)} - \left( \frac{\gamma M^{(p+1)}}{2} - \frac{\gamma C^k M^k}{2(\kappa + C^k)} \right) C \right) \Delta t. \quad (3.25)$$

461 To simplify the notation, we let  $\bar{a} := \frac{\gamma M^{(p+1)}}{2} - \frac{\gamma C^k M^k}{2(\kappa + C^k)}$  and  $\bar{b} := \frac{\gamma C^k M^k}{2(\kappa + C^k)}$ .

462 We analyze both the left-hand-side and right-hand-side independently by letting  $f_l = (C)^2 + (\kappa - C^k) C -$   
 463  $\kappa C^k$  and  $f_r = (\bar{b} - \bar{a}C) \Delta t$ .  $f_l$  is a quadratic equation with positive concavity everywhere and  $C$ -  
 464 intercept at  $-\kappa C^k < 0$ .  $f_r$  is a line with a slope opposite to the sign of  $\bar{a}$  and has  $C$ -intercept at  
 465  $\bar{b} \Delta t > 0$ .

466 There exist four cases here, each visualized in Figure 3.2 It is clear that since the  $f_l$  is a quadratic  
 467 function and  $f_r$  is a linear function we have that  $f_l$  will attain a larger value at some value of  $C$ .  
 468 Since  $f_l$  is quadratic we know there can only exist two intersections between  $f_l$  and  $f_r$ . Because we  
 469 always have  $f_r(0) > f_l(0)$ , we can show, using the intermediate value theorem that there must exist  
 470 a intersection for both  $C > 0$  and  $C < 0$ . This means that we have exactly one positive solution and  
 471 one negative solution since there is a maximum of two intersections. □

472 To determine which branch of (3.23) to use, we look at the function logically. If we know that one  
 473 positive solution will always exist then the only branch for that to occur is the positive branch. This is  
 474 because the square root term,  $\sqrt{b^2 - 4c}$  will never be negative. The addition of two negative numbers  
 475 cannot result in a positive solution therefore the positive branch must be used for the positive solution  
 476 that we desire.

477 Now that computable solutions for  $M$  and  $C$  at a single time step have been found, an algorithm to  
 478 solve for the next time step can be established. Algorithm 1 shows the organization of solving (3.11 -  
 479 3.10).

480 Note that Algorithm 1 actually describes both a fully-implicit and a semi-implicit method for solving  
 481 (2.16). Recall that the final number of iterations is recorded as  $P$ , if  $P = 1$  then only a single iteration

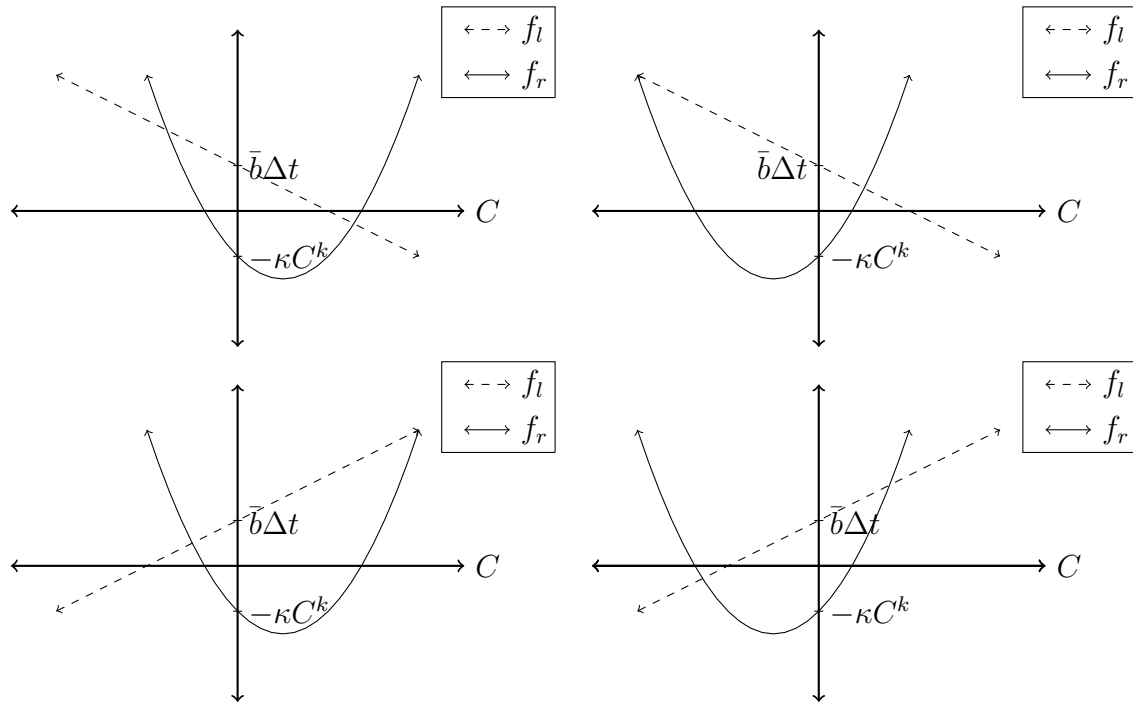


**Figure 3.2:** Graph of  $f_l = (C^2 + (\kappa - C^k)C - \kappa C^k)$  and  $f_r = (\bar{b} - \bar{a}C)\Delta t$  for all four possible cases. Notice that because  $-\kappa C^k < 0$  and  $\bar{b}\Delta t > 0$  for all realistic parameter values the two functions will always intersect in the positive  $C$  region. The top left graph is for  $\bar{a} > 0$  and  $\kappa - C^k < 0$ . The top right graph is for  $\bar{a} > 0$  and  $\kappa - C^k > 0$ . The bottom left graph is for  $\bar{a} < 0$  and  $\kappa - C^k < 0$ . The bottom right graph is for  $\bar{a} < 0$  and  $\kappa - C^k > 0$ .

**Data:**  $M^k, C^k$  are vectors with values from the previous time step and  $p = 0$ .

**begin**

```

    Let  $M^{(p=0)} = M^k$  and  $C^{(p=0)} = C^k$ ;
    while Convergence is not achieved do
        | Solve  $A^{(p)}M^{(p+1)} = \frac{1}{\Delta t}M^{(p)}$ ;
        | Solve  $C^{(p+1)} = \frac{1}{2}(b \pm \sqrt{b^2 - 4c})$ ;
        | Check convergence, (3.13);
        | Let  $p = p + 1$ ;
    end
    Let  $P := p$ ;
    Let  $M^{(k+1)} = M^{(P)}$  and  $C^{(k+1)} = C^{(P)}$ ;
end

```

**Algorithm 1:** Algorithm for the fully-implicit solving of (2.16)

482 of the algorithm is applied, which correlates to the behaviour of the semi-implicit method. This can be  
 483 produced by selecting a sufficiently large enough tolerance so that the convergence check, (3.13), is  
 484 always resolved after the first iteration. The resulting semi-implicit method is effectively the method  
 485 described in Sirca and Horvat (2012), which was first introduced in Eberl and Demaret (2007).

486 **3.3 Computational Setup**

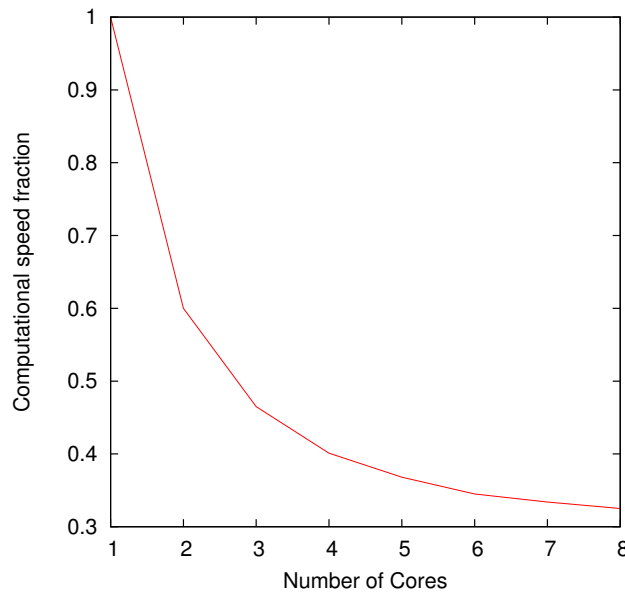


**Figure 3.3:** A graph showing the computation speed of simulations run with different number of cores. The  $y$ -axis represents the fraction of time each core has in comparison to the 1-core result. The simulation is the same setup as the travelling wave simulation that is defined in the next section. The simulation was stopped at  $t = 2$  and was run with a grid of  $2049 \times 2049$ .

487 The implementation of Algorithm 1 was done with Fortran. The system matrix  $A$  in (3.16) is stored  
 488 in the sparse data format called Compressed Diagonal Storage (CDS) (Barrett et al., 1987). For each  
 489 iteration step the linear system is solved using the Conjugate Gradient method (Saad, 2003).  
 490 All the computations were run on a custom built workstation with an Intel Xeon CPU E5-2650 (1.2  
 491 GHz, 20MB cache size) and 32 GB RAM under Red Hat Enterprise Linux Server release 6.5 (Santi-  
 492 ago). Running the computations with OpenMP, took advantage of 4 out of the 16 threads of the Intel  
 493 Xeon CPU, with 2 threads to each core. The choice of 4 cores is that the computational gain for each  
 494 additional core becomes less significant after 4, as shown in Figure 3.3. The GNU Fortran compiler,

495 version 4.4.7, was used for all computations; the compiler arguments were

496 `-O3 -fdefault-real-8 -fopenmp`

## 497 3.4 Method Validation

498 With a defined method and computational setup we assess the behavior and accuracy of the method in  
 499 a variety of simulations. An examination of a typical simulation will show if the expected behaviour is  
 500 observed. A convergence analysis for the method can be done to confirm that solutions from different  
 501 grid sizes approach a single solution as they become more precise. This convergence test will also  
 502 show the thresholds for an accurate simulation result, to help reduce the computation times. Once the  
 503 fully-implicit method has been tested, it can be compared against the semi-implicit method.

### 504 3.4.1 Basic Simulations

505 Using Algorithm 1, simple scenarios can be tested as a first verification on the method.

506 A simple test would be to check if the spatial discretization can preserve specific characteristics of the  
 507 solutions. One example of this would be seeing if a 1D initial condition could be preserved as time  
 508 progresses. Having all of the biomass on one boundary of  $\Omega$ , for example across the  $y$ -axis, would  
 509 qualify as a 1D initial condition. These initial conditions will be defined as:

$$510 M(0, x, y) = \begin{cases} -\left(\frac{h}{d^4}\right)x^4 + h & , \text{if } y \leq d \\ 0 & , \text{otherwise} \end{cases} \quad (3.26)$$

$$C(0, x, y) = 1$$

511 where  $h = 0.1$  and  $d = \frac{5}{128}$ . Here,  $h$  and  $d$  represent the height and depth of the inoculation site.

512 The solution shown in Figure 3.4 shows that the 1D characteristic of the biomass stays at a later time.

513 Another characteristic to observe would be if a spherical initial condition remains spherical. Using

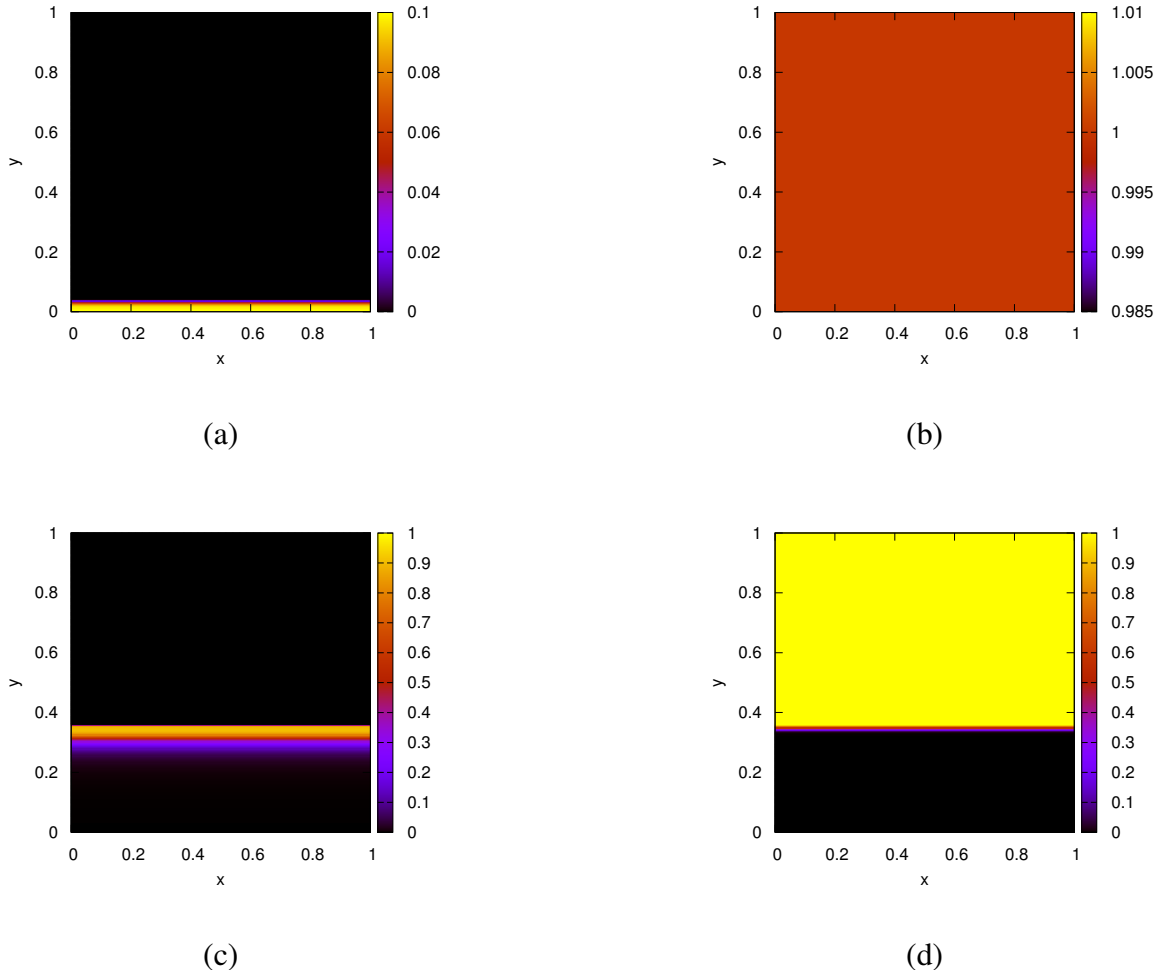


**Figure 3.4:** Solutions for (ac)  $M$  and (bd)  $C$  with 1D initial conditions defined in (3.26) at (ab)  $t = 0$  and (cd)  $t = 40$ . Computed with a  $1025 \times 1025$  grid and a time step of  $\Delta t = 10^{-3}$ .

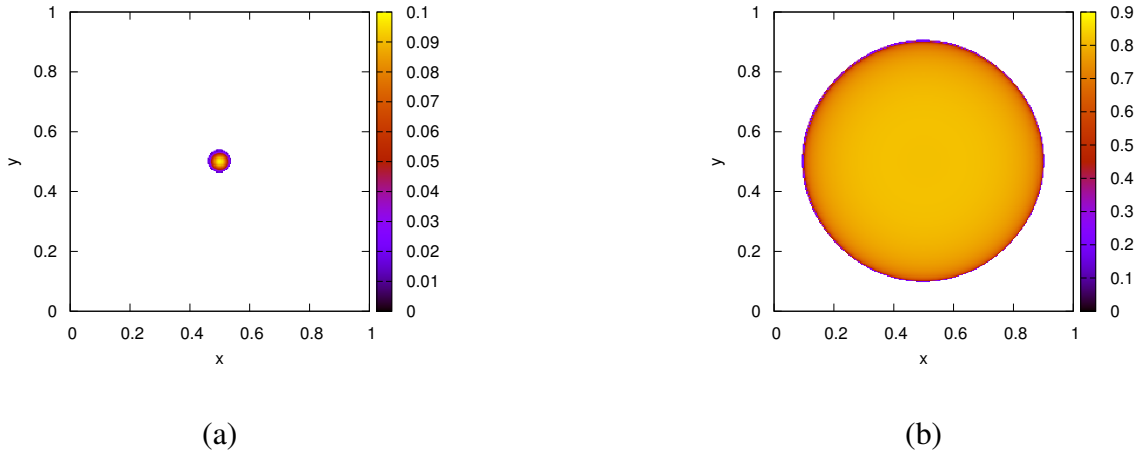


**Figure 3.5:** Solutions for  $M$  with spherical initial conditions defined by (3.27) at (a)  $t = 0$  and (b)  $t = 40$ . Computed with a  $1025 \times 1025$  grid and a time step of  $\Delta t = 10^{-3}$ .

514 initial conditions for the biomass,

$$515 \quad M(0, x, y) = \begin{cases} -\frac{h}{d^2} ((x - 0.5)^2 + (y - 0.5)^2) + h & , \text{if } (x - 0.5)^2 + (y - 0.5)^2 < d^2 \\ 0 & , \text{otherwise} \end{cases}, \quad (3.27)$$

516 a test can be tried to see if the spherical nature of the solution is kept as time progresses. We still have  
 517  $C(0, x, y) = 0$  here. The solution shown in Figure 3.5 shows that the spherical shape of the solution  
 518 is maintained at later times.

519 Both Figure 3.4 and Figure 3.5 increase the confidence that the spatial discretization did not introduce  
 520 any loss of characteristics for the solutions.

521 The global mass conservation may be lost from possible sources or sinks of biomass caused by the  
 522 implementation. To ensure this is not the case, the total amount of biomass can be used to compare  
 523 the simulated amount against the theoretical amount. However, the total biomass cannot be exactly  
 524 determined with the given growth rate function. This means that there will not be anything to measure  
 525 the validity of the simulation solution against. If we let the growth rate be some constant,  $a$ , the exact  
 526 total biomass can be calculated.

527 The expected total biomass,  $T_M(t)$ , can be found by using the divergence theorem and integrating  
 528 over the region from equation (2.1) with  $F(C) = a$ ,

$$\begin{aligned}
 \frac{\partial M}{\partial t} &= \nabla_x(D(M)\nabla_x M) + aM \\
 \implies \int_{\Omega} \frac{\partial M}{\partial t} dA &= \int_{\Omega} (\nabla_x(D(M)\nabla_x M)) + aM dA \\
 \implies \int_{\Omega} \frac{\partial M}{\partial t} dA &= \int_{\partial\Omega} (D(M)\nabla_n M \cdot n) dA + \int_{\Omega} aM dA \\
 \implies \int_{\Omega} \frac{\partial M}{\partial t} dA &= \int_{\partial\Omega} (\nabla_x(D(M)(0) \cdot n)) + \int_{\Omega} aM dA \\
 \implies \frac{\partial}{\partial t} \int_{\Omega} M dA &= a \int_{\Omega} M dA \\
 &\text{Let } T_M = \int_{\Omega} M dA \\
 \implies \frac{\partial T_M}{\partial t} &= aT_M \\
 \implies T_M(t) &= T_M(0)e^{at}
 \end{aligned} \tag{3.28}$$

530 Numerically, this is computed by grid-wise summation,

$$531 T_M(t^k) \approx T_M^k = \frac{\sum_i^n \sum_j^m M_{i,j}^k}{nm}. \tag{3.29}$$

532 The simulation setup used will be analogous to that used for Figure 3.5. The one difference will be  
 533 that the simulation here is ran for a longer time to allow the biomass to diffuse along the boundary,  
 534 showing the boundary effects.

535 From Figure 3.6 we can see that the total biomass only differs between the computed value and the  
 536 theoretical value by a relative error less than 0.003. The cases where the error becomes significant are  
 537 from the region being completely filled with biomass, at which point diffusion is no longer possible.  
 538 The error fluctuates violently here because of this. This suggests that the method does not introduce  
 539 any significant sources or sinks of biomass at the boundary of the region.

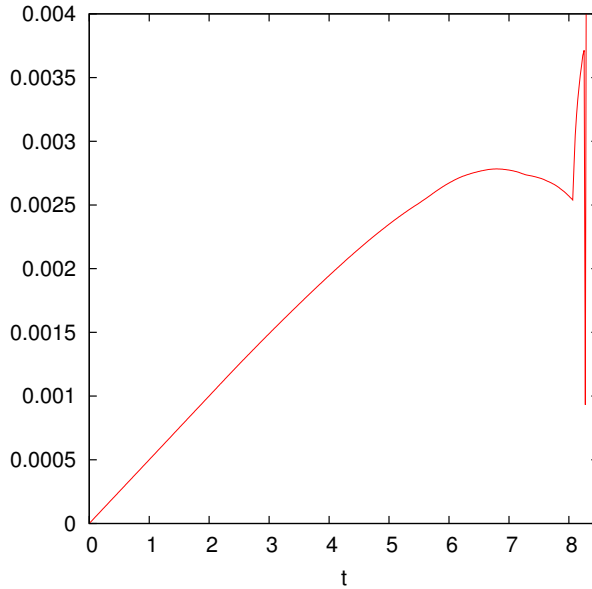


**Figure 3.6:** Plot of the relative error,  $\frac{|f_1 - f_2|}{|f_2|}$ , between the computed total biomass,  $f_1 = T_M(t)$ , and the theoretical total biomass,  $f_2 = y_0 e^x$ . The changes after  $t = 8$  are from the biomass having completely filled the region  $\Omega$ . This means that there is no physical space for the biomass to occupy and thus the growth slows down to a stop.

540 **3.4.2 Convergence Analysis**

541 To validate the accuracy of the method, convergence analyses on the spatial discretizations will need  
 542 to be made. Then the comparison between the semi- and fully-implicit method established in Algo-  
 543 rithm 1 can investigated. First, a metric must be formed to enable consistent comparisons between  
 544 different simulation solutions. This metric will be referred to as the normed difference. Only  $M$  will  
 545 be considered for the normed difference calculations. This is because  $C$  depends on  $M$  and including  
 546 it does not qualitatively change the results.

547 **3.4.2.1 Normed Difference Computations**

548 The normed difference is computed by taking the relative normed-difference between two solution in  
 549 the following fashion:

550 
$$\epsilon_{sol} = \frac{\|u_1 - u_2\|}{\|u_2\|} \quad (3.30)$$

551 where  $u_1$  represents one simulation solution and  $u_2$  references the solution that is expected to be  
 552 more accurate. The theoretical accuracy of  $u_2$  derives from the fact that most comparisons will be

553 done between solutions where one is trivially expected to be more precise. For our purposes, the  
 554 solutions we compare will typically vary in only  $\Delta x$  or between semi- and fully- implicit. These are  
 555 understood to have the relation that a smaller  $\Delta x$ , and that the fully-implicit method with the highest  
 556 tolerance is to be more accurate. There is an assumption that both  $u_1$  and  $u_2$  have the same number  
 557 of grid points, so that the difference can be taken grid-wise. In the case where there are difference  
 558 between the number of grid points of  $u_1$  and  $u_2$ , the coarser grid point refinement is for both  $u_1$  and  
 559  $u_2$ . This is done by projecting the finer grid onto the coarser grid.

560 The results of the normed difference computations, named  $\epsilon_{sol}$ , is a numerical value for the difference  
 561 between two solutions. This depends on the norm used during the computations. Here three norms  
 562 will be used:

$$563 \quad \ell_1 : \|u\|_1 = \frac{1}{nm} \sum_i^{nm} |u_i| \quad (3.31)$$

$$564 \quad \ell_2 : \|u\|_2 = \sqrt{\frac{1}{nm} \sum_i^{nm} (u_i)^2} \quad (3.32)$$

$$566 \quad \ell_\infty : \|u\|_\infty = \max_{i=1,\dots,nm} |u_i| \quad (3.33)$$

568 These different norms will all be used to create a broader understanding of the normed difference.  
 569 This creates three distinct values for  $\epsilon_{sol}$ , named  $\epsilon_{\ell_1}$ ,  $\epsilon_{\ell_2}$ , and  $\epsilon_{\ell_\infty}$ ; each named for the norm used  
 570 during the computation. Note that these norms are for the vector of the solution, through the use of  
 571 the grid-ordering  $\pi(i, j)$ .

### 572 3.4.2.2 Grid Size Convergence

573 To observe the validity of the method, a test on the convergence of solutions based on the spatial  
 574 discretization is done. This will involve using the same simulation described in (3.26) due to the  
 575 simplicity.

576 The convergence will be tracked with only two forms of  $\epsilon_{sol}$ ;  $\epsilon_1$  and  $\epsilon_2$ . This is because the value of  
 577  $\epsilon_\infty$  does not vary with the grid size, since the wave front has a steep interface and tends to lead to

	$s(n) = 2^n + 1$				
	1	2	3	4	5
$n = 2$	+	+	+	+	+
$n = 3$	+	+	+	+	+

**Figure 3.7:** Visualization in 1D to illustrate the choice of  $s(n) = 2^n + 1$  instead of  $2^n$  for the grid size selection. Here it can be seen that successive grid size selections using  $s(n)$  line up on certain grid points and when using  $2^n$  no grid points are equivalent.

578 inconsistent changes in normed difference. Since the use of  $\epsilon_\infty$  is not a suitable method for measuring  
 579 the normed difference, the inconsistency does not suggest an invalidity with the method. Because of  
 580 the difference in the number of grid points between different solutions,  $u_1$  and  $u_2$ , only the grid points  
 581 in the coarser refinement will be used. This places a limitation on the selection of grid-sizes since  
 582 there must be some grid points locations that are the same for two different chosen grid sizes. For  
 583 this purpose, we define the function  $s(n) = 2^n + 1$  for  $n \in \mathbb{N}$  to be used as the grid size selection  
 584 function. Now certain grid points will match without the use of linear interpolation, as illustrated in  
 585 Figure 3.7.

586 Using the same simulation setup as was done in Figure (3.4), solutions resulting from different grid  
 587 sizes based on  $s(n)$  are computed for  $n = 5, 6, \dots, 12$ . In this case, when calculating  $\epsilon_{sol} = \frac{|u_1 - u_2|}{|u_2|}$ ,  
 588 we let  $u_1$  be the grid size under investigation and  $u_2$  be the solutions of the most refined grid size,  
 589  $n = 12$ . This would show the converging solutions for smaller grid sizes because the change to the  
 590 finest grid size will be monotonically decreasing.

591 The results from Figure 3.8 show that the solutions converge as the grid size become refined with the  
 592 grid size.

### 593 3.5 Comparison of Semi-implicit and Fully-implicit Method

594 We are now in a position to compare the fully-implicit time-integration scheme that we introduced  
 595 here with the semi-implicit time-integration that has been used for problems with a diffusive substrate  
 596 in the literature (Khassehkhan et al., 2009). Recall that the semi-implicit method is a special case

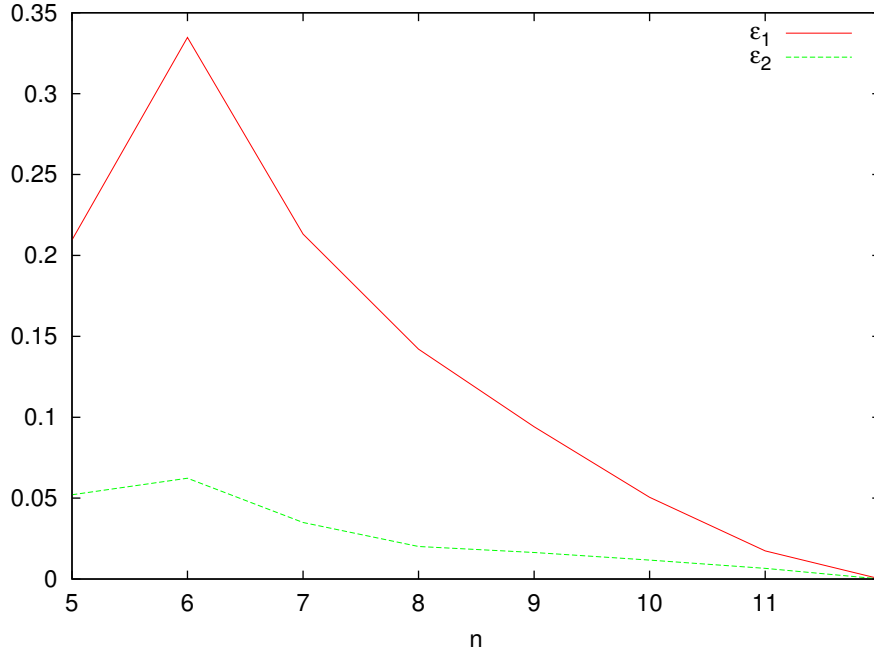


**Figure 3.8:** Plot showing the convergence of solutions based on changes in  $\Delta x$ . The computations are of  $\epsilon_{\ell_1}$  and  $\epsilon_{\ell_2}$  with grid-size following  $s(n) = 2^n + 1$ .

597 of the fully-implicit method if the non-linear iteration is stopped after one step. This can be forcibly  
 598 achieved, for example, by choosing a very large tolerance threshold for the non-linear iteration.

599 The simulation used is the same as described in (3.4) and is stopped at  $t = 40$ . The comparison will  
 600 be on multiple metrics: the average number of iterations of Algorithm 1, the value of  $\epsilon_1$  and  $\epsilon_2$ , the  
 601 computation time of the simulation, and the height of the wave peak.

602 The average number of iterations are tracked so that the amount of work done for each tolerance can  
 603 be better quantified. It is based on the average number of iterations of the fully-implicit method taken  
 604 over all the times steps, from  $t = 0$  to the current  $t$ . This value is used since it represents the number  
 605 of iterations in a way that is easy to read and understand. As the tolerance decreases the amount of  
 606 iterations the algorithm must perform will increase, the degree of increase will help relate the amount  
 607 of work.

608 The value of  $\epsilon_1$  and  $\epsilon_2$  act as a measure of accuracy. Here, these values quantify the difference between  
 609 the solution of the semi-implicit method (Recall, Tol. =  $1.0e - 0$ ) which is  $u_1$  and the solution of  
 610 the fully-implicit method for different tolerances as  $u_2$ . This results in a relative difference from the

611 semi-implicit method and would show the change in solution as the tolerance decreases. Each row of  
 612 Table 3.1 refers to the  $u_1$  values used in the comparison. Each difference was taken at the last time  
 613 step.

614 Along with accuracy, the simulation time is tracked. This is because it represents another metric for  
 615 which the viability of the fully-implicit method can be verified. Intuitively there should be a decrease  
 616 in the normed difference with the fully-implicit method as the value for  $tol$  decreases. Therefore, this  
 617 needs to be weighted against the cost of computational intensity and the increase of the simulation  
 618 time.

619 The location of the wave peak is a tracked quality of the solution that reveals how consistent the  
 620 results are. The wave peak is described here as the maximum value of the solution at the final time  
 621 step calculated. The ultimate goal is that the simulation solutions be converging towards the exact  
 622 solution. To see this here the  $x$ -coordinate of the wave peak is tracked as well as the height of the  
 623 wave peak.

624 The results of the method comparison can be seen in Table 3.1.

Tol.	Avg. Iter.	$\epsilon_1$	$\epsilon_2$	Time	Wave Height
1.0e-0	1.0000	0.000000000000	0.000000000000	12.1830	0.96366123
1.0e-1	1.0000	0.000000000000	0.000000000000	12.2080	0.96366123
1.0e-2	1.0000	0.000000000428	0.000000000167	12.3379	0.96366123
1.0e-3	1.0000	0.000000000428	0.000000000167	12.2310	0.96366123
1.0e-4	1.0000	0.000000001098	0.000000000329	12.3200	0.96366123
1.0e-5	1.9650	0.002573969658	0.001066499658	18.9869	0.96391491
1.0e-6	2.0000	0.002574057907	0.001066505860	19.0910	0.96391479
1.0e-7	2.0018	0.002573959764	0.001066498736	19.0940	0.96391492
1.0e-8	2.5856	0.002577916965	0.001066781565	20.5169	0.96390966
1.0e-9	2.9012	0.002577461054	0.001066759099	21.3080	0.96390979
1.0e-10	3.2278	0.002581334868	0.001067029069	22.2280	0.96390490
1.0e-11	16.0990	0.002632955188	0.001070709373	57.5589	0.96383105
1.0e-12	36.3184	0.002647234923	0.001071748013	113.9940	0.96380854
1.0e-13	57.6812	0.002648733848	0.001071857564	173.8489	0.96380614

**Table 3.1:** Results from running simulations with different Tol.

625 There are a number of observations that can be made from these results.

- 626     ● A direct relationship between computation time and average number of iterations exists.
- 627     ● There is no significant difference between solutions unless the tolerance is set high enough to  
628       force multiple iterations. This means the semi-implicit method results in a tolerance between  
629        $10^{-4}$  and  $10^{-5}$  as any smaller tolerance does not require additional iterations.
- 630     ● The differences in Wave Height are a result of additional iterations and monotonically approach  
631       a specific value as the tolerance becomes smaller.
- 632     ● The greatest gain in accuracy while weighing the increased computation time is from a tolerance  
633       around  $10^{-5}$  at which point only one extra iteration is completed.
- 634     ● The main takeaway is that the semi-implicit method results in 4 digits of accuracy and when a  
635       second iteration is forced (from additional tolerance) a 5<sup>th</sup> digit is gained for the 50% increase  
636       in computation time.
- 637     ● After 36 iterations a 6<sup>th</sup> digit of accuracy is gained for a 900% increase in computation time.

638 **Chapter 4**

639 **Simulation Results**

640 **4.1 Typical Simulation**

641 A typical simulation refers to the parameter values and the choice of initial condition. It will show  
642 the behaviour of the system under normal circumstances and help reveal interesting characteristics.

643 The typical initial condition attempts to emulate the biological situation of biomass growing inwards  
644 on a sheet of cellulose. This will show how the biomass moves and how two separate masses interact  
645 when merging. The initial condition used will initialize a number of random spherical inoculation  
646 points near the  $y = 0$  and  $y = 1$  axis. We let  $(x_r, y_r)$  be the random point used as the center for  
647 inoculation. To separate the inoculation points we have  $x_r \in [0, 1]$  and  $y_r \in [0, 0.1] \cup [0.9, 1]$ . The  
648 number of inoculation points are the same for both the  $y = 0$  region and  $y = 1$  region. Multiple  
649 inoculation points combine additively. Each spherical inoculation point is computed as,

650 
$$M(0, x, y) = \frac{-h}{d^2} ((x - x_r)^2 + (y - y_r)^2) + h, \quad M \geq 0. \quad (4.1)$$

651 Note that  $M(0, x, y)$  is for points within circles of radius  $d$  centered at  $(x_r, y_r)$ , otherwise  $M(0, x, y) =$   
652 0. For the substratum we have  $C(0, x, y) = 1$  everywhere.

653 The choice of parameter value is based on the default values given in Table A.1. There are 40 inocu-

654 lation points on each side, totalling 80. The fully-implicit method is used here with  $tol = 10^{-8}$ .

655 **4.1.1 Biomass Ratio**

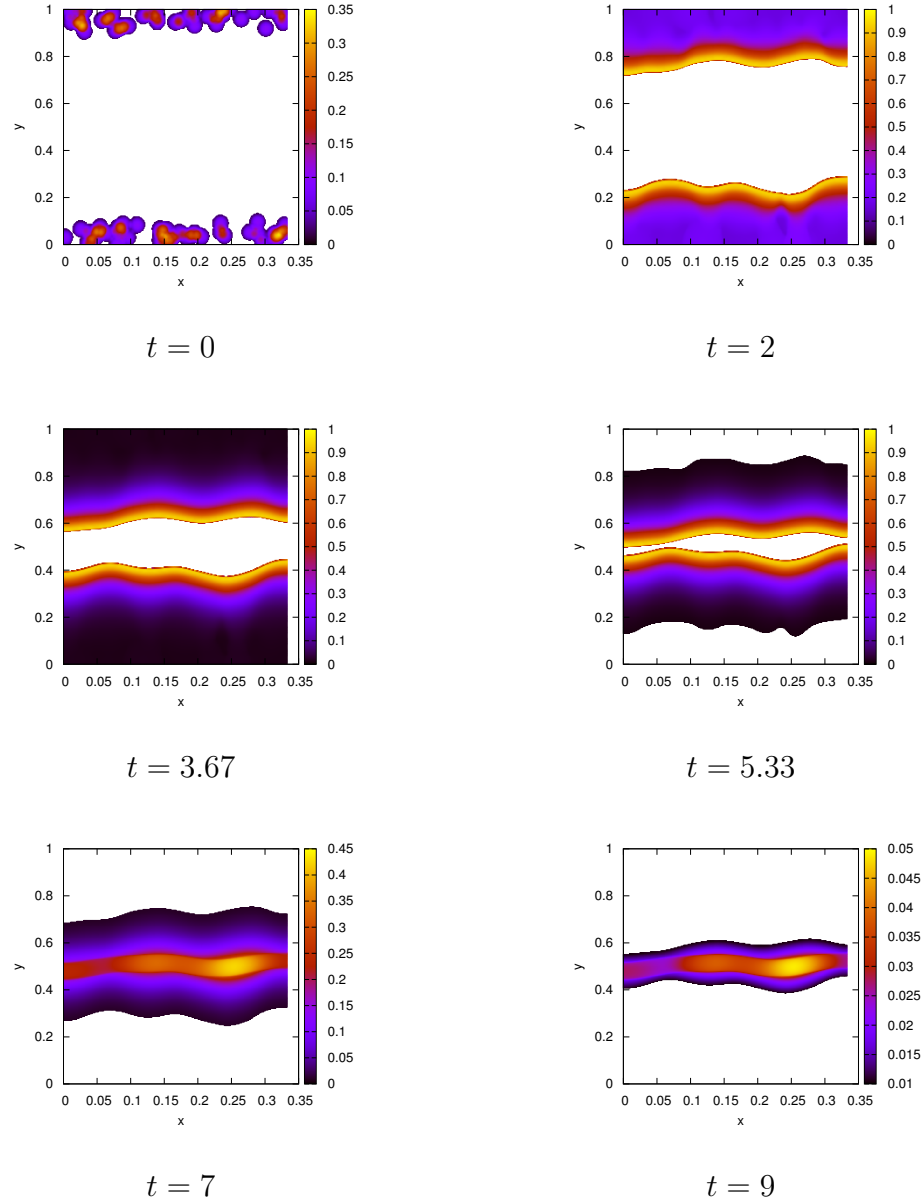


**Figure 4.1:** A graph showing the  $M$  solution of a typical simulation at different time steps. The initial condition is 80 random spherical inoculation points evenly divided between each of the  $y = 0$  and  $y = 1$  sides. A  $513 \times 513$  grid was used.

656 Figure 4.1 shows the time evolution of  $M$  for the simulation. Here, the random inoculations on both  
657 sides of the region propagate towards each other and eventually combine at the center. By looking at

658  $t = 2$ ,  $t = 3.67$ , and  $t = 5.33$  it appears as though the wave front is moving with a constant shape and  
 659 at a constant speed. This suggest that there may be the existence of a travelling wave solution which  
 660 will be explored in the next section.

661 One important feature to notice is that the time evolution in Figure 4.1 matches the conceptual model  
 662 proposed in Dumitrache et al. (2015). This model can be seen in Figure 1.2. The different stages of  
 663 the conceptual model can be observed in our simulation results:

- 664 • Stage I:  $t = 2$  and  $t = 3.67$  show the biomass growing towards the center of the sheet, which is  
 665 the center white area.
- 666 • Stage II/III:  $t = 5.33$  shows the consumed substrate region as the outer white.
- 667 • Stage IV: Not shown. Only occurs at the moment when the two bands first collide and the  
 668 biomass concentration at that point still remains at the actual carrying capacity.
- 669 • Stage V:  $t = 7$  and  $t = 9$  show the combined center band, now at a biomass concentration  
 670 lower then the actual carrying capacity.

### 671 4.1.2 $CO_2$ Production

672 Some important quantities to track are the total amount of biomass,  $M$ , and substrate,  $C$ . These  
 673 approximations across the discretization will be called  $T_M(t)$  and  $T_C(t)$  to represent the total biomass  
 674 and total substrate, respectively. The computation for these values can be done by integrating over  
 675 the region,  $\Omega$ :

$$676 \quad T_M(t) = \int_{\Omega} M dA, \quad T_C(t) = \int_{\Omega} C dA \quad (4.2)$$

677 These values can be seen in Figure 4.3 (bd) for  $T_M(t)$  and (c) for  $T_C(t)$ .

678 Since *C. thermocellum* produces  $CO_2$  as the substrate is consumed, we can track the production of  
 679  $CO_2$ . Following the idea from Dumitrache et al. (2015), we can equate the change in production of

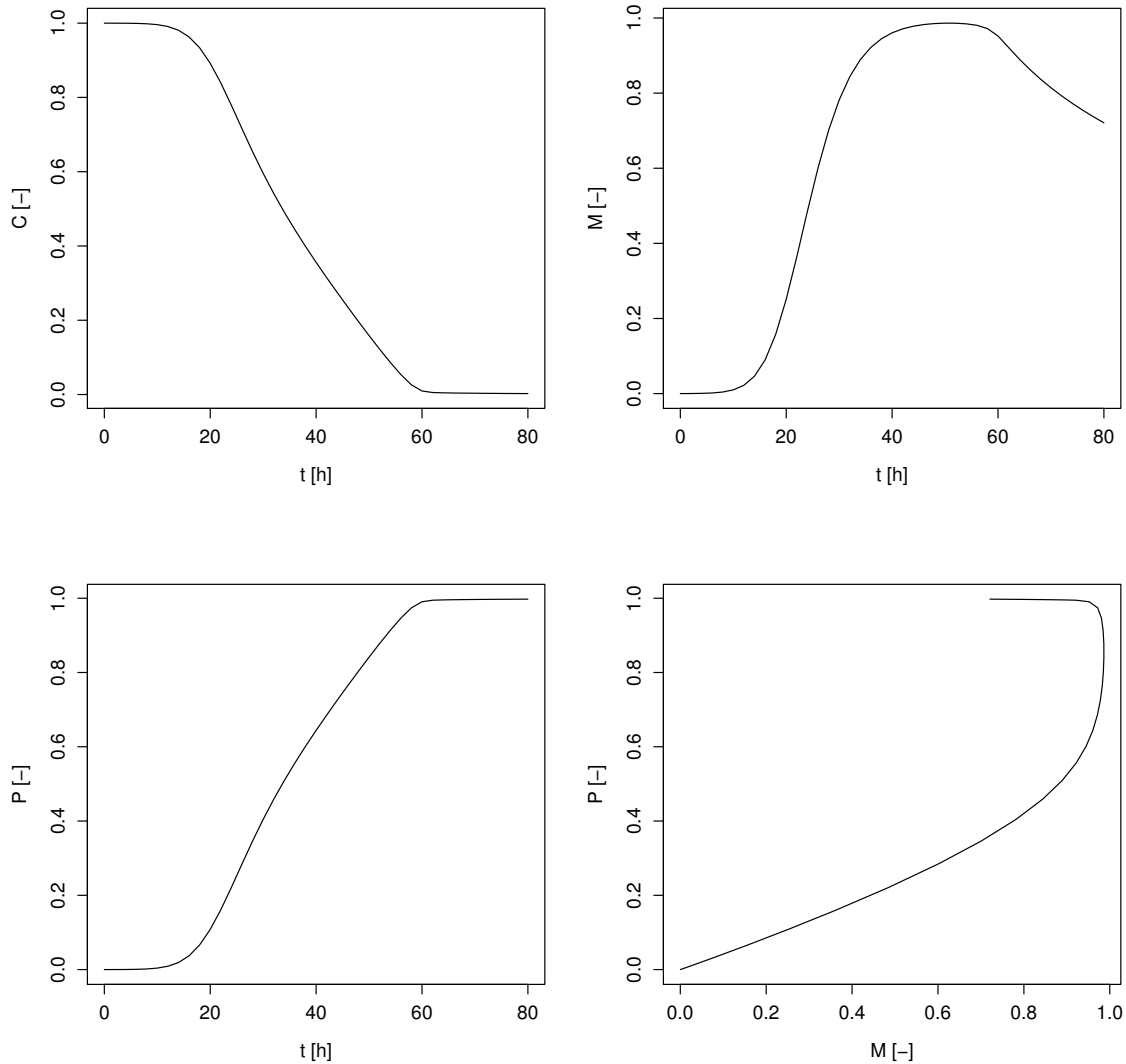


**Figure 4.2:** A typical model simulation from the simple ODE model. Shown are substrate concentration  $C$  (top left, normalised), effective sessile biomass  $M$  (top right, relative to the ideal carrying capacity  $M_\infty$ ), and  $CO_2$  product  $P$  (bottom left, in moles) as functions of time  $t$ ; Also shown is the product  $P$  vs sessile biomass  $M$  (bottom right, in moles). Figure originally from Dumitrache et al. (2015).

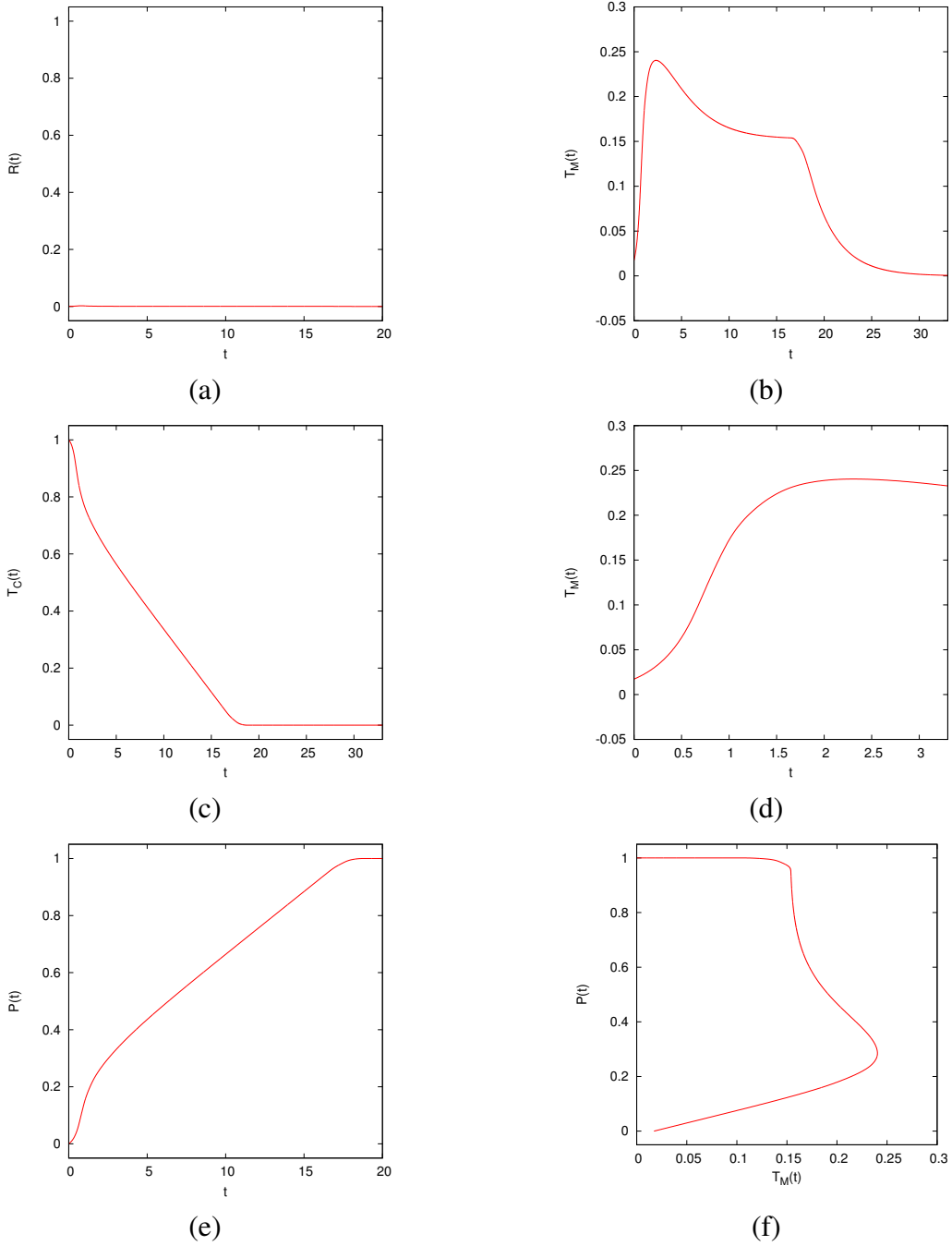


**Figure 4.3:** Total value of certain qualities from the typical simulation. Here we have: (a)  $\mathcal{R}(t)$ , the rate of  $CO_2$  production, (b) total  $M$  as a function of time, (c) total  $C$  as a function of time, (d) total  $M$  as a function of time zoomed in from  $t = 0$  to  $t = 3$ , (e)  $\mathcal{P}(t)$ , the total  $CO_2$  produced, (f)  $\mathcal{P}(t)$  as a function of total  $M$ . All the graphs are from the same simulation with initial condition of 40 random spherical inoculation points along the  $y = 0$  side of the region and another 40 on  $y = 1$ . A grid of  $257 \times 257$  was used for this graph. Default parameter set (Appendix A) was used except for  $\delta = 10^{-8}$ .

680  $CO_2$  as time changes by the following equation:

681 
$$p_t = \rho G(C)M. \quad (4.3)$$

682 To get the amount of  $CO_2$  produced at a specific time we get,

683 
$$\mathcal{R}(t) = \int_{\Omega} p_t dA = \int_{\Omega} \rho G(C) M dA. \quad (4.4)$$

684 From this we can get the more useful value, the total  $CO_2$  produced until this point.

685 
$$\mathcal{P}(t) = \int_0^t \mathcal{R}(s) ds. \quad (4.5)$$

686 The  $CO_2$  amount is calculated by letting  $\rho = 1$  and using the numerically computed values for  
 687  $G(C)M$  as a measure. For the same simulation as Figure 4.1, the  $CO_2$  information can be seen in  
 688 Figure 4.3 (a e).

689 The results from Figure 4.3 (c d e f) seems to match the results from the ordinary differential equation  
 690 model proposed in Dumitrache et al. (2015). Their results can be seen in Figure 4.2. It is important  
 691 to note that in our system  $T_M = 1$  means that  $\Omega$  is completely filled with biomass. However, in  
 692 Dumitrache et al. (2015) they scaled the biomass to the ideal carrying capacity of biomass, i.e. they  
 693 have  $T_M = 1$  when all the biomass is in stage II or III. The overall result from this experiment is that  
 694 the spatial two dimension model confirms the conceptual model from Dumitrache et al. (2015) based  
 695 on which the reactor-scale model was formulated. The reactor-scale model consolidated the spatial  
 696 effects into the carrying capacity of the growth and yet still managed to agree with the results of the  
 697 actual spatial model.

**698 4.2 Travelling Wave Analysis****699 4.2.1 Spatial Simplification**

700 To simplify the travelling wave analysis we reduce the spatial dimensions to that of a one dimensional  
701 problem. This can be done if initial conditions that are homogenous with respect to  $y$  are chosen. The  
702 purpose of this spatial simplification is that this will speed up the computations considerable. It will  
703 also make visualizations easier as certain figures would become too cluttered in two dimensions.  
704 What is done here is more of a pseudo-reduction of dimensions. By reducing the grids from an  $n \times m$   
705 grid to an  $n \times 4$  grid we have changed the way the problem size scales with finer grids. The problem  
706 is still two dimensional, just now one dimension has been reduced to only 4 grid points of accuracy  
707 instead of  $m$  points. This does not effect the final result since we only apply this change to problems  
708 with appropriate initial conditions. These initial conditions are homogenous in the  $y$  direction and  
709 thus we do not have any fluctuation between  $y$  values for a given  $x$  value.

710 One main benefit of changing the grid from  $n \times m$  to  $n \times 4$  is that the growth of the problem with  
711 respect to the resolution of the grid is reduced dramatically. This changes the problem from a  $O(n^2)$   
712 problem to a  $O(n)$ . Using the one dimensional travelling wave initial conditions, (3.26), one simula-  
713 tion is computed with a  $513 \times 513$  grid, seen at Figure 4.4, and another with a  $513 \times 4$  grid, seen at  
714 Figure 4.6.

715 Before any changes to the grid can be made, it must be confirmed that fluctuations are sufficiently  
716 small. To this end, the standard deviation is used as a measure. The standard deviation is calculated  
717 along the  $y$ -direction for each  $x$  value. This gives a numerical quantity for the measure of dispersal  
718 each  $y$  value has with another. Here, we use the sample standard deviation for the sole reason that  
719 this single simulation does not represent its own population. Initially, at  $t = 0$  the standard deviation  
720 is 0 everywhere (DATA NOT SHOWN). At  $t = 40$ , Figure 4.5 show the standard deviation of each  
721  $y$  value. After many time steps have passed the amount of spread is always less then  $10^{-14}$ , which  
722 is an acceptable degree of consistency. Note that the main inconsistency is at the wave front, around

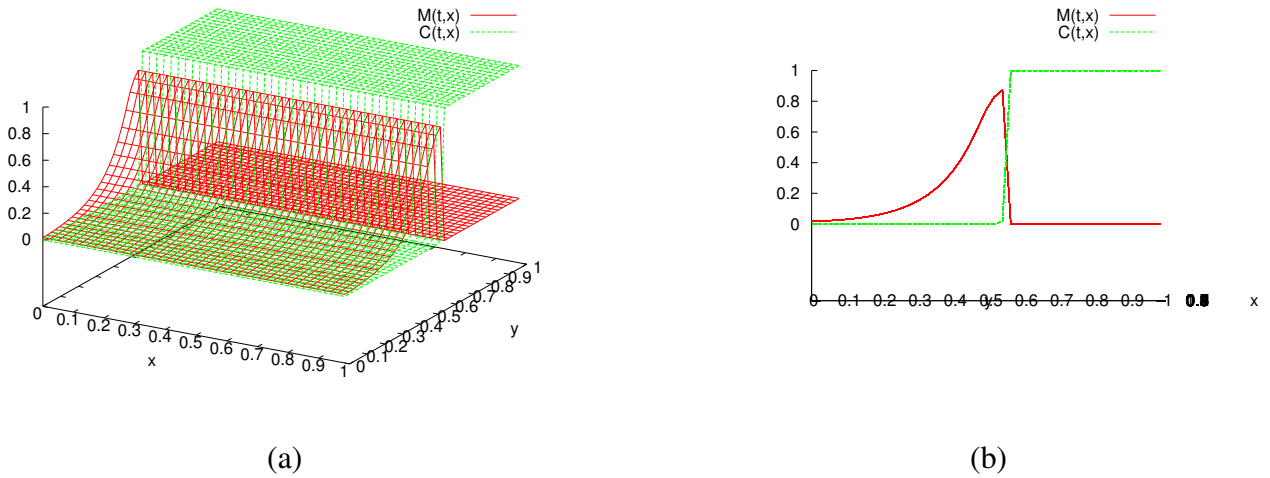


**Figure 4.4:** Graph of (a) 3D view of  $M(t, x, y)$  and  $C(t, x, y)$ , (b) Side profile view of  $M(t, x, y)$  and  $C(t, x, y)$  at  $t = 40$ .

<sup>723</sup>  $x = 5.75$ , which is mainly because of the sharp change in values.

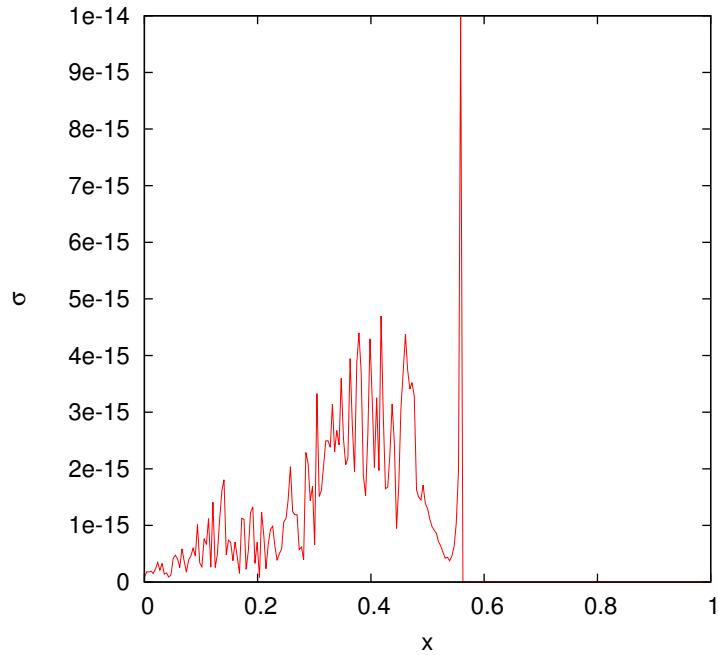


**Figure 4.5:** The standard deviation at the same time as the above graphs

- <sup>724</sup> When simulations are computed with a  $n \times 4$  grid, a two dimensional solution is still computed.  
<sup>725</sup> With regards to visualizations, side profiles could be used on these solutions to present pseudo-one  
<sup>726</sup> dimensional visualizations; this is not ideal. To visualize the solutions in true one dimension we use  
<sup>727</sup>  $\bar{M}$  and  $\bar{C}$  as averaged values of the solutions along the y-axis. This is computed after the solution has

728 been determined and is independent of the actual computations for  $M$  and  $C$ . So by taking the average  
 729 of the points along the  $y$ -axis we can get a two dimensional plot as seen in Figure 4.6.

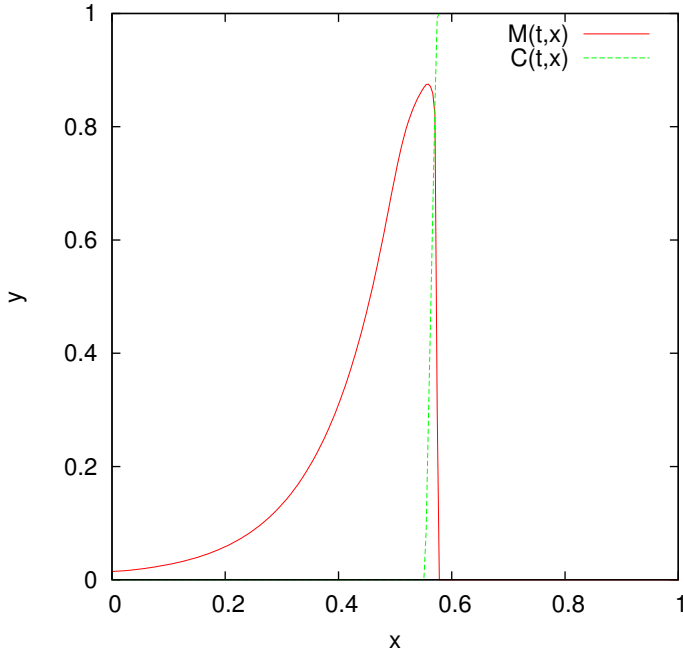


**Figure 4.6:** Graph of  $M(2,y)$  and  $C(2,y)$ , now reduced to a one dimensional solution.

730 This means that the system (2.16) - (2.18) can be reduced to a one dimensional problem. With initial  
 731 conditions that are homogenous with respect to  $y$ , we can greatly reduce the required number of grid  
 732 points in the one axis. Once the  $y$ -axis reduced, we can also ignore it for visualizations, only using  
 733 the  $x$ - $z$  axis and plotting the values of  $\bar{M}$  and  $\bar{C}$ .

### 734 4.2.2 Travelling Wave Solution

735 Classical travelling wave solutions are solutions that propagate with an *a priori* unknown constant  
 736 speed without any change in shape. This means that the solutions can be defined as

$$737 \quad M(t, x) = M(x - ct) \quad (4.6)$$

738 Figure 4.7 shows the time evolution of the single time snapshot from Figure 4.6. Given the above  
 739 definition and by looking at the consistent appearance of the solution, it suggests that it is a travelling

740 wave. It is clear here that the shape of the solution is consistent enough to suggest the existence of a  
 741 travelling wave solution.

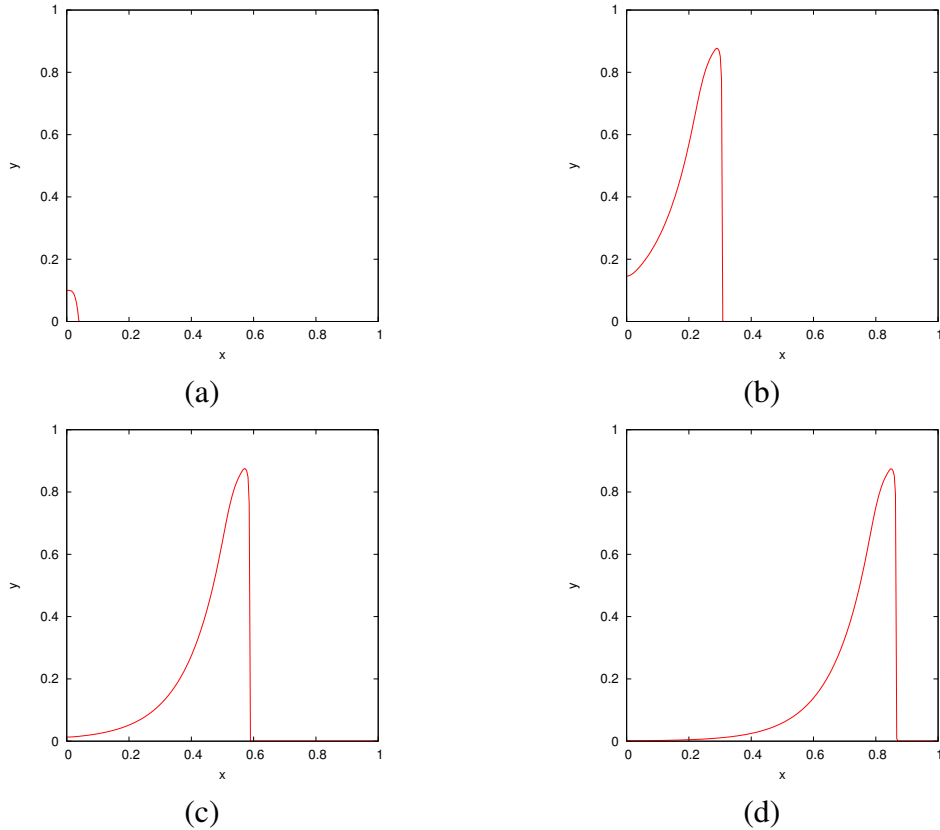


**Figure 4.7:** Solutions of  $M(x, t)$  and  $C(x, t)$  at (a)  $t = 0$ , (b)  $t = 20$ , (c)  $= 40$ , (d)  $= 60$ . This was run on a  $513 \times 4$  grid.

742 The existence of a travelling wave solution for this simulation can be confirmed if the solution  $M(x, t)$   
 743 can be shown as  $M(x - ct)$ , where  $c$  is the *a priori* unknown wave speed. This can be graphically  
 744 confirmed by horizontally translating the solution at different time steps on top of each other. If  
 745 the superimposed solutions are of similar shape and have been translated by multiples of the same  
 746 value then evidence of a travelling wave would be shown. This would suggest that the value used for  
 747 horizontal translations is an approximation for the wavespeed  $c$ . We can numerically approximate the  
 748 value for  $c$  by looking at how fast the peak of the wave travels. The location of the wave peak is the  
 749  $x$  coordinate that corresponds to the largest  $M$  value. Recall that we are dealing with a pseudo-one  
 750 dimensional problem, so there does not need to be any consideration for an  $(x, y)$  coordinate. For this  
 751 case, we used the GNUPLOT software to fit a linear model,  $f(x) = mx + b$ , to the last half of the  
 752 wave peaks path, seen in Figure 4.8. The last half of the values were used instead of the whole set

753 of values because only for the former do we have a fully formed travelling wave. The value of  $m$  in  
 754  $f(x)$  is the approximation for the wave speed,  $c$ .

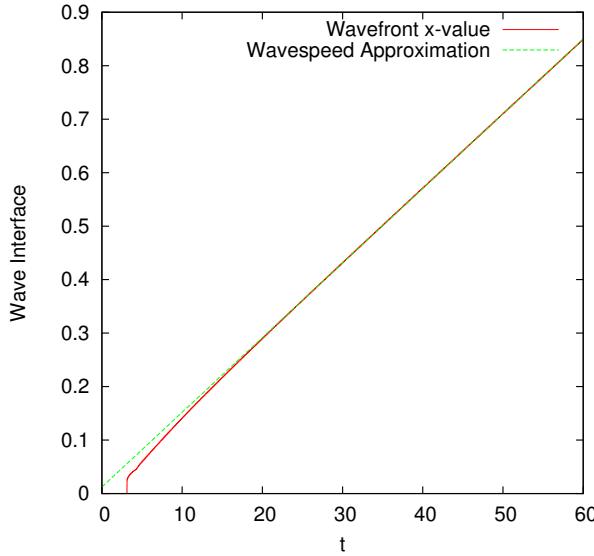


**Figure 4.8:** The  $x$  location of the wave peak as a function of  $t$ . The red line is the wave peak location extracted from the simulation results. The green line is the function  $f(x) = cx + b$  with  $c$  as the wave speed, found by fitting the model to the second half of  $x$  values. The simulation results used here are from the solution shown in the previous Figure.

755 With an approximation for  $c$ , the solutions of Figure 4.7 can be represented as  $M(x - c(t_0 - t_n))$ ,  
 756 where  $t_0 = 60$  is a reference point for the other time steps. The values of  $t_n$  are the times for the other  
 757 solutions. By translating along the  $x$ -axis multiple solution profiles can be superimposed, as seen in  
 758 Figure 4.9. The shape of each time step is very similar throughout, only differing slightly at the tail.  
  
 759 Based on the above evidence, we can say that a travelling wave solution has been suggested to exist  
 760 numerically for a single initial condition and particular set of parameters. This leads to two logical  
 761 extensions, looking at the stability of the travelling wave solution based on initial condition and  
 762 investigating the effect the parameters have on the travelling wave solution.

### 763 4.2.3 Travelling Wave Stability

764 Based on the previous example, there seems to exist a travelling wave solution for the intial condi-  
 765 tion given in (3.26). The next step is looking at how different initial conditions could still result in a  
 766 travelling wave solution. For this we specifically look at the stability of the solution, does it attract

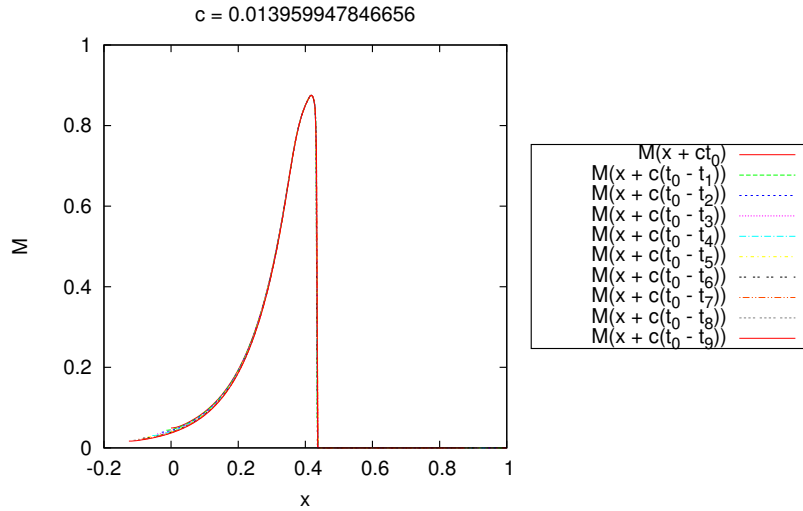


**Figure 4.9:** Solutions of  $M$  that are represented as  $M(x - ct)$  *a priori*. The multiple time steps are translated on top of another by horizontal movements of  $c(t_0 - t_n)$  for each time step.

767 each nearby solution into becoming a travelling wave solution or do only special cases become trav-  
 768 elling wave solutions. This will help confirm that the existence of the travelling wave solution is not  
 769 dependent on the single choice of initial condition.

770 To test this we take an initial condition that is not inherently one dimensional and see if it approaches  
 771 the one dimensional property. The choice of IC is to have multiple random spherical inoculation  
 772 points along the  $y = 0$  side of the region. Specifically, we use  $(x_r, y_r)$  to represent the center of each  
 773 random inoculation point. Here  $x_r \in \mathcal{R}$  and  $y_r \in [0, 0.1]$ .

774 The equation used for each random spherical inoculation point is,

$$775 \quad M = \frac{-h}{d^2} ((x - x_r)^2 + (y - y_r)^2) + h, \quad M \geq 0. \quad (4.7)$$

776 Random inoculation points add to each other if they overlap. After all the inoculation points have  
 777 been generated, every value is divide by the total amount of biomass. This lets the initial condition  
 778 become a representation for the distribution of random inoculation points in terms of the total amount  
 779 generated. A time evolution of the simulation with the above initial condition can been seen in Figure  
 780 4.10. Here it can be observed that the solution  $M$  appears to slowly converge to a one dimensional

781 problem. This cannot be fully seen since the wave propagation reaches the end of the region before it  
 782 can become fully one dimensional.

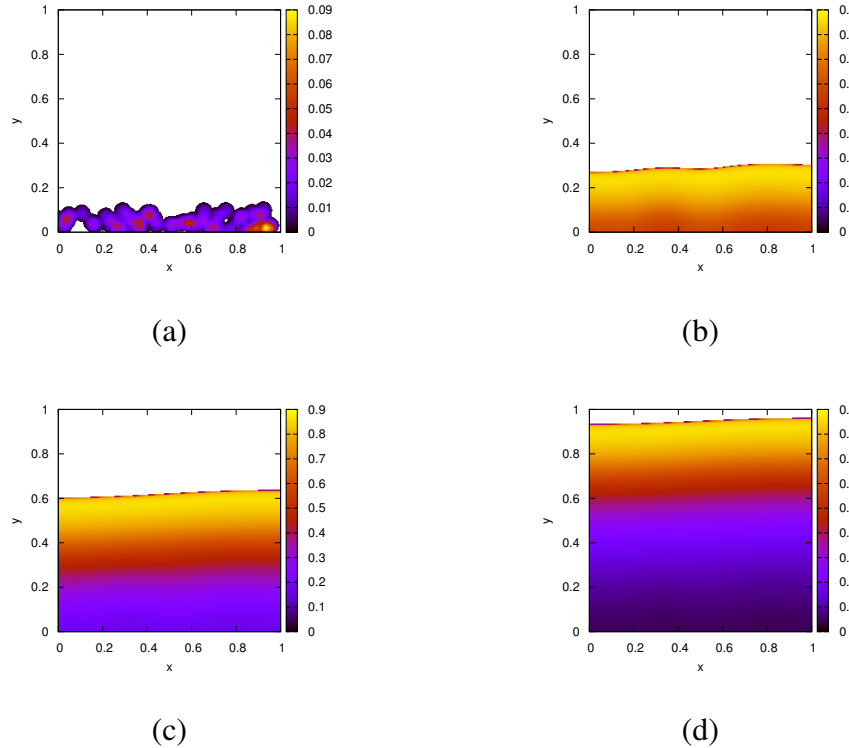


**Figure 4.10:** Plots of the simulation with random spherical inoculation points centered in the region  $(x, y) \in [0, 0] \times [1, 0.1]$ . The solutions are shown at (a)  $t = 0$ , (b)  $t = 10$ , (c)  $t = 20$ , and (d)  $t = 30$ . Each solution is computed on a  $513 \times 513$  grid.

783 We can quantitatively see the behaviour of this convergence by calculating the measure of spread at  
 784 the wave front. This can be achieved by calculating the standard deviation of  $y$  coordinate for each  
 785  $x$  coordinate. By tracking the largest  $y$  value with a non-zero  $M$  for each  $x$  value we can generate a  
 786 sample data set of the wavefront. The wavefront is used instead of other points of interest, such as the  
 787 wave peak, because it is the most consistent of characteristics that can be easily tracked. As seen in  
 788 Figure 4.5, the wave peak had the largest spread among all other values.

789 Taking the sample standard deviation of this set results in the measure of spread for the wavefront. The  
 790 sample standard deviation was used since this one example does not represent the whole population  
 791 of solutions. The idea is that, for a solution that converges to one-dimensionality, the  $y$  location of  
 792 the wavefront should be converging to similar values. This means that the standard deviation would

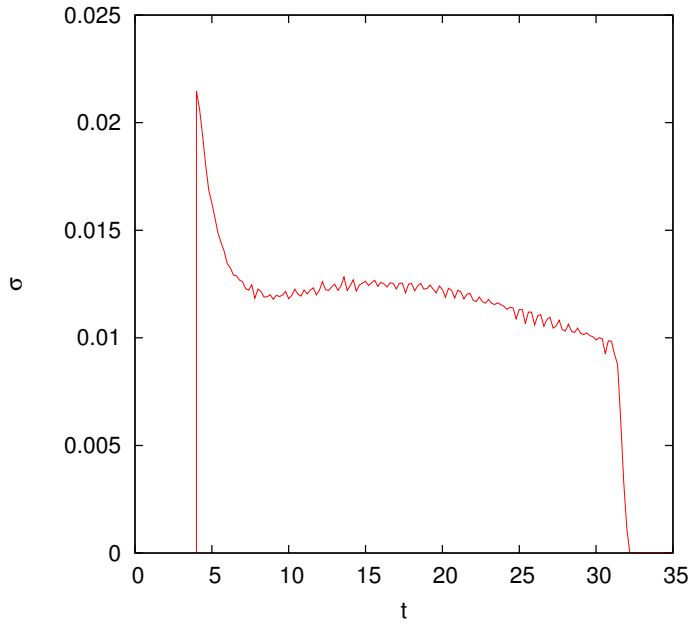


**Figure 4.11:** The standard deviation of the wavefront interface as a function of time. The wavefront references the largest  $y$  coordinate with  $M > 0.001$  for each  $x$  coordinate. The choice of using  $M > 0.001$  is because we want to ignore the small values ( $10^{-100}$ ) that arise from the diffusion right at the wave front. This simulation is the same as the previous Figure.

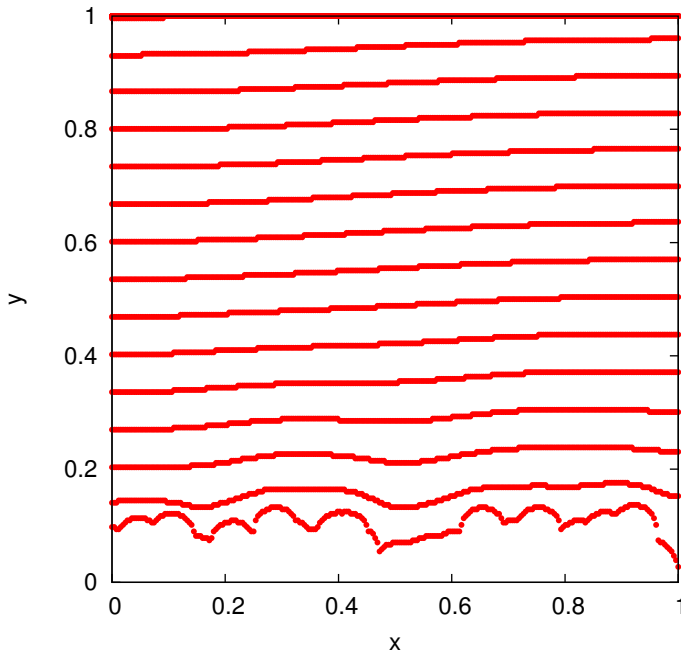


**Figure 4.12:** The wavefront shape of multiple time steps. Each wavefront has a difference in time by 2, i.e. they are at  $t = 4, 6, 8, \dots, 58, 60$ . The simulation results are the same as the previous Figures, using the default parameter values with a grid size  $513 \times 513$ .

793 converge to zero. The standard deviation of the wavefront as a function of time of the simulation  
794 ran in Figure 4.10 can be seen in Figure 4.11. Here is shown that the solution is converging to zero,  
795 however not monotonically.

796 For the numerical computation of the wavefront, the largest  $y$  values greater than 0.001 was used  
797 instead of 0. The reason is that there are very small values of around  $10^{-200}$  that arise due to the  
798 diffusion that were not adequate representations of the wavefront.

799 Another interesting item to investigate is the actual shape of the wavefront. Figure 4.12 shows only  
800 the wavefront shape for multiple time steps. The wavefront shape is the same dataset of points used  
801 to calculate the standard deviation of the wavefront interface. Of interest is that the wavefront seems  
802 to move at a constant speed, since each wavefront shown is equidistant from the next.

803 **4.2.4 Parameter Effect on Wave Speed**

804 The travelling wave solutions seen before have all existed for a single set of parameters. Here the four  
805 main system parameters,  $\delta$ ,  $\kappa$ ,  $\nu$ , and  $\gamma$  are independently varied and the effect on the travelling wave  
806 solutions are observed. From this we can also see how the wave speed of the travelling wave solution  
807 changes as a function of the different model parameters.

808 For this an automated script was created that checks, for each time step, if  $M$  is travelling wave  
809 solution based on the solution  $M$  from a number of time steps previous. From this check, a wave speed  
810 needs to be approximated based on the distance between the two solutions. If this approximated wave  
811 speed is matched throughout all the  $x$  values, then a travelling wave solution is assumed to exist at  
812 that time step. With this script, we can try the same simulation as Figure 4.7 with different parameter  
813 values.

814 For each parameter,  $\delta$ ,  $\kappa$ ,  $\nu$ ,  $\gamma$ , the range of values chosen were arbitrarily. Figure 4.13 shows the  
815 results of the wave speed for each parameter changes. Mainly it was so that the solution did not  
816 propagate too fast and hit the end of the region before developing into a full travelling wave solution.  
817 Generally when the travelling wave does not form it is because the wave front propagates to the end

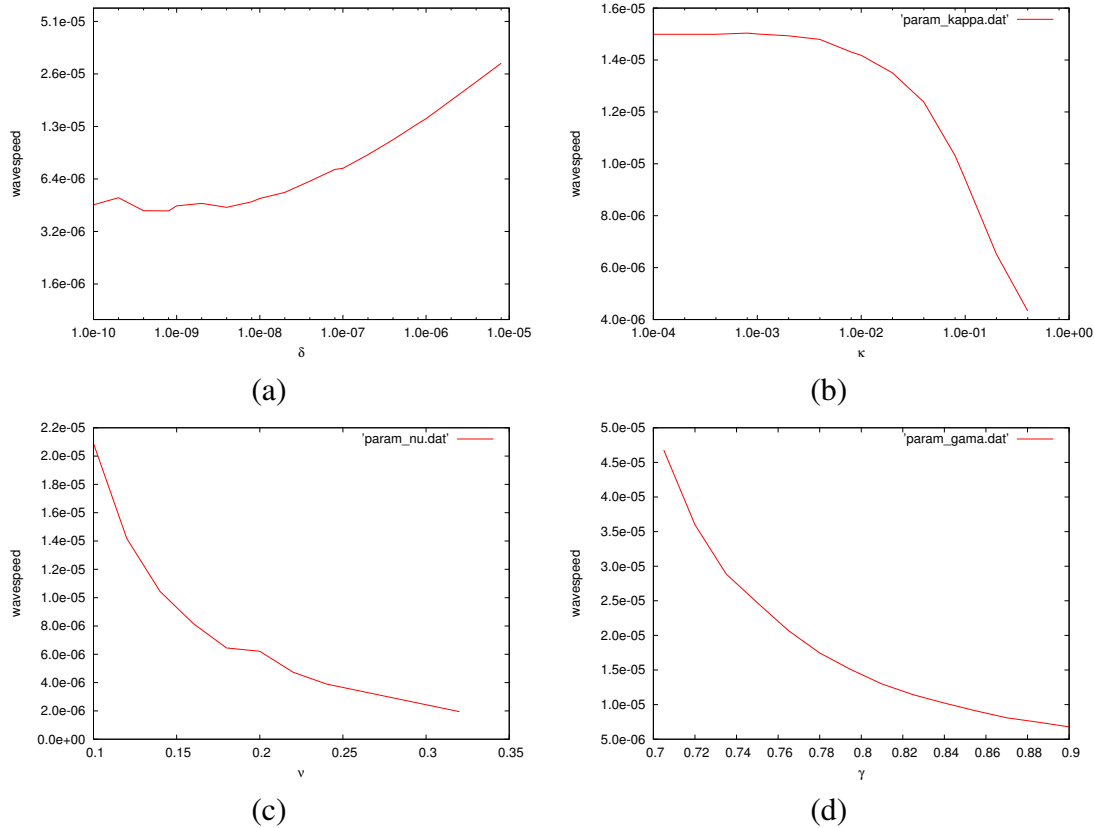


**Figure 4.13:** The value of  $c$  as parameter (a)  $\delta$ , (b)  $\kappa$ , (c)  $\nu$ , and (d)  $\gamma$  are changed. Note that (a) and (b) have logscales due to the selection of parameter values. Each of these were calculated with the same setup as the travelling solution previously done. The grid size for each was  $513 \times 4$  and a time step of  $\Delta t = 0.001$  was used.

818 of the region faster than the tail of the travelling wave can decrease to 0. In the case of  $\nu$ , any larger  
819 values than the selected range resulted in biomass that died faster than it could grow, and thus no  
820 travelling wave solution exists. There did not appear to be any cases where a travelling wave solution  
821 could not form.

822 The behaviour of the wave speed as a result of changing the parameters can be explained by the  
823 biological meaning of each parameter. For  $\delta$ , the diffusion constant, a large value results in a larger  
824 local biomass growth as a result of diffusion. This speeds up the spreading of the biomass and  
825 the propagation of the interface. For  $\kappa$ , the half-saturation concentration, this value depicts at what  
826 substrate concentration we achieve half-maximum growth for the biomass. When this value is large,  
827 the required amount of substrate for optimal growth speed is increased and thus the overall growth of  
828 the biofilm is slowed down. For  $\nu$ , the decay and loss rate of biomass, a larger value results in more  
829 biomass being ejected from the system and thus the amount of biomass available to grow become  
830 smaller and growth propagations are slowed. For  $\gamma$ , the biomass yield coefficient, a larger value  
831 correlates to a substrate that is quickly consumed which produces less total biomass for growth. This  
832 inhibits the propagation of the biomass interface and lowers the wave speed. The simulated values  
833 recorded in Figure 4.13 agree with the expected behaviour for each parameter.

### 834 4.3 Spatial Effects

835 There are many spatial effects that can exist here because of the diffusion term in the biomass. We  
836 now try observing any differences in the behaviour of the system based on spatially different initial  
837 conditions. This will show if there is any noticeable differences in the behaviour of the system based  
838 solely on the placement of initial biomass. There will be two methods to compare the different  
839 simulations: visually and by monitoring the amount of  $CO_2$  produced. The visual inspection is a  
840 logical comparison to use, the  $CO_2$  is chosen since it essentially provides a measure of the activity in  
841 the system. The  $CO_2$  is also used in the experiments conducted in Dumitrache (2014). Looking at the  
842  $CO_2$  production, a lumped measurement of the biomass activity, shows whether local spatial effects  
843 change the global reactor scale behaviour.

844 To measure the difference, two simulations will be run with varying initial conditions. One simulation  
 845 will have the initial condition evenly spread along one side of the region. The other will have all  
 846 the initial condition clumped in single corner. This will replicate the two possible extremes for the  
 847 location of biomass.

848 Since the simulation is comparing the difference between two initial conditions, the initial amount  
 849 of total biomass,  $T_M(0)$ , must be the same between both simulations. The equally dispersed initial  
 850 condition needs to have as much surface area exposed as reasonably possible. To this end, *num*  
 851 spherical inoculation points, equidistance from each other, are used along the  $y = 0$  side of  $\Omega$ . Here  
 852 we use  $(x_e, y_e)$  as the center of the evenly distributed inoculation points. The value of  $(x_e, y_e)$  depends  
 853 on the number of points chosen for the simulation. Each spherical inoculation point is computed as,

$$854 \quad M(0, x, y) = \frac{-h}{d^2}((x - x_e)^2 + (y - y_e)^2) + h, \quad M \geq 0. \quad (4.8)$$

855 Note that  $M(0, x, y)$  is for points within circles of radius  $d$  centered at  $(x_e, y_e)$ , otherwise  $M(0, x, y) =$   
 856 0. For the substratum we have  $C(0, x, y) = 1$  everywhere.

857 For the clumped initial condition, we choose another spherical inoculation point so that it is similar  
 858 to the evenly distributed initial condition. Here, we need only a single inoculation point, centered at  
 859 the corner  $(0, 0)$ . The choice of inoculation center is so that the initial biomass is as concentrated as  
 860 possible, while still retaining a spherical shape. The initial condition for the clumped biomass is as  
 861 follows,

$$862 \quad M = \frac{-1}{(2hd^2 \cdot num)^{\frac{1}{3}}}(x^2 + y^2) + (2hd^2 \cdot num)^{\frac{1}{3}}. \quad (4.9)$$

863 Here the coefficients have been chosen so that the two initial conditions have the same amount of  
 864 biomass. The value of *num* is to represent the number of inoculation points in the evenly distributed  
 865 initial condition.

866 Figure 4.14 - 4.15 shows the time evolution of both initial conditions. Here we arbitrarily select  
 867  $num = 6$ .

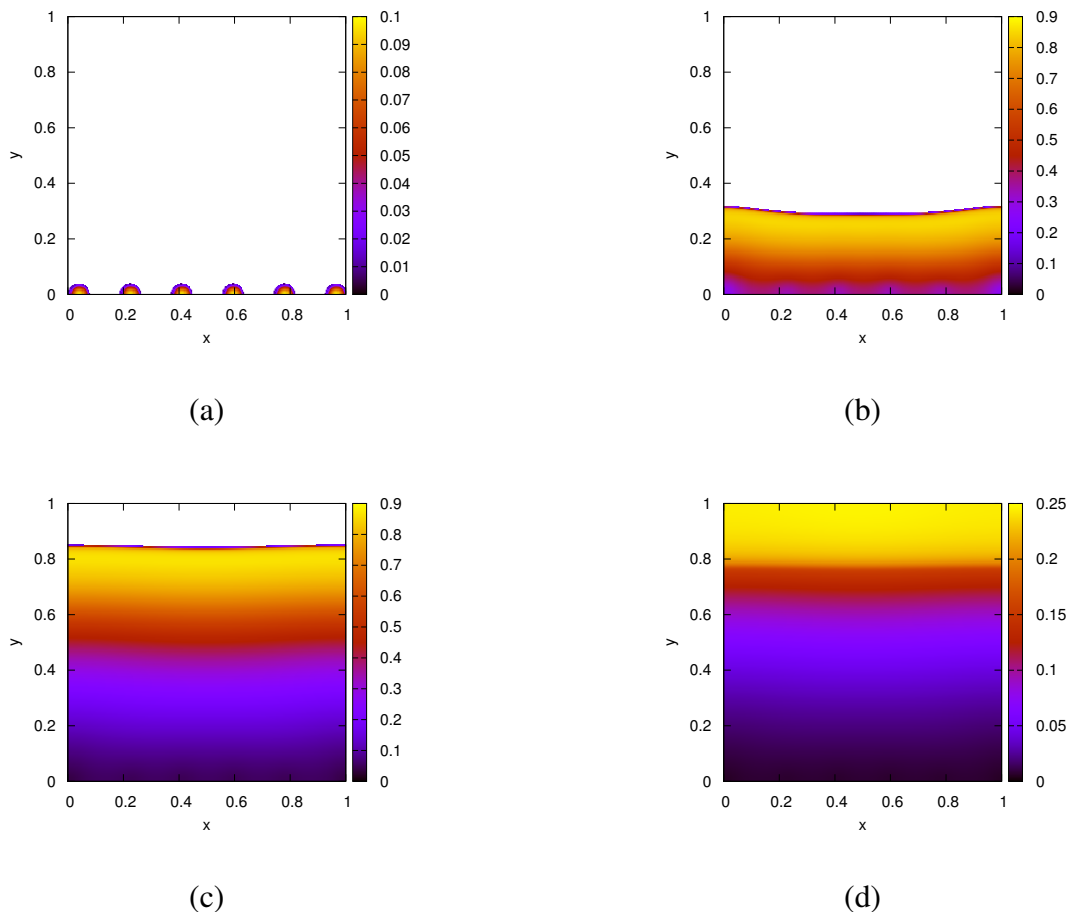


**Figure 4.14:** This shows the time evolution for the evenly distributed initial condition at (a)  $t = 0$ , (b)  $t = 16$ , (c)  $t = 32$ , (d)  $t = 48$ . Here default parameters are used on a grid size of  $513 \times 513$ .

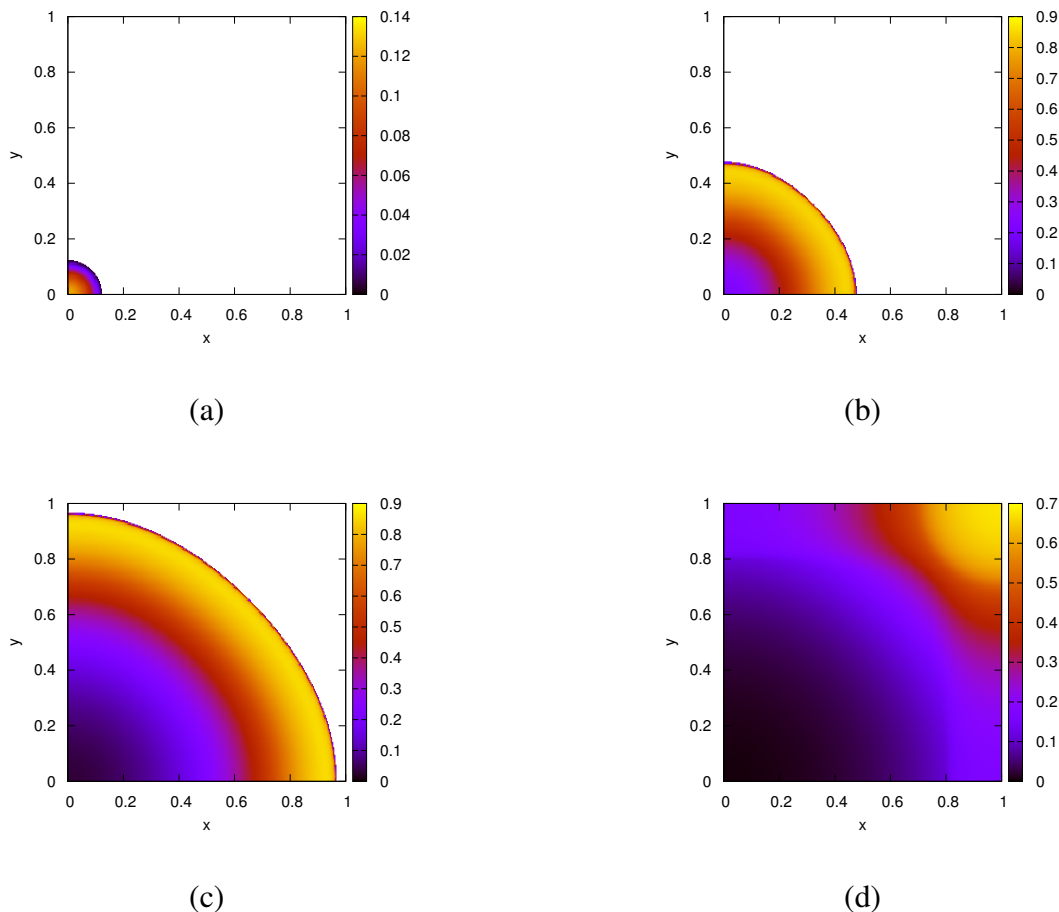


**Figure 4.15:** This shows the time evolution for the clumped initial condition at (a)  $t = 0$ , (b)  $t = 16$ , (c)  $t = 32$ , (d)  $t = 48$ . Here default parameters are used on a grid size of  $513 \times 513$ .

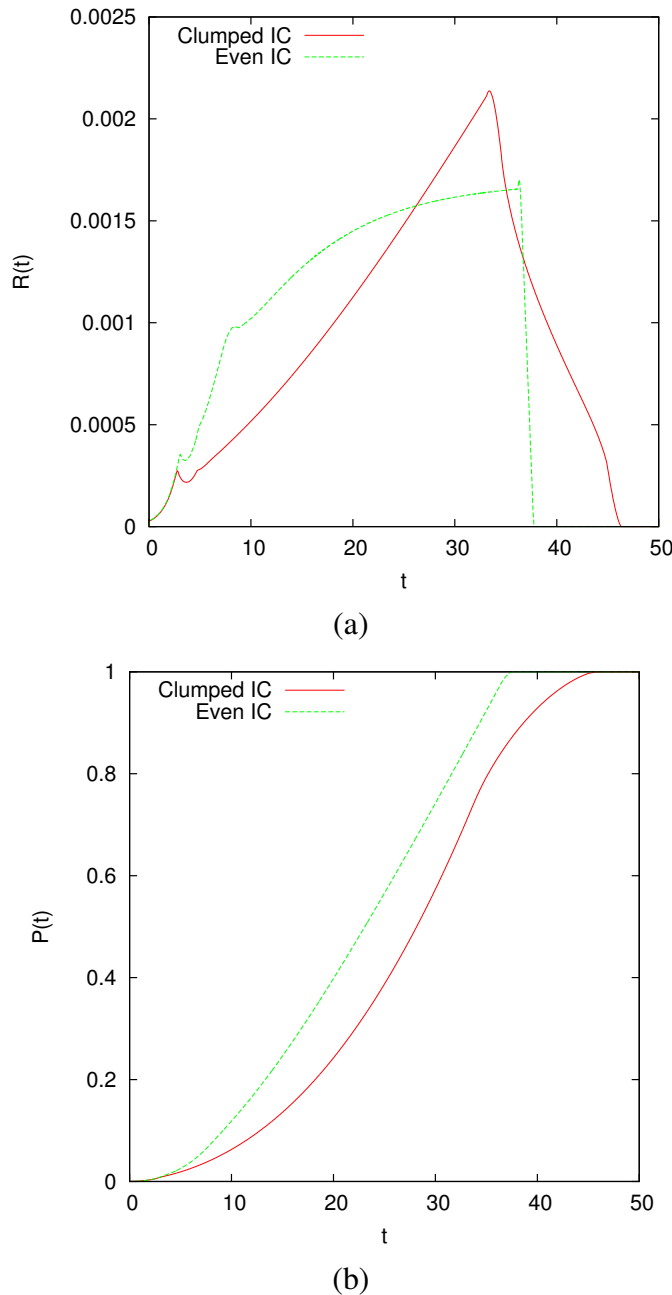


**Figure 4.16:** A plot of (a) the rate of  $CO_2$  production,  $\mathcal{R}(t)$ , and (b) the total amount of  $CO_2$  produced until time  $t$ ,  $\mathcal{P}(t)$ . These are extracted from the same simulation done in the two previous figures.

868 It becomes easier to see the difference between the two spatially different problems when  $CO_2$  pro-  
869 duction is taken into account. In Figure 4.16 it is clear that there is a substantial difference between the  
870  $CO_2$  production of both cases. This shows that the initial distribution of biomass can affect a lumped,  
871 global measurement and change the reactor-scale behaviour when compared to a meso-scaled system.

872 **Chapter 5**

873 **Conclusions**

874 **5.1 Lessons Learned**

- From the numerics chapter of the thesis, the validity and usefulness of a newly developed fully-implicit method was investigated. By comparing it to the standard semi-implicit method, which it extends, it was determined that a significant accuracy gain results from a single extra iteration of the fully-implicit method. Multiple iterations increase this gain since the increase in accuracy is positively correlated to the number of iterations performed. However, the computational effort required from the fully-implicit method grows exponentially with lower tolerance. The ratio for solution accuracy when weighed against heavier computation times suggests that two iterations of the fully-implicit method is best (one extra from the semi-implicit method). This resulted in an extra digit of accuracy at the cost of approximately 150% the computational effort.
- From the simulation chapter of the thesis, a number of useful characteristics were observed in the system. The existence of travelling wave solutions was strongly suggested from all the evidence gathered. The stability of this wave suggests that it always exists, but this cannot be verified due to the analytic complexity of the problem. Testing two sets of initial conditions, chosen at opposing extremes of spatial spreading (all biomass in one location versus equally

distributed across one boundary), and measuring the  $CO_2$  production showed a large difference between the two solutions at a reactor-scale. This suggests that two dimensional models are better for accurately mimicking the behaviour of the system.

## 5.2 Future Work

- A full travelling wave analysis could be conducted. The existence of travelling wave solutions might be proven and the travelling wave speed could be solved for in terms of parameters. The issue with this is the high degeneracy of the diffusion term. One way of handling this would be to try regularising the system to eliminate the degeneracy.
- The reaction parameters of the diffusion-reaction model from the experimental data in Dumitrache et al. (2015) could be determined. This is an ill-posed problem since the data is lumped for only  $CO_2$  production rates; there is no data for  $C$ ,  $M$ , and any initial data for  $M$ .
- The two dimensional model can be upscaled to obtain a reactor-scale model as in Dumitrache et al. (2015) where the spatial effects were accounted for by introducing the concept of a carrying capacity. This could be accomplished by using volume averaging to consolidate the spatial terms in with the growth terms.
- A rigorous proof could be attempted, showing that the nonlinear iteration of the fully-implicit method always converges or that the conditions required for convergence is so far missing.

907 **References**

- 908 Alternative Fuel Data Center (2014). Ethanol vehicle emissions. Online; accessed 1-December-2015.
- 909 Barrett, R., Berry, M., T.F., C., Demmel, J., Donato, J., Dongarra, J., Eijkhout, V., Pozo, R., Romine,  
910 C., and van der Vorst, H. (1987). *Templates for the Solution of Linear Systems: Building Blocks for*  
911 *Iterative Methods*. Society for Industrial and Applied Mathematics, 1st edition.
- 912 Burden, R. and Faires, J. (2010). *Numerical Analysis*. Brooks/Cole, 9th edition.
- 913 Butcher, J. (2008). *Numerical Methods for Ordinary Differential Equations*. Wiley, 2nd edition.
- 914 Dumitrache, A. (2014). *Understanding Biofilms of Anaerobic, Thermophilic and Cellulolytic Bac-*  
915 *teria: A Study towards the Advancement of Consolidated Bioprocessing Strategies*. PhD thesis,  
916 University of Toronto.
- 917 Dumitrache, A., Eberl, H., Wolfaardt, G., and Allen, D. (2015). Mathematical modeling to validate  
918 on-line  $CO_2$  measurements as a metric for cellulolytic biofilm activity in continuous-flow bioreac-  
919 tors. *Biochemical Engineering Journal*, 101:55–67.
- 920 Dumitrache, A., Wolfaardt, G., Allen, D., Liss, S., and Lynd, L. (2013a). Form and function of  
921 clostridium thermocellum biofilms. *Applied and Environmental Microbiology*, 79:231–239.
- 922 Dumitrache, A., Wolfaardt, G., Allen, D., Liss, S., and Lynd, L. (2013b). Tracking the cellulolytic  
923 activity of clostridium thermocellum biofilms. *Biotechnology for Biofuels*, 6:175.
- 924 Eberl, H. and Demaret, L. (2007). A finite difference scheme for a doubly degenerate diffusionreac-  
925 tion equation arising in microbial ecology. *Electronic Journal of Differential Equations*, CS15:77–  
926 95.

- 927 Eberl, H., Khassehkhan, H., and Demaret, L. (2010). A mixed-culture model of a probiotic biofilm  
928 control system. *Computational and Mathematical Methods in Medicine*, 11(2):99–118.
- 929 Eberl, H., Parker, D., and van Loosdrecht, M. (2001). A new deterministic spatio-temporal continuum  
930 model for biofilm development. *Journal of Theoretical Medicine*, 3:161–175.
- 931 Efendiev, M., Eberl, H., and Zelik, S. (2002). Existence and longtime behaviour of solutions of a  
932 nonlinear reaction-diffusion system arising in the modeling of biofilms. *RIMS Kokyuroko*, 1258:49–  
933 71.
- 934 Gurtin, M.E., M. (1977). On the diffusion of biological populations. *Mathematical Biosciences*,  
935 33:35–49.
- 936 Jalbert, E. and Eberl, H. (2014). Numerical computation of sharp travelling waves of a degenerate  
937 diffusion-reaction equation arising in biofilm modelling. *Communications in Nonlinear Science  
938 and Numerical Simulation*, 19(7):2181–2190.
- 939 Khassehkhan, H. and Eberl, H. (2008). Modeling and simulation of a bacterial biofilm that is con-  
940 trolled by ph and protonated lactic acids. *Computation and Mathematical Methods in Medicine*,  
941 9(1):47–67.
- 942 Khassehkhan, H., Hillen, T., and Eberl, H. (2009). A nonlinear master equation for a degenerate  
943 diffusion model of biofilm growth. *Lecture Notes in Computer Science*, 5544:735–744.
- 944 Kreft, J.-U., Picioreanu, C., Wimpenny, J., and van Loosdrecht, M. (2001). Individual-based mod-  
945 elling of biofilms. *Microbiology*, 147(11):2897–2912.
- 946 Lynd, L. (2008). Energy biotechnology. *Current Opinion in Biotechnology*, 19(3):199–201.
- 947 Macías-Díaz, J., Macías, S., and Medina-Ramírez, I. (2013). An efficient nonlinear finite-difference  
948 approach in the computational modeling of the dynamics of a nonlinear diffusion-reaction equation  
949 in microbial ecology. *Computational Biology and Chemistry*, 47:24–30.

- 950 Noguera, D., Pizarro, G., Stahl, D., and Rittmann, B. (1999). Simulation of multispecies biofilm  
951 development in three dimensions. *Water Science and Technology*, 39:123–130.
- 952 Picioreanu, C., van Loosdrecht, M., and Heijnen, J. (1998). A new combined differential-discrete cel-  
953 lular automaton approach for biofilm modeling: application for growth in gel beads. *Biotechnology*  
954 and *Bioengineering*, 57:718–731.
- 955 Rittmann, B. and McCarty, P. (1980). Model of steady-state-biofilm kinetics. *Biotechnology and*  
956 *Bioengineering*, 22(11):2343–2357.
- 957 Saad, Y. (2003). *Iterative Methods for Sparse Linear Systems*. Society for Industrial and Applied  
958 Mathematic, 2nd edition.
- 959 Sirca, S. and Horvat, M. (2012). *Computational Methods for Physicistsl: Compendium for Students*.  
960 Springer.
- 961 Varga, R. (2004). *Geršgorin and His Circles*. Berlin: Springer-Verlag.
- 962 Wang, Z.-W., Lee, S.-H., Elkins, J., and Morrell-Falvey, J. (2011). Spatial and temporal dynamics  
963 of cellulose degradation and biofilm formation by caldicellulosiruptor obsidiansis and clostridium  
964 thermocellum. *AMB Express*, 1:30.
- 965 Wanner, O., Eberl, H., Morgenroth, E., Noguera, D., Picioreanu, C., Rittmann, B., and van Loos-  
966 drecht, M. (2005). *Mathematical modeling of biofilms*. IWA Scientific and Technical Report no  
967 18., UK: IWA Publishing.

968 **Appendix A**

969 **Default Parameter Values**

970 The default parameter values used for simulations are listed in the follow table. Unless stated, every  
971 simulation uses these values.

Parameter	Symbol	Value
-	$\alpha$	4
-	$\beta$	4
Decay-Loss rate	$\nu$	0.12
Half-concentration rate	$\kappa$	$10^{-3}$
Yield rate	$\gamma$	0.80
Diffusion constant	$\delta$	$10^{-4}$
Initial condition height	$h$	0.1
Initial condition depth	$d$	$\frac{5}{127}$
Number of grid points	$nm$	$513 \times 513$
Grid size	$\Delta x$	$\frac{1}{513}$
Time step	$\Delta t$	$10^{-3}$

**Table A.1:** The listing of default parameter values used for most simulations.

972 **Appendix B**

973 **Source Code**

**Listing B.1:** PDE-ODEsolver.f90 main source code

```
974 !=====
975 !     PDE - ODE Coupled Solver
976 !-----
977 !     This fortran code solves the PDE - ODE coupled system that describes
978 !     the growth of Clostridium Thermocellum and its consumption of the carbon
979 !     substrait.
980 !
981 !     The system is based off the following system:
982 !         M_t = nabla (D(M) nabla M ) + f(C,M)
983 !         C_t = - g(C,M)
984 !     where M is the biomass of C. Thermocellum and C is the concentration of
985 !     Carbon. D(M) is the diffusion coeffient for the biomass movement. f(C,M)
986 !     is the growth and death term for the biomass. g(C,M) is the consumption
987 !     of carbon substrait.
988 !-----
989 !     The method of solving is by trapzidral rule for C, and by finite
990 !     difference for M
991 !=====

992
993 program cThermoPDEODE
994 !     use omp_lib
995 implicit none
996 INTERFACE
997     subroutine solveLSDIAG(n,ndiag,ioff,a,sol,rhs,nit,err1,err2,stopcrit)
998 !-----
999     ! input: n      problem size
1000    !       ndiag: number of diagonals
1001    !       ioff: offsets (distance of sub diagonals to main diagonal)
1002    !       Mnew:      matrix values
1003    !       sol:      initial guess for iteration ( overwritten by result)
1004    !       rhs:      the righ hand side of the linear system
1005    !       nit:      max num of iter to be carried out (overwritten)
1006    !       err1:     tol for 1st stopping criterion (will be overwritten)
1007    !       err2:     tol for 2nd stopping criterion (will be overwritten)
1008    ! output: sol:      solution of Ax=b
1009    !       nit:      number of iterations taken
1010    !       err1:     computed value for 1st stopping criterion
1011    !       err2:     computed value for 2nd stopping criterion
1012    !       stopcrit: value that tells which stopping criti activated
1013 !-----
```

```

1014      implicit none
1015      integer, intent(in)          :: n,ndiag
1016      real,dimension(n,ndiag),intent(in):: a
1017      integer, dimension(ndiag),intent(in)::ioff
1018      real,dimension(n),intent(in)   :: rhs
1019      real,dimension(n),intent(inout) :: sol
1020      real,intent(inout)           :: err1,err2
1021      integer,intent(inout)        :: nit
1022      integer,intent(out)          :: stopcrit
1023      end subroutine
1024
1025  END INTERFACE
1026
1027 !=====
1028 ! Variable Descriptions
1029 !=====
1030
1031 ! filename Variables
1032 character(100) :: filename
1033
1034 ! Problem Parameters
1035 real :: kappa,delta,nu,gama
1036 integer :: alpha,beta
1037 real :: depth,height
1038 integer :: fSelect, dSelect, gSelect, MinitialCond
1039 integer :: num_innocu_points
1040
1041 ! Numerical Method Parameters
1042 integer :: pSize,row,col,n,ndiag,nit,nOuts
1043 real :: tEnd,tDel,xDel,e1,e2,eSoln,eTrav
1044 integer :: true2D, checkTrav
1045
1046 ! Solution variables
1047 real,dimension(:),allocatable :: C, M
1048
1049 ! Reporting variables
1050 real :: avgIters, maxIters
1051 real :: avgNit, maxNit
1052 integer :: startTime, endTime, clock_rate, clock_max
1053 real :: elapsedTime
1054
1055 write(*,*) "Enter parameter file name: ex. 'parameter.txt' "
1056 write(*,'(A)', advance="no") "      "
1057 read(*,*) filename
1058
1059 write(*,*) "Setting Parameters that shouldn't change"
1060 ndiag = 5
1061 write(*,'(A,I5)') "      ndiag = ", ndiag
1062
1063 write(*,*) "Getting problem size from file"
1064 call getProbSize(pSize, true2D, checkTrav, filename, len(filename))
1065 if (true2D == 1) then
1066     write(*,*) "      Problem is 2D"
1067     col = 4
1068 else if (true2D == 0) then
1069     write(*,*) "      Problem is 3D"

```

```

1069     col = pSize
1070   end if
1071   write(*,*) "      pSize = ", pSize
1072   row = pSize
1073   n = row * col
1074   write(*,*) "      row    = ", row
1075   write(*,*) "      col    = ", col
1076   write(*,*) "      n      = ", n
1077
1078   write(*,*) "Opening Parameter file"
1079   call paramSet(depth, height, num_innocu_points, alpha, beta, kappa, &
1080                 gama, nu, delta, nOuts, tEnd, tDel, e1, e2, eTrav, &
1081                 eSoln, fSelect, dSelect, gSelect, MinitialCond, filename, &
1082                 len(filename))
1083   xDel = 1/real(row)
1084   nit = n * 100
1085   write(*,*) "Parameters set:"
1086   write(*,*) "      depth      = ", depth
1087   write(*,*) "      height     = ", height
1088   write(*,*) "      alpha      = ", alpha
1089   write(*,*) "      beta       = ", beta
1090   write(*,*) "      gama       = ", gama
1091   write(*,*) "      nu         = ", nu
1092   write(*,*) "      delta      = ", delta
1093   write(*,*) "      nOuts     = ", nOuts
1094   write(*,*) "      tEnd       = ", tEnd
1095   write(*,*) "      tDel       = ", tDel
1096   write(*,*) "      e1         = ", e1
1097   write(*,*) "      e2         = ", e2
1098   write(*,*) "      eSoln     = ", eSoln
1099   write(*,*) "      nit        = ", nit
1100   write(*,*) "      xDel       = ", xDel
1101   write(*,*) "      fSelect    = ", fSelect
1102   write(*,*) "      dSelect    = ", dSelect
1103   write(*,*) "      gSelect    = ", gSelect
1104   write(*,*) "      MinitialCond= ", MinitialCond
1105   write(*,*) "Allocating the size of arrays"
1106   allocate(C(n),M(n))
1107   write(*,'(A,I12,A)') "      C and M are now dimension(", n, ") arrays"
1108
1109   write(*,*) "Setting Initial Conditions"
1110   call setInitialConditions(C,M,row,col,n,depth,height,xDel,MinitialCond, &
1111                 num_innocu_points)
1112
1113   write(*,*) "Starting Solver"
1114   call system_clock(COUNT_RATE=clock_rate, COUNT_MAX=clock_max)
1115   call system_clock(startTime)
1116   call solveOrder2(tEnd,nOuts,tDel,n,row,col,M,C,xDel,&
1117                 gama,nu,alpha,beta,kappa,delta,ndiag,e1,e2,nit,eSoln,dSelect,&
1118                 fSelect,gSelect,avgIters,maxIters,avgNit,maxNit,true2D,checkTrav,eTrav)
1119   call system_clock(endTime)
1120
1121   ! Convert times into seconds
1122   elapsedTime = real(endTime - startTime)/real(clock_rate)
1123

```

```

1124
1125 ! Report Statistics
1126 write(*,*) "-----"
1127 write(*,*) "Statsitcs:"
1128 write(*,*) "-----"
1129 write(*,*) "Time to compute = ", elapsedTime
1130 write(*,*) ""
1131 write(*,*) "Avg Iters for iterating betn. soln. =", avgIter
1132 write(*,*) "Max Iters for iterating betn. soln. =", maxIter
1133 write(*,*) "Avg Iters for linear solver =", avgNit
1134 write(*,*) "Max Iters for linear solver =", maxNit
1135 write(*,*) "Writing statistics to file"
1136 call reportStats(avgIter,maxIter,avgNit,maxNit,elapsedTime)
1137
1138 write(*,*) "Execution completed"
1139
1140 end program
1141
1142
1143 !=====
1144 ! Sets the problem size and checks for auxillary settings
1145 !-----
1146 ! This must be done first since the problem size is used in the variable
1147 ! declaration of the arrays.
1148 ! The auxillary settings are if the problem is 2D in nature; this means
1149 ! that the computation time can be drastically reduced by letting col = 4
1150 ! instead of col = pSize.
1151 ! Also, the option for checking for the existance of travelling wave
1152 ! solutions is done here.
1153 !=====
1154 subroutine getProbSize(pSize, true2D, checkTrav, filename, nameLen)
1155 implicit none
1156 integer,intent(out) :: pSize, true2D, checkTrav
1157 integer,intent(in) :: nameLen
1158 character(nameLen),intent(in) :: filename
1159 character :: dum ! Dummy variable
1160 write(*,*) filename
1161 open(UNIT = 19, FILE = filename, STATUS = "old", ACTION = "read")
1162 read(19,*); read(19,*); read(19,*)
1163 ! Skip first 3 lines
1164 read(19,*)
1165 dum, dum, pSize
1166 read(19,*)
1167 dum, dum, true2D
1168 read(19,*)
1169 dum, dum, checkTrav
1170 close(19)
1171
1172 end subroutine getprobSize
1173
1174 !=====
1175 ! Sets the all the parameter values
1176 !-----
1177 ! Opens the parameter.txt file, which holds all the parameter values and
1178 ! function uses, and sets the variables accordingly.
1179 ! Takes in all the parameters on entry and outputs them with the appropriate
1180 ! value.
1181 !=====
1182 subroutine paramSet(depth, height, numInnocu, alpha, beta, kappa, &

```

```

1179         gama, nu, delta, nOuts, tEnd, tDel, e1, e2, eTrav, &
1180         eSoln, fSelect, dSelect, gSelect, MinitialCond, filename, &
1181         nameLen)
1182 implicit none
1183 real, intent(out) :: depth, height, kappa, delta, nu
1184 real, intent(out) :: tEnd, tDel, e1, e2, eSoln, eTrav, gama
1185 integer, intent(out) :: alpha, beta, numInnocu, nOuts
1186 integer, intent(out) :: fSelect, dSelect, gSelect, MinitialCond
1187 integer, intent(in) :: nameLen
1188 character(nameLen), intent(in) :: filename
1189
1190 character :: dum, dum2      ! Dummy variable
1191
1192 open(UNIT = 19, FILE = filename, STATUS = "old", ACTION = "read")
1193 ! Skip first 6 lines
1194 read(19,*); read(19,*); read(19,*); read(19,*); read(19,*);
1195
1196 read(19,*)
1197 read(19,*)
1198 read(19,*)
1199 read(19,*)
1200 read(19,*)
1201 read(19,*)
1202 read(19,*)
1203 read(19,*)
1204 read(19,*)
1205 read(19,*)
1206 read(19,*)
1207 read(19,*)
1208 read(19,*)
1209 read(19,*)
1210 read(19,*)
1211 read(19,*)
1212 read(19,*)
1213
1214 ! Skip xDel
1215 read(19,*)
1216 read(19,*)
1217 read(19,*)
1218 read(19,*)
1219
1220 close(19)
1221
1222 end subroutine paramSet
1223
1224
1225 !=====
1226 ! Sets the initial conditions for the system
1227 !-----
1228 ! For C, we have homogenous initial conditions, trivial to do
1229 ! For M, the inoculation point has a smooth curve to avoid sharp numerical
1230 ! artifacts in the system. This is done with a polynomial  $f(x) = a*x^8+b$ ,
1231 ! this function is computed based on the depth and height parameters,
1232 ! calculating  $b = height$  and  $a = b/(depth)^8$ 
1233 !=====

```

```

1234 subroutine setInitialConditions(C,M,row,col,n,depth,height,xDel,MinitialCond, &
1235                               num_innocu_points)
1236 implicit none
1237 integer,intent(in) :: row,col,n,MinitialCond, num_innocu_points
1238 real,intent(in) :: depth, height, xDel
1239 real,dimension(n),intent(out) :: C,M
1240
1241 integer :: i,j,x,y, xi, yi, p
1242 real :: f,a           ! function for IC curve
1243 real :: innoc         ! Placeholder for new IC value at point
1244 real :: total          ! Counts total innoculation height
1245 real :: mIC, cIC      ! Used to store previous simulation values while reading
1246 real :: xr, yr
1247
1248 C = 1.; j = 0; M = 0
1249
1250 ! 2D trav wave smooth curve
1251 if (MinitialCond == 1) then
1252   a = -height/(depth)**4
1253   !$omp parallel do private(f) shared(height,a)
1254   do i = 1, n
1255     x = (i-1)/col
1256     f = a*(x*xDel)**4 + height
1257     M(i) = f
1258     if (f .LE. 0) M(i) = 0
1259   enddo
1260   !$omp end parallel do
1261
1262 ! homogenous everywhere
1263 else if (MinitialCond == 2) then
1264   M = height
1265
1266 ! 3D initial conditions
1267 else if (MinitialCond == 3) then
1268   a = -height/(depth)**2
1269   !$omp parallel do private(f,x,y) shared(height,a)
1270   do i = 1, n
1271     x = MOD(i-1, col)
1272     y = i / row
1273     f = a*((x*xDel-0.5)*(x*xDel-0.5) + (y*xDel-0.5)*(y*xDel-0.5)) + height
1274     M(i) = f
1275     if (M(i) .LE. 0) M(i) = 0
1276   enddo
1277   !$omp end parallel do
1278
1279 !(Random innoculation points over whole domain [3D])
1280 else if (MinitialCond == 4) then
1281   a = -height/(depth*depth)
1282   call init_random_seed()
1283   do i = 1, num_innocu_points
1284     call random_number(xr)
1285     call random_number(yr)
1286     do j = 1, n
1287       if (M(j) .LE. 0) then
1288         x = MOD(j-1, col)

```

```

1289         y = j / row
1290         M(j) = M(j) + a*((x*xDel-xr)*(x*xDel-xr) + (y*xDel-yr)*(y*xDel-yr)) + height
1291         if (M(j) .LE. 0) M(j) = 0
1292     endif
1293   enddo
1294 enddo
1295
1296 ! (Random inoculation points on y=0 side [3D])
1297 else if (MinitialCond == 5) then
1298   a = -height/(depth*depth)
1299   call init_random_seed()
1300   do i = 1, num_innoco_points
1301     call random_number(xr)
1302     call random_number(yr)
1303     yr = yr*0.1
1304     do j = 1, n
1305       x = MOD(j-1, col)
1306       y = j / row
1307       innoc = a*((x*xDel-xr)*(x*xDel-xr) + (y*xDel-yr)*(y*xDel-yr)) + height
1308       if (innoc .GE. 0) M(j) = M(j) + innoc
1309     enddo
1310   enddo
1311   ! Divide inoculation height by average non-zero value
1312   i = 0
1313   do j = 1, n
1314     if (M(j) .GT. 0) then
1315       i = i + 1
1316       total = total + M(j)
1317     endif
1318   enddo
1319   do j = 1, n
1320     M(j) = M(j) * height/(total/real(i))
1321   enddo
1322
1323
1324 ! sharp IC. homogenous in y-dir
1325 else if (MinitialCond == 6) then
1326   do i = 1, n
1327     x = (i-1) / col
1328     if ( x*xDel .LE. depth) then
1329       M(i) = height
1330     endif
1331   enddo
1332
1333 ! pertubations in y-dir; check trav.wave. stability
1334 else if (MinitialCond == 7) then
1335   call init_random_seed()
1336   do i = 1, n
1337     if ( i*xDel/col .LE. depth) then
1338       call random_number(xr)
1339       M(i) = xr*0.2
1340     endif
1341   enddo
1342
1343 ! Test the grid ordering/ printing

```

```

1344 else if (MinitialCond == 8) then
1345 ! do i = 1, row
1346 ! do j = 1, col
1347 ! if (i*xDel .LE. depth) then
1348 ! p = j + (i-1)*col
1349 ! M(i) = real(p)/real(n)/4.0
1350 ! endif
1351 ! enddo
1352 ! enddo
1353 do i = 1, n
1354 M(i) = real(i)/real(n)/10
1355 enddo
1356
1357 ! (Evenly spaced innoculation points on y=0 side [3D])
1358 else if (MinitialCond == 9) then
1359 a = -height/(depth*depth)
1360 do i = 1, num_innocu_points
1361 xr = depth + (i-1)*2*depth + real((i-1)*(1-num_innocu_points*depth*2))/real(num_innocu_points)
1362 do j = 1, n
1363 if (M(j) .LE. 0) then
1364 x = MOD(j-1, col)
1365 y = j / row
1366 M(j) = M(j) + a*((x*xDel-xr)*(x*xDel-xr) + (y*yDel)*(y*yDel)) + height
1367 if (M(j) .LE. 0) M(j) = 0
1368 endif
1369 enddo
1370 enddo
1371
1372 ! Random innoculation points on y=0 and y = 1
1373 else if (MinitialCond == 10) then
1374 a = -height/(depth*depth)
1375 call init_random_seed()
1376 do i = 1, 2*num_innocu_points
1377 call random_number(xr)
1378 call random_number(yr)
1379 yr = yr*0.1
1380 if (i .GT. num_innocu_points) then
1381 yr = yr + 0.9 ! For y = 1 side
1382 endif
1383 do j = 1, n
1384 x = MOD(j-1, col)
1385 y = j / row
1386 innoc = a*((x*xDel-xr)*(x*xDel-xr) + (y*yDel-yr)*(y*yDel-yr)) + height
1387 if (innoc .GE. 0) M(j) = M(j) + innoc
1388 enddo
1389 enddo
1390
1391 ! Read IC from output file... (Continues a previous sim) CANNOT GET WORKING>>>
1392 ! else if (MinitialCond == 11) then
1393 ! open(UNIT = 119, FILE = "initialCond.dat", STATUS = "old", ACTION = "read")
1394 ! read(119,*) ! Skip first line
1395 ! do i = 1, n/2+1
1396 ! read(119,*) innoc, innoc, innoc, innoc
1397 ! enddo
1398 ! do i = n/2+1, n      <<<< THIS IS THE PROBLEM AREA, Can't divide the region in two

```

```

1399 !      read(119,*) innoc, innoc, mIC, cIC ! innoc is used as a dummy variable here
1400 !
1401 !      M(i) = mIC
1402 !
1403 !      C(i) = cIC
1404 !
1405 !
1406 ! Clumped up innoculation at origin. Same total as MinitCond == 9
1407 else if (MinitialCond == 12) then
1408     innoc = (2*height*depth*depth*num_innocu_points) ** (1.0/3.0)
1409     a = -1.0/(innoc)
1410     do j = 1, n
1411         x = MOD(j-1, col)
1412         y = j / row
1413         M(j) = a*((x*xDel)*(x*xDel) + (y*xDel)*(y*xDel)) + innoc
1414         if (M(j) .LE. 0) M(j) = 0
1415     enddo
1416
1417 ! Evenly Spaced innocu point in cubes (exact total)
1418 else if (MinitialCond == 13) then
1419     xr = real(col)/real(num_innocu_points)
1420     do j = 1, n
1421         x = MOD(j-1, col)
1422         y = j / row
1423         if (y*xDel .LE. depth .AND. MOD(x+xr/4.0, xr) >= xr/2.0) M(j) = height
1424     enddo
1425
1426 ! Clumped up like ==12, but exact cube
1427 else if (MinitialCond == 14) then
1428     xr = (num_innocu_points * depth * height * real(col)/(2*real(num_innocu_points))) **
1429     do j = 1, n
1430         x = MOD(j-1, col)
1431         y = j / row
1432         if (y*xDel .LE. xr .AND. x*xDel .LE. xr) M(j) = xr
1433     enddo
1434
1435 endif
1436
1437 end subroutine setInitialConditions
1438
1439 !
1440 !=====
1441 ! Function f(C,M)
1442 !=====
1443 subroutine fFunc(M,C,f,kappa,nu,fSelect)
1444     implicit none
1445     integer, intent(in) :: fSelect
1446     real, intent(in) :: M,C,kappa,nu
1447     real, intent(out) :: f
1448     real :: eps
1449     eps = C*0.00000001
1450     if (fSelect == 1) f = C/(kappa+C)-nu
1451     if (fSelect == 2) f = C/(kappa+C)
1452     if (fSelect == 3) f = C/(kappa*M+C+eps)-nu
1453     if (fSelect == 4) f = C/(kappa*M+C+eps)

```

```

1454     if (fSelect == 5) f = 1
1455     if (fSelect == 6) f = C/(kappa+C)*(1-M/(C+eps))-nu
1456 end subroutine fFunc
1457
1458
1459 !=====
1460 ! Function d(M)
1461 !=====
1462 subroutine dFunc(M,d,delta,alpha,beta,dSelect)
1463     implicit none
1464     integer,intent(in) :: alpha, beta, dSelect
1465     real, intent(in) :: M, delta
1466     real, intent(out) :: d
1467     if (dSelect == 1) d = delta
1468     if (dSelect == 2) d = delta * M**alpha
1469     if (dSelect == 3) d = delta * M**alpha / ((1 - M)**beta)
1470 end subroutine dFunc
1471
1472
1473 !=====
1474 ! Solves the solution, C
1475 !-----
1476 ! Uses the trapizoidal rule for an ODE and solves for C.
1477 ! Different gSelects give different values for b and c.
1478 ! gSelect = 1 --> g = gama*C/(kappa+C)
1479 !=====
1480 subroutine solveC(M,Mnew,Csol,Cnew,n,kappa,gama,tDel,gSelect)
1481     implicit none
1482     integer,intent(in) :: n,gSelect
1483     real,intent(in) :: kappa,tDel,gama
1484     real,dimension(n),intent(in) :: M,Mnew,Csol
1485     real,dimension(n),intent(out) :: Cnew
1486
1487     integer :: i,j      ! grid index
1488     integer :: g        ! current grid point
1489     real :: b,c        ! quadratic equation terms
1490     real :: f          ! f(C,M) value at gridpoint
1491     real :: aux
1492
1493     real :: r,s
1494     r = 1
1495     s = 0.5
1496
1497     aux = tDel*0.5*gama
1498
1499     if (gSelect == 1) then
1500         !$omp parallel do private(b,c) shared(kappa,Csol,aux,Mnew,M)
1501         do i = 1,n
1502             b = kappa - Csol(i) + aux*(Mnew(i) + Csol(i)*M(i)/(kappa+Csol(i)))
1503             c = -kappa*Csol(i) + aux*kappa*Csol(i)*M(i)/(kappa + Csol(i))
1504             Cnew(i) = 0.5 * (-b + SQRT(b*b - 4 * c))
1505         enddo
1506         !$omp end parallel do
1507     end if
1508

```

```

1509 end subroutine solveC
1510
1511 !=====
1512 ! Generates matrix M in diagonal format for the current timestep
1513 !=====
1514
1515 subroutine GenMatrixM(M,C,MatrixM,Mioff,Mrhs,row,col,n,ndiag,delta,nu,&
1516 alpha,beta,kappa,tDel,xDel,dSelect,fSelect)
1517 implicit none
1518 integer,intent(in) :: row,col,n,ndiag,alpha,beta,dSelect,fSelect
1519 real,intent(in) :: delta,kappa,xDel,tDel,nu
1520 real,dimension(n),intent(in) :: M,C
1521
1522 real,dimension(n,ndiag),intent(out) :: MatrixM
1523 real,dimension(n),intent(out) :: Mrhs
1524 integer,dimension(ndiag),intent(out) :: Mioff
1525
1526 real :: xCof
1527 real :: f
1528 real,dimension(n) :: diff
1529 !integer :: x,y,g
1530 integer :: i
1531
1532 real :: tDela
1533 tDela = tDel      ! Used for testing purposes
1534
1535 xCof = 1/(xDel*xDel)
1536
1537 Mioff = (/ -col, -1, 0, 1, col /)
1538 MatrixM(:,:) = 0
1539
1540 ! Compute all the diffusion coefficients
1541 !$omp parallel do shared(M,diff,delta,alpha,beta,dSelect)
1542 do i = 1,n
1543   call dFunc(M(i), diff(i), delta, alpha, beta, dSelect)
1544 enddo
1545 !$omp end parallel do
1546
1547 !$omp parallel do shared(MatrixM,xCof,diff,Mrhs,tDel,M,C,kappa,nu,fSelect) private(i, i)
1548 !$omp parallel do private(f)
1549 do i = 1,n
1550   if (i .LE. col) then
1551     MatrixM(i,5) = MatrixM(i,5) - xCof*0.5*(diff(i+col)+diff(i))
1552     MatrixM(i,3) = MatrixM(i,3) + xCof*0.5*(diff(i+col)+diff(i))
1553   else
1554     MatrixM(i,1) = MatrixM(i,1) - xCof*0.5*(diff(i-col)+diff(i))
1555     MatrixM(i,3) = MatrixM(i,3) + xCof*0.5*(diff(i-col)+diff(i))
1556   endif
1557
1558   if (MOD(i,col) == 1) then
1559     MatrixM(i,4) = MatrixM(i,4) - xCof*0.5*(diff(i+1)+diff(i))
1560     MatrixM(i,3) = MatrixM(i,3) + xCof*0.5*(diff(i+1)+diff(i))
1561   else
1562     MatrixM(i,2) = MatrixM(i,2) - xCof*0.5*(diff(i-1)+diff(i))
1563     MatrixM(i,3) = MatrixM(i,3) + xCof*0.5*(diff(i-1)+diff(i))

```

```

1564         endif
1565
1566     if (MOD(i,col) == 0) then
1567         MatrixM(i,2) = MatrixM(i,2) - xCof*0.5*(diff(i-1)+diff(i))
1568         MatrixM(i,3) = MatrixM(i,3) + xCof*0.5*(diff(i-1)+diff(i))
1569     else
1570         MatrixM(i,4) = MatrixM(i,4) - xCof*0.5*(diff(i+1)+diff(i))
1571         MatrixM(i,3) = MatrixM(i,3) + xCof*0.5*(diff(i+1)+diff(i))
1572     endif
1573
1574     if (i .GE. n-col) then
1575         MatrixM(i,1) = MatrixM(i,1) - xCof*0.5*(diff(i-col)+diff(i))
1576         MatrixM(i,3) = MatrixM(i,3) + xCof*0.5*(diff(i-col)+diff(i))
1577     else
1578         MatrixM(i,5) = MatrixM(i,5) - xCof*0.5*(diff(i+col)+diff(i))
1579         MatrixM(i,3) = MatrixM(i,3) + xCof*0.5*(diff(i+col)+diff(i))
1580     endif
1581
1582     call fFunc(M(i),C(i),f,kappa,nu,fSelect)
1583     MatrixM(i,3) = MatrixM(i,3) - f + (1/tDel)
1584     Mrhs(i) = M(i)/tDel
1585
1586 enddo
!$omp end parallel do
1587
1588 end subroutine GenMatrixM
1589
1590
1591 !=====
1592 !   Solve Order 2
1593 !-----
1594 !   1. Solves for M_{i+1} using C_i and M_i
1595 !   2. Solves for C_{i+1} using C_i, M_i, and M_{i+1}
1596 !   ... repeat until convergence
1597 !=====
1598 subroutine solveOrder2(tEnd,nOuts,tDel,n,row,col,M,C,xDel,&
1599 gama,nu,alpha,beta,kappa,delta,ndiag,e1,e2,nit,eSoln,dSelect,fSelect,&
1600 gSelect,avgIters,maxIters,avgNit,maxNit,true2D,checkTrav,eTrav)
1601 implicit none
1602 integer,intent(in) :: nOuts,n,row,col,alpha,beta,ndiag
1603 integer,intent(in) :: dSelect,fSelect,gSelect,true2D,checkTrav
1604 real,intent(in) :: tEnd,tDel,xDel,kappa,delta,nu,gama
1605 real,intent(in) :: eSoln,eTrav
1606 real,intent(inout) :: e1,e2
1607 integer,intent(inout) :: nit
1608 real,dimension(n),intent(out) :: M,C
1609 real,intent(out) :: avgIters,maxIters,avgNit,maxNit
1610
1611 integer :: counter      ! Counts the num. of iter. in system solver
1612 integer :: endLoop       ! endLoop = 1 -> solving loop can stop
1613 integer :: filter        ! Controls frequency of outputs written
1614
1615 real :: stored_e1, stored_e2
1616
1617 real :: totalMassM      ! Total Biomass over region
1618 real :: totalMassC      ! Total Substrait over region

```

```

1619 real :: prevMassC           ! Total Substrait from X timesteps ago
1620
1621 real,dimension(n) :: Mnew
1622 real,dimension(n) :: Cnew
1623 real,dimension(n,ndiag) :: MatrixM
1624 real,dimension(n) :: Mrhs
1625 real,dimension(n) :: Cprev, Mprev
1626 integer,dimension(ndiag) :: Mioff
1627 integer :: stopcritria
1628 integer :: stat
1629 real :: diffC, diffM
1630 integer :: countIters
1631 real :: peak, height, intfac ! Track Interface and wave peak
1632 integer :: travExist          ! 1 if trav wave exist at this timestep
1633 real :: waveSpeed            ! calculated wavespeed at current timestep
1634 real,dimension(n) :: Mprev_10 ! M from 10-ish timesteps ago, for travCheck
1635
1636 stored_e1 = e1
1637 stored_e2 = e2
1638
1639 filter = int(tEnd/(nOuts*tDel))
1640 endLoop = 0
1641 counter = 0
1642 countIters = 0
1643 avgIters = 0
1644 avgNit = 0
1645 Mprev_10 = M    ! To initiatize for travCheck
1646 travExist = 0
1647
1648 prevMassC = 1
1649
1650 open(UNIT = 124, IOSTAT = stat, FILE = "total.dat", STATUS = "old")
1651 if (stat .EQ. 0) close(124, STATUS = "delete")
1652 open(UNIT = 120, FILE = "total.dat", POSITION = "append", ACTION = "write")
1653
1654 open(UNIT = 124, IOSTAT = stat, FILE = "COprod.dat", STATUS = "old")
1655 if (stat .EQ. 0) close(124, STATUS = "delete")
1656 open(UNIT = 126, FILE = "COprod.dat", POSITION = "append", ACTION = "write")
1657
1658 if (true2D == 1) then
1659   open(UNIT = 124, IOSTAT = stat, FILE = "peakInfo.dat", STATUS = "old")
1660   if (stat .EQ. 0) close(124, STATUS = "delete")
1661   open(UNIT = 121, FILE = "peakInfo.dat", POSITION = "append", ACTION = "write")
1662 endif
1663
1664 if (checkTrav == 1) then
1665   open(UNIT = 124, IOSTAT = stat, FILE = "travCheck.dat", STATUS = "old")
1666   if (stat .EQ. 0) close(124, STATUS = "delete")
1667   open(UNIT = 138, FILE = "travCheck.dat", POSITION = "append", ACTION = "write")
1668 endif
1669
1670 write(*,*) "      time      avgIter      maxIter      avgNit      maxNit      avgM
1671 avgC"
1672
1673 do while((counter) * tDel <= tEnd)

```

```

1674 ! Output every 100 times more then nOuts for the peak info
1675 if (MOD(counter, int(filter/100)+1) == 0) then
1676   ! Get total M and C
1677   call calcMass(M, totalMassM, n, row, col)
1678   call calcMass(C, totalMassC, n, row, col)
1679   write(120,*) counter*tDel, totalMassM, totalMassC
1680
1681   ! CO_2 production: t, current produced CO2, total produced CO2
1682   write(126,*) counter*tDel, prevMassC - totalMassC, 1 - totalMassC
1683   prevMassC = totalMassC
1684
1685   ! peak-interface, only availbale for 2D graphs
1686   if (true2D == 1) then
1687     call calcPeakInterface(M, row, col, peak, height, intfac)
1688     write (121,*) tDel*counter, peak, height, intfac
1689   end if
1690 endif
1691 if (true2D == 1 .AND. checkTrav == 1 .AND. MOD(counter, int(filter))==0) then
1692   call checkTravWave(M, Mprev_10, row, col, travExist, wavespeed, height, eTrav)
1693   wavespeed = wavespeed/filter ! Makes wavespeed independent of number of outputs
1694   write (138,*) tDel*counter, travExist, wavespeed
1695   Mprev_10 = M
1696 endif
1697
1698 ! Write to file / report Total Mass
1699 if (MOD(counter, filter) == 0) then
1700   if (true2D == 1) then
1701     call printToFile2D(n, row, col, M, C)
1702   else
1703     call printToFile(n, row, col, M, C)
1704   end if
1705
1706   if (counter == 0) then
1707     write(*,'(F8.2,F12.2,I8,F12.2,I8,F12.6,F12.6)') 0.0, 0.0, &
1708     int(maxIters), 0.0, int(maxNit), totalMassM, totalMassC
1709   else
1710     write(*,'(F8.2,F12.2,I8,F12.2,I8,F12.6,F12.6)') tDel*counter, &
1711     real(avgIters/counter), int(maxIters), real(avgNit/avgIters), &
1712     int(maxNit),totalMassM, totalMassC
1713   endif
1714 endif
1715
1716 diffC = 1
1717 diffM = 1
1718 countIters = 0
1719 Cprev = C
1720 Mprev = M
1721
1722 do while(diffC + diffM > eSoln)
1723   nit = 100*n
1724   e1 = stored_e1
1725   e2 = stored_e2
1726
1727   ! Solve M
1728   call GenMatrixM(Mprev,C,MatrixM,Mioff,Mrhs,row,col,n,ndiag,delta,nu,&

```

```

1729           alpha,beta,kappa,tDel,xDel,dSelect,fSelect)
1730   call solveLSDIAG(n,ndiag,Mioff,MatrixM,Mnew,Mrhs,nit,e1,e2,stopcritria)
1731
1732 ! Solve C
1733 call solveC(Mprev,Mnew,Cprev,Cnew,n,kappa,gama,tDel,gSelect)
1734
1735 ! Solve CO_2 production
1736
1737
1738 if(nit > maxNit) maxNit = nit
1739 avgNit = avgNit + nit
1740
1741 call calcDiff(diffC, C, Cnew, row, col)
1742 call calcDiff(diffM, M, Mnew, row, col)
1743
1744 C = Cnew
1745 M = Mnew
1746 countIters = countIters+1
1747
1748 if (countIters > 10000) then
1749   write(*,*) "[!] Over 10000 iterations in one timestep"
1750   write(*,*) "[!] Solutions not converging. Exit!"
1751   stop
1752 end if
1753 !
1754   write(*,*) countIters, diffC, diffM, C(12),M(12)
1755 enddo
1756 if(countIters > maxIters) maxIters = countIters
1757 avgIters = avgIters + countIters
1758
1759 counter = counter + 1
1760 enddo
1761 avgNit = avgNit/(avgIters) ! avgIters right now is the total
1762 avgIters = avgIters/counter
1763
1764 ! Print final solution
1765 ! if (true2D == 1) then
1766 !   call printToFile2D(n,row,col,M,C)
1767 ! else
1768 !   call printToFile(n,row,col,M,C)
1769 ! end if
1770 ! write(*,'(F8.2,F12.2,I8,F12.2,I8,F12.6,F12.6)') tDel*counter, &
1771 !       real(avgIters), int(maxIters), real(avgNit), &
1772 !       int(maxNit),totalMassM, totalMassC
1773 close(120)
1774 close(138)
1775 close(126)
1776 if (true2D == 1) then
1777   close(121)
1778 endif
1779
1780 end subroutine solveOrder2
1781
1782
1783 =====

```

```

1784 !      Calculate the Total Mass
1785 !-----
1786 !      Uses Riemann Sums kind of concept to check if the program runs correctly
1787 !      since the total mass of the region can be computed and checked.
1788 !=====
1789 subroutine calcMass(X,totalMass,n,row,col)
1790     implicit none
1791     integer,intent(in) :: n,row,col
1792     real,dimension(n),intent(in) :: X
1793
1794     real,intent(out) :: totalMass
1795
1796     integer :: i,j,g
1797
1798     totalMass = 0
1799
1800     !$omp parallel do reduction(+:totalMass)
1801     do i=1,n
1802         totalMass = totalMass + X(i)
1803     enddo
1804     !$omp end parallel do
1805
1806     totalMass = totalMass / n
1807
1808 end subroutine calcMass
1809
1810
1811 !=====
1812 !      Prints out the solution in a format accepted by gnuplot, used for graphing
1813 !-----
1814 !      Runs through the grid, row-by-row. The MOD and filter act to reduce the
1815 !      number of grid points written, useful when comparing different grid
1816 !      sizes.
1817 !-----
1818 !      Input:
1819 !      n      = The problem size
1820 !      row    = The number of rows
1821 !      col    = The number of columns
1822 !      M      = The solution vector for biomass
1823 !      C      = The solution for substrait
1824 !      Output:
1825 !      none
1826 !=====
1827 subroutine printToFile(n,row,col,M,C)
1828     implicit none
1829
1830     integer,intent(in) :: n, row, col
1831     real,dimension(n),intent(in) :: M,C
1832
1833     integer :: p
1834     integer :: i,j
1835     integer :: stat
1836     integer :: filter
1837
1838     !-----

```

```

1839 ! Deletes the old output file if it exist
1840 !-----
1841 open(UNIT = 123, IOSTAT = stat, FILE = "output.dat", STATUS = "old")
1842 if (stat .EQ. 0) close(123, STATUS = "delete")
1843
1844 open(UNIT = 11, FILE = "output.dat", POSITION = "append", ACTION = "write")
1845
1846 filter = 1
1847 if (row .gt. 257) then
1848   filter = (row-1)/256
1849 endif
1850
1851 do i=1,row
1852   if (MOD(i-1, filter) == 0) then
1853     do j=1,col
1854       if (MOD(j-1, filter) == 0) then
1855         p = (j + (i-1)*col)
1856         write(11,*) real(j-1)/real(col-1), &
1857                   real(i-1)/real(row-1), M(p), C(p)
1858       endif
1859     enddo
1860     write(11,*) ' '
1861   endif
1862 enddo
1863 write(11,*)
1864
1865
1866 end subroutine printToFile
1867
1868 !=====
1869 ! Prints out the solution in a 2D format, used for graphing the Travelling
1870 ! Wave Example.
1871 !-----
1872 !
1873 ! Runs through the grid, row-by-row. The MOD and filter act to reduce the
1874 ! number of grid points written
1875 ! Unique here is that the average of the x-axis is taken so that the system
1876 ! can be reduced to just y. Also written are the max and min for each y
1877 ! value; this is used for showing that the system can be reduced.
1878 !-----
1879 !
1880 ! Input:
1881 !   n      = The problem size
1882 !   row    = The number of rows
1883 !   col    = The number of columns
1884 !   M      = The solution vector for biomass
1885 !   C      = The solution for substrait
1886 !
1887 ! Output:
1888 !   none
1889 !=====
1890
1891 subroutine printToFile2D(n, row, col, M, C)
1892   implicit none
1893
1894   integer,intent(in) :: n, row, col
1895   real,dimension(n),intent(in) :: M,C
1896
1897
1898
1899
1900
1901
1902
1903
1904
1905
1906
1907
1908
1909
1910
1911
1912
1913
1914
1915
1916
1917
1918
1919
1920
1921
1922
1923
1924
1925
1926
1927
1928
1929
1930
1931
1932
1933
1934
1935
1936
1937
1938
1939
1940
1941
1942
1943
1944
1945
1946
1947
1948
1949
1950
1951
1952
1953
1954
1955
1956
1957
1958
1959
1960
1961
1962
1963
1964
1965
1966
1967
1968
1969
1970
1971
1972
1973
1974
1975
1976
1977
1978
1979
1980
1981
1982
1983
1984
1985
1986
1987
1988
1989
1990
1991
1992
1993
1994
1995
1996
1997
1998
1999
2000
2001
2002
2003
2004
2005
2006
2007
2008
2009
2010
2011
2012
2013
2014
2015
2016
2017
2018
2019
2020
2021
2022
2023
2024
2025
2026
2027
2028
2029
2030
2031
2032
2033
2034
2035
2036
2037
2038
2039
2040
2041
2042
2043
2044
2045
2046
2047
2048
2049
2050
2051
2052
2053
2054
2055
2056
2057
2058
2059
2060
2061
2062
2063
2064
2065
2066
2067
2068
2069
2070
2071
2072
2073
2074
2075
2076
2077
2078
2079
2080
2081
2082
2083
2084
2085
2086
2087
2088
2089
2090
2091
2092
2093
2094
2095
2096
2097
2098
2099
2100
2101
2102
2103
2104
2105
2106
2107
2108
2109
2110
2111
2112
2113
2114
2115
2116
2117
2118
2119
2120
2121
2122
2123
2124
2125
2126
2127
2128
2129
2130
2131
2132
2133
2134
2135
2136
2137
2138
2139
2140
2141
2142
2143
2144
2145
2146
2147
2148
2149
2150
2151
2152
2153
2154
2155
2156
2157
2158
2159
2160
2161
2162
2163
2164
2165
2166
2167
2168
2169
2170
2171
2172
2173
2174
2175
2176
2177
2178
2179
2180
2181
2182
2183
2184
2185
2186
2187
2188
2189
2190
2191
2192
2193
2194
2195
2196
2197
2198
2199
2200
2201
2202
2203
2204
2205
2206
2207
2208
2209
2210
2211
2212
2213
2214
2215
2216
2217
2218
2219
2220
2221
2222
2223
2224
2225
2226
2227
2228
2229
2230
2231
2232
2233
2234
2235
2236
2237
2238
2239
2240
2241
2242
2243
2244
2245
2246
2247
2248
2249
2250
2251
2252
2253
2254
2255
2256
2257
2258
2259
2260
2261
2262
2263
2264
2265
2266
2267
2268
2269
2270
2271
2272
2273
2274
2275
2276
2277
2278
2279
2280
2281
2282
2283
2284
2285
2286
2287
2288
2289
2290
2291
2292
2293
2294
2295
2296
2297
2298
2299
2300
2301
2302
2303
2304
2305
2306
2307
2308
2309
2310
2311
2312
2313
2314
2315
2316
2317
2318
2319
2320
2321
2322
2323
2324
2325
2326
2327
2328
2329
2330
2331
2332
2333
2334
2335
2336
2337
2338
2339
2340
2341
2342
2343
2344
2345
2346
2347
2348
2349
2350
2351
2352
2353
2354
2355
2356
2357
2358
2359
2360
2361
2362
2363
2364
2365
2366
2367
2368
2369
2370
2371
2372
2373
2374
2375
2376
2377
2378
2379
2380
2381
2382
2383
2384
2385
2386
2387
2388
2389
2390
2391
2392
2393
2394
2395
2396
2397
2398
2399
2400
2401
2402
2403
2404
2405
2406
2407
2408
2409
2410
2411
2412
2413
2414
2415
2416
2417
2418
2419
2420
2421
2422
2423
2424
2425
2426
2427
2428
2429
2430
2431
2432
2433
2434
2435
2436
2437
2438
2439
2440
2441
2442
2443
2444
2445
2446
2447
2448
2449
2450
2451
2452
2453
2454
2455
2456
2457
2458
2459
2460
2461
2462
2463
2464
2465
2466
2467
2468
2469
2470
2471
2472
2473
2474
2475
2476
2477
2478
2479
2480
2481
2482
2483
2484
2485
2486
2487
2488
2489
2490
2491
2492
2493
2494
2495
2496
2497
2498
2499
2500
2501
2502
2503
2504
2505
2506
2507
2508
2509
2510
2511
2512
2513
2514
2515
2516
2517
2518
2519
2520
2521
2522
2523
2524
2525
2526
2527
2528
2529
2530
2531
2532
2533
2534
2535
2536
2537
2538
2539
2540
2541
2542
2543
2544
2545
2546
2547
2548
2549
2550
2551
2552
2553
2554
2555
2556
2557
2558
2559
2560
2561
2562
2563
2564
2565
2566
2567
2568
2569
2570
2571
2572
2573
2574
2575
2576
2577
2578
2579
2580
2581
2582
2583
2584
2585
2586
2587
2588
2589
2590
2591
2592
2593
2594
2595
2596
2597
2598
2599
2600
2601
2602
2603
2604
2605
2606
2607
2608
2609
2610
2611
2612
2613
2614
2615
2616
2617
2618
2619
2620
2621
2622
2623
2624
2625
2626
2627
2628
2629
2630
2631
2632
2633
2634
2635
2636
2637
2638
2639
2640
2641
2642
2643
2644
2645
2646
2647
2648
2649
2650
2651
2652
2653
2654
2655
2656
2657
2658
2659
2660
2661
2662
2663
2664
2665
2666
2667
2668
2669
2670
2671
2672
2673
2674
2675
2676
2677
2678
2679
2680
2681
2682
2683
2684
2685
2686
2687
2688
2689
2690
2691
2692
2693
2694
2695
2696
2697
2698
2699
2700
2701
2702
2703
2704
2705
2706
2707
2708
2709
2710
2711
2712
2713
2714
2715
2716
2717
2718
2719
2720
2721
2722
2723
2724
2725
2726
2727
2728
2729
2730
2731
2732
2733
2734
2735
2736
2737
2738
2739
2740
2741
2742
2743
2744
2745
2746
2747
2748
2749
2750
2751
2752
2753
2754
2755
2756
2757
2758
2759
2760
2761
2762
2763
2764
2765
2766
2767
2768
2769
2770
2771
2772
2773
2774
2775
2776
2777
2778
2779
2780
2781
2782
2783
2784
2785
2786
2787
2788
2789
2790
2791
2792
2793
2794
2795
2796
2797
2798
2799
2800
2801
2802
2803
2804
2805
2806
2807
2808
2809
2810
2811
2812
2813
2814
2815
2816
2817
2818
2819
2820
2821
2822
2823
2824
2825
2826
2827
2828
2829
2830
2831
2832
2833
2834
2835
2836
2837
2838
2839
2840
2841
2842
2843
2844
2845
2846
2847
2848
2849
2850
2851
2852
2853
2854
2855
2856
2857
2858
2859
2860
2861
2862
2863
2864
2865
2866
2867
2868
2869
2870
2871
2872
2873
2874
2875
2876
2877
2878
2879
2880
2881
2882
2883
2884
2885
2886
2887
2888
2889
2890
2891
2892
2893
2894
2895
2896
2897
2898
2899
2900
2901
2902
2903
2904
2905
2906
2907
2908
2909
2910
2911
2912
2913
2914
2915
2916
2917
2918
2919
2920
2921
2922
2923
2924
2925
2926
2927
2928
2929
2930
2931
2932
2933
2934
2935
2936
2937
2938
2939
2940
2941
2942
2943
2944
2945
2946
2947
2948
2949
2950
2951
2952
2953
2954
2955
2956
2957
2958
2959
2960
2961
2962
2963
2964
2965
2966
2967
2968
2969
2970
2971
2972
2973
2974
2975
2976
2977
2978
2979
2980
2981
2982
2983
2984
2985
2986
2987
2988
2989
2990
2991
2992
2993
2994
2995
2996
2997
2998
2999
2999

```

```

1894 integer :: p
1895 integer :: i,j
1896 integer :: stat
1897 integer :: filter
1898 real :: averageM, averageC
1899 real :: maxM, minM, maxC, minC
1900 real :: y
1901
1902 !-----
1903 ! Deletes the old output file if it exist
1904 !-----
1905 open(UNIT = 124, IOSTAT = stat, FILE = "2D_output.dat", STATUS = "old")
1906 if (stat .EQ. 0) close(124, STATUS = "delete")
1907
1908 open(UNIT = 12, FILE = "2D_output.dat", POSITION = "append", ACTION = "write")
1909
1910 filter = 1
1911 if (row .gt. 257) then
1912   filter = (row-1)/256
1913 endif
1914
1915 do, i=1,row
1916   if (MOD(i-1, filter) == 0) then
1917     averageM = 0
1918     averageC = 0
1919     maxM = 0
1920     maxC = 0
1921     minM = 1
1922     minC = 1
1923     do, j=1,col
1924       p = j + (i-1)*col
1925       averageM = averageM + M(p)
1926       averageC = averageC + C(p)
1927       if(M(p) .ge. maxM) then
1928         maxM = M(p)
1929       endif
1930       if(M(p) .le. minM) then
1931         minM = M(p)
1932       endif
1933       if(C(p) .ge. maxC) then
1934         maxC = C(p)
1935       endif
1936       if(C(p) .le. minC) then
1937         minC = C(p)
1938       endif
1939     enddo
1940     averageM = averageM/(col)
1941     averageC = averageC/(col)
1942     y = real(i-1)/real(row-1)
1943     write(12,'(f20.12,f20.12,f20.12)') y,averageM,averageC
1944 !write(12,'(f14.10,f14.10,f14.10,f14.10,f14.10,f14.10,f14.10)') y, averageM, averageC, minM,
1945   endif
1946 enddo
1947 write(12,*)
1948

```

```

1949
1950 end subroutine printToFile2D
1951
1952
1953 !=====
1954 ! Calculates the difference between each grid point for the solutions at
1955 ! different iterations
1956 !-----
1957 ! Input:
1958 ! row = The number of rows
1959 ! col = The number of columns
1960 ! C = The previous solution for substrait
1961 ! Cnew = The current solution for substrait
1962 ! Output:
1963 ! diff = The average difference between the two C's
1964 !=====
1965 subroutine calcDiff(diff, C, Cnew, row, col)
1966   integer, intent(in) :: row, col
1967   real, dimension(row*col), intent(in) :: C, Cnew
1968   real, intent(out) :: diff
1969
1970   integer :: i
1971
1972   diff = 0
1973   !$omp parallel do reduction(+:diff)
1974   do i=1, row*col
1975     diff = diff + abs(C(i) - Cnew(i))
1976   enddo
1977   !$omp end parallel do
1978   diff = diff/real(row*col)
1979
1980 end subroutine calcDiff
1981
1982
1983 !=====
1984 ! Calculates the peak and interface info at a single timestep
1985 !-----
1986 ! Input:
1987 ! row = The number of rows
1988 ! col = The number of columns
1989 ! M = The solution for biomass, array size (n)
1990 ! Output:
1991 ! peak = Peak location
1992 ! height = Peak height
1993 ! intfac = Interface location
1994 !=====
1995 subroutine calcPeakInterface(M, row, col, peak, height, intfac)
1996   implicit none
1997   integer, intent(in):: row,col
1998   real, dimension(row*col), intent(in) :: M
1999   real, intent(out) :: peak, height, intfac
2000
2001   real :: hei
2002   real :: y
2003   integer :: i,j,p

```

```

2004
2005     hei = 0
2006     do, i=1, row
2007         y = real(i-1)/real(row-1)
2008         do, j=1, col
2009             p = (j + (i-1)*col)
2010             if (M(p) >= hei) then
2011                 peak = y
2012                 hei = M(p)
2013             endif
2014             if (M(p) > 0.1) then
2015                 intfac = y
2016             endif
2017         enddo
2018     enddo
2019     height = hei
2020
2021 end subroutine
2022
2023
2024
2025 !=====
2026 !   Check if there is evidence of a travelling wave solution
2027 !-----
2028 !   Makes an educated guess for the wavespeed (which would be incorrect
2029 !   by, at worst, 2*eTrav) and then uses this wavespeed to check if the
2030 !   difference between M and Mprev is consistently wavespeed +- eTrav
2031 !   Reports 1 or 0 for travExists based on if travelling exists (1)
2032 !   or not (0). Also reports the approximated wavespeed.
2033 !=====
2034 subroutine checkTravWave(M, Mprev, row, col, travExist, wavespeed, height, eTrav)
2035     implicit none
2036     integer, intent(in) :: row, col
2037     real, intent(in) :: height, eTrav
2038     real, dimension(row * col), intent(in) :: M, Mprev
2039
2040     integer, intent(out) :: travExist
2041     real, intent(out) :: wavespeed
2042
2043     integer :: i, wavePoint1, wavePoint2
2044     real :: diff ! placeholder for difference between M and Mprev
2045     wavePoint1 = -1
2046     wavePoint2 = -1
2047
2048     do, i=row, 1, -1
2049         ! -3 because each column is 4 and I want to start at 1
2050         if (M(i*col-3) > 0.09 - eTrav .AND. M(i*col-3) < 0.09 + eTrav) then
2051             wavePoint1 = i
2052             exit
2053         endif
2054     enddo
2055
2056     do, i=row, 1, -1
2057         if (Mprev(i*col-3) > 0.09 - eTrav .AND. Mprev(i*col-3) < 0.09 + eTrav) then
2058             wavePoint2 = i

```

```

2059      exit
2060    endif
2061 enddo
2062
2063 ! Here the wavespeed is in 'i' units
2064 wavespeed = abs(wavePoint1 - wavePoint2)
2065
2066
2067 travExist = 1
2068 do i = 1, row-int(wavespeed)
2069   !write(*,*) wavespeed, i, M((i - int(wavespeed))* col - 3), Mprev(i*col - 3)
2070   diff = abs(M((i+int(wavespeed)) * col - 3) - Mprev(i * col - 3))
2071   if ( diff > eTrav*10 ) travExist = 0
2072 enddo
2073 if (wavespeed == 0) travExist = 0 ! Can't have trav wave with 0 speed
2074
2075 ! Here wavespeed is converted to dimensionless units over X time
2076 wavespeed = wavespeed / float(row)
2077
2078
2079 end subroutine checkTravWave
2080
2081
2082
2083 !=====
2084 !   Writes a bunch of statistics to file
2085 !-----
2086 !   Input:
2087 !       avgIters = average number of iterations from between solutions
2088 !       maxIters = maximum number of iterations from between solutions
2089 !       avgNit   = average number of iterations from linear solver
2090 !       maxNit   = maximum number of iterations from linear solver
2091 !       time     = time to complete solveOrder
2092 !   Output:
2093 !       write everything to the file.
2094 !=====
2095 subroutine reportStats(avgIters,maxIters,avgNit,maxNit,time)
2096 implicit none
2097 real,intent(in)::avgIters,maxIters,avgNit,maxNit
2098 real,intent(in)::time
2099 integer :: stat
2100
2101 open(UNIT = 125, IOSTAT = stat, FILE = "statReport.dat", STATUS = "old")
2102 if (stat .EQ. 0) close(125, STATUS = "delete")
2103 open(UNIT = 128, FILE = "statReport.dat", POSITION = "append", ACTION = "write")
2104
2105 write(128,*) "Statsitcs:"
2106 write(128,*) "-----"
2107 write(128,*) "Time to compute = ", time
2108 write(128,*) ""
2109 write(128,*) "Avg Iters for iterating betn. soln. =", avgIters
2110 write(128,*) "Max Iters for iterating betn. soln. =", maxIters
2111 write(128,*) "Avg Iters for linear solver =", avgNit
2112 write(128,*) "Max Iters for linear solver =", maxNit
2113

```

```

2114 close(128)
2115
2116 end subroutine
2117
2118
2119
2120 subroutine amuxd (n,x,y,diag,idiag,ioff)
2121 !-----
2122 !      Mnew times a vector in Diagonal storage format (DIA)
2123 !      f90/f95 version of the sparskit f77 subroutine
2124 !-----
2125 ! multiplies a matrix by a vector when the original matrix is stored
2126 ! in the diagonal storage format.
2127 !-----
2128 !
2129 ! on entry:
2130 !-----
2131 ! n      = row dimension of Mnew
2132 ! x      = real array of length equal to the column dimension of
2133 !          the Mnew matrix.
2134 ! ndiag  = integer. The first dimension of array adiag as declared in
2135 !          the calling program.
2136 !          (obsolete (=n always))
2137 ! iddiag = integer. The number of diagonals in the matrix.
2138 ! diag   = real array containing the diagonals stored of Mnew.
2139 ! iddiag = number of diagonals in matrix.
2140 ! diag   = real array of size (ndiag x iddiag) containing the diagonals
2141 !
2142 ! ioff   = integer array of length iddiag, containing the offsets of the
2143 !          diagonals of the matrix:
2144 !          diag(i,j) contains the element a(i,i+ioff(j)) of the matrix.
2145 !
2146 ! on return:
2147 !-----
2148 ! y      = real array of length n, containing the product y=Mnew*x
2149 !
2150 !-----
2151 implicit none
2152     integer, intent(in):: n, iddiag
2153     integer, intent(in),dimension(iddiag) :: ioff
2154     real, dimension(n), intent(in) :: x
2155     real, dimension(n,iddiag), intent(in) :: diag
2156     real, dimension(n), intent(out) :: y
2157     integer :: j, io, il, i2, i
2158
2159     !$omp parallel shared(y,diag,x,n) private(j,io,il,i2)
2160
2161     !$omp workshare
2162     !$omp do
2163     do i=1,n
2164         y(i)=0.
2165     enddo
2166     !$omp enddo
2167     !$omp end workshare
2168

```

```
2169  do j=1, iddiag
2170    io = ioff(j)
2171    i1 = max0(1,1-io)
2172    i2 = min0(n,n-io)
2173    !$omp do
2174    do i=i1,i2
2175      y(i) = y(i)+diag(i,j)*x(i+io)
2176    enddo
2177    !$omp end do
2178  enddo
2179  !$omp end parallel
2180
2181 end subroutine amuxd
```